Neuronal and Circuit Architecture Underlying Feeding Behavior in *Drosophila*

Dissertation

zur Erlangung des

Doktorgrades (Dr. rer. nat.)

der Mathematisch-Naturwissenschaftlichen Fakultät

der Rheinischen Friedrich-Wilhelms-Universität Bonn

vorgelegt von

Anton Miroschnikow

aus Chemnitz (Karl-Marx-Stadt)

BONN 2020

Angefertigt mit Genehmigung der Mathematisch-Naturwissenschaftlichen Fakultät der Rheinischen Friedrich-Wilhelms-Universität Bonn.

1. Gutachter: Prof. Dr. Michael Pankratz
2. Gutachter: PD Dr. Reinhard Bauer

Tag der Promotion: 18.06.2021
Erscheinungsjahr: 2021

„If our brains were simple enough for us to understand them,
we'd be so simple that we couldn't." **- Ian Stewart**

ZUSAMMENFASSUNG

Nahrungsaufnahme ist überlebenswichtig und eine der häufigsten Aktivitäten von Tieren. Über die Organisation der neuronalen Schaltkreise, die die Nahrungsaufnahme im Zentralnervensystem steuern, ist wenig bekannt. In dieser Arbeit wurde, in einem ssTEM-Volumen des gesamten Gehirns, die Konnektivität aller Ein- und Ausgangsneurone, die der Nahrungsaufnahme von larvalen *Drosophila* zugrunde liegen auf der Ebene von Synapsen untersucht.

Die Eingangsneurone stammen aus enterischen, pharyngealen und externen Organen, projizieren durch die drei pharyngealen Nerven und konvergieren basierend auf Modalität und peripherem Ursprung auf sieben topografisch unterschiedliche sensorische synaptische Kompartimente innerhalb des Zentralnervensystems. Die Ausgangsneurone bestehen aus pharyngealen Motorneuronen, serotonergen modulatorischen Neuronen und neuroendokrinen Neuronen, die in die Ringdrüse, ein wichtiges endokrines Organ von *Drosophila,* ziehen. Sensorische Neurone aus drei sensorischen Kompartimenten bilden, in überlappenden Domänen, eine signifikante Menge an monosynaptischen Verbindungen zu motorischen, modulatorischen und neuroendokrinen Ausgangsneuronen und unterscheiden sich von jenen, die polysynaptische Verbindungen zum Pilzkörper, dem Zentrum des assoziativen Lernens im Insektengehirn, bilden. Eine frühe Konvergenz von Geruchs- und Geschmacksinformation wird auf der Ebene von Neuronen zweiter Ordnung beobachtet, die sich mit der Pilzkörper-Calyx verbinden.

Polysynaptische Routen werden über die monosynaptischen Verbindungen gelegt, was zu einer Reihe paralleler divergierender sensorischer Pfade führt, die auf gemeinsame Ausgangsneurone konvergieren. Die Mehrheit der Prämotorneuronen, aus denen die verschiedenen parallelen Pfade bestehen, integriert jeweils geringfügig unterschiedliche und wiederholt sensorische Eingänge verschiedener Modalität. Einige der Pilzkörper-Ausgangsneuronen verschalten direkt auf diese Prämotorneuronen.

Diese Ergebnisse schlagen eine Netzwerksarchitektur für die Nahrungsaufnahme vor, in der monosynaptische und polysynaptische Pfade über eine Reihe von konvergierenden Pfaden von sensorischen Eingangsneuronen zu Ausgangsneuronen durchlaufen werden können, was für das Verständnis der Mechanismen der Aktionsauswahl relevant ist.

ABSTRACT

Feeding is elemental for survival and one of the most common activities of animals. Little is known about the organization of neuronal circuits controlling feeding behavior in the central nervous system. This study maps, from a whole brain ssTEM volume, the connectivity of all input and output neurons that underlie food intake behavior of *Drosophila* larvae on synaptic level.

The input neurons originate from enteric, pharyngeal and external organs, project through the three pharyngeal nerves and converge, based on modality and peripheral origin, onto seven topographical distinct sensory synaptic compartments within the CNS. The output neurons consist of pharyngeal motor neuron, serotonergic modulatory neurons, and neuroendocrine neurons, that target the ring gland, a major endocrine organ of *Drosophila*. Strikingly, sensory neurons from three sensory compartments form a significant amount of monosynaptic connections to motor, modulatory and neuroendocrine targets in overlapping domains and are distinct from those that form polysynaptic connections to the mushroom body, a center of insect associative learning. An early convergence of olfactory and gustatory information is observed at the level of second order neurons connecting to the mushroom body calyx.

Polysynaptic routes are superimposed on top of the monosynaptic connections, resulting in a series of parallel divergent sensory pathways that converge onto common motor outputs. The majority of the premotor neurons constituting the different parallel paths integrate each slightly different and recurrently cross-modal sensory inputs. A set of mushroom body output neurons connects directly to these premotor neurons.

These results propose a circuit architecture for feeding behavior in which monosynaptic and multisynaptic pathways can be traversed from sensory inputs to output neurons via a series of converging paths, which has relevance for understanding the mechanisms of action selection.

DEDICATION

At this point I would like to express my gratitude to all the people who have supported me and without whose help, this work would not have been possible.

First, I am in particular grateful to my parents and my brother for their imperturbable and unconditional support through the years. Thank you for always standing behind me, supporting my dreams, championing my projects, encouraging my pursuits and guiding me in the right direction.

I am grateful to my supporting and caring wife, Viktoria. Thank you for being my best friend, my beloved partner, my strength when I need it and for boosting my confidence during my low moments.

I would like to offer my sincere gratitude to Prof. Michael Pankratz for his constant support, his infectious enthusiasm, the lively discussions in his office, his consistent sympathetic ear for my ideas and challenges and his trust in me when sending me across the globe to develop my skills and represent the work we have been doing. Working under his leadership was a great opportunity for me to grow professionally and personally. Thank you, Mike, for being the kind, generous, open-minded and humorous person that you are.

Special thanks to my fellow colleagues and friends Dr. Philipp Schlegel, Dr. Andreas Schoofs and Dr. Sebastian Hückesfeld. Thank you, guys, for your continuous help, support and encouragement and for seeing the potential in me. I appreciate all the good times we've shared. I really mean it when I say you guys are the best.

I would like to thank the whole Pankratz lab and especially Dr. Ingo Zinke, Tanja Gross, Anne Stone and former colleague Sarah Brenner. Your energy and enthusiasm set the bar at work and is tough to beat. Thanks for being the life of the lab.

Table of Contents

LIST OF TABLES

LIST OF FIGURES

CHAPTER 1

INTRODUCTION

1.1 Roads towards mapping the brain

Understanding the brain, its lifelong attempts to make sense of our inner and outer world, how it controls behaviors and how it embodies the essence of the mind was and will remain arguably the greatest challenge facing neuroscience and adjoining fields. With around 84,000,000,000 (84 billion) neurons (Azevedo et al., 2009) that communicate via trillions of connections, the human brain is a network of extraordinary complexity and the underlying connectivity serves as the structural basis of all our capabilities. Thus, for investigating brain function it is essential to denote '*a comprehensive, structural blueprint of all network elements and connections of the brain*', i.e. a map of the brain – the "connectome" (Sporns et al., 2005).

In the last decade, the importance of this effort became evident by the amount of political and public attention it received as well as the financial investments that have been made to launch, for example, the Brain Research through Advancing Innovative Neurotechnologies® (BRAIN) initiative[1] (USA) and the Human Brain Project[2] (Europe). These programs aim at "developing new experimental tools" and "empowering brain research toward

[1] https://braininitiative.nih.gov

[2] https://www.humanbrainproject.eu

understanding the human brain and its diseases to advance brain medicine and computing technology".

Although the field of neuronal circuit mapping is experiencing rapid development, the sheer complexity of the nervous system and associated technical challenges make the human brain connectome at synaptic level appear a vision for the far distant future (DeFelipe, 2010; Kornfeld and Denk, 2018; Schlegel et al., 2017; Swanson and Lichtman, 2016). Moreover, it is doubtful whether a complete map would come with a sudden understanding of the brain. Instead understanding of brain function is more likely to be built from a combination of sources and approaches. Research on smaller and simpler nervous systems of invertebrates, for example, has successfully brought insights into fundamental organizational principles, computations applicable to larger, presumed to be more complex vertebrate neural circuits (Bargmann and Marder, 2013; Gelperin, 2019; Katz et al., 2013). Hence, invertebrates like the fruit fly *Drosophila melanogaster,* with their relatively small brains yet wide range of complex behaviors, offer a great platform to comprehensively map and functionally dissect brain circuits. Just as the fully sequenced genome of the fly has helped the human genome projects, insights from fly brains might well be foundational for the understanding of our own brains (Adams et al., 2000; International Human Genome Sequencing Consortium, 2001).

1.2 The dawn of connectomics

There is still a long road to be covered before we break the code of the brain, but we need to remind ourselves that we already achieved a great deal in illuminating and dissecting neuronal circuits.

Towards the end of the 19th century, Santiago Ramón y Cajal's (Nobel Laureate 1906) anatomical and histological studies in lower vertebrates, performed with Golgi's (Nobel Laureate 1906) stain method, were seminal for the field of neuronal circuit mapping and the current understanding of brain structure and function (Grant, 2007). The neuron doctrine and the law of dynamic polarization of Cajal became two of the founding assumptions of modern brain science (Llinás, 2003). The neuron doctrine, a universally accepted concept of nervous system organization, states that the nervous system of all animals is made up of discrete individual functional units, the neurons, which connect to other neurons and

effector cells (such as muscle and gland) by specialized intercellular contacts, the synapses, and not cytoplasmic continuity (Bullock, 1959; Foster and Sherrington, 1897; Ramón y Cajal, 1894; Sherrington, 1906; Waldeyer-Hartz, 1891). The law of functional polarization, a consequence of the neuron doctrine, states that nerve cells are polarized, receiving information on their dendrites and cell bodies and conducting information to distant locations through axons.

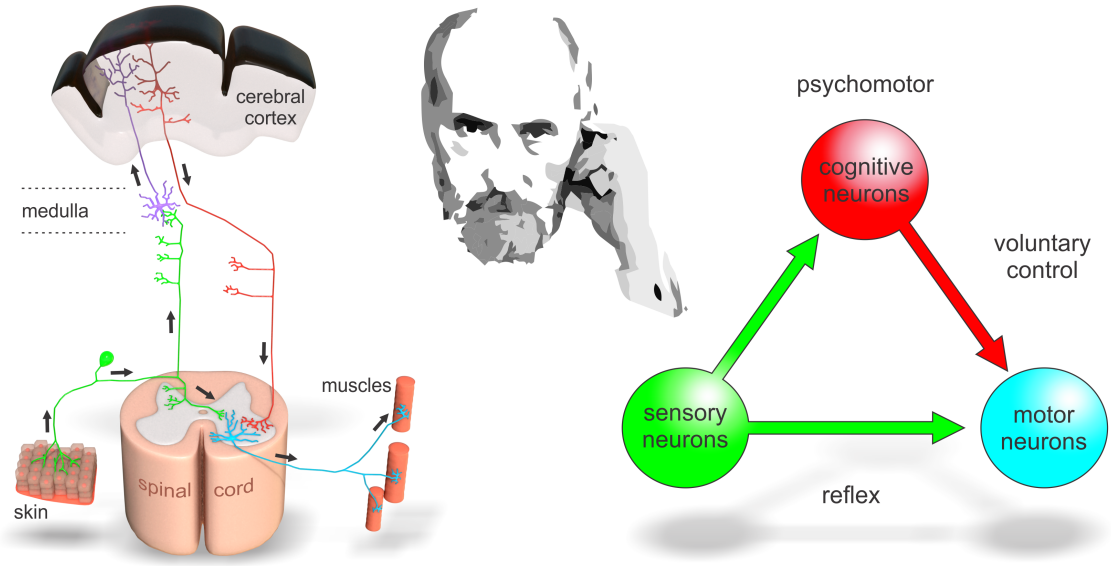

FIGURE 1.1 A simple connectome. Left**:** 3D-reconstruction of Cajal's vertebrate spinal reflex arc based on the neuron doctrine. *"Schèma de la marche des incitations motrices volontaires et des excitations sensitives conscientes"* (Ramón y Cajal, 1894). The schematic wiring diagram shows the information flow (arrows) from peripheral sensory neurons to the spinal cord. Middle: Santiago Ramón y Cajal. Right: Connectivity motif reflecting the circuit organization of Cajal's spinal reflex arc and clarifying his fundamental observations. "Motor neurons have at least two functionally different sources of axonal inputs or synapses: reflex inputs from sensory neurons and voluntary inputs from cerebral cortical neurons. Sensory information bifurcates in the central nervous system: part of it goes to the motor system for initiating reflex responses, and part of it goes to the psychomotor or cognitive neurons for influencing voluntary responses". From Swanson, 2011.

These generalizations, linking structure and function, led to the first accurate circuit diagrams aimed at explaining how behavior is regulated by a network of sensory neurons, interneurons and output neurons. For example, Cajal's description of the architecture of a vertebrate spinal reflex arc **(Fig 1.1)** can be summarized as follows: sensory neurons project to the central nervous system (CNS) where they bifurcate. One branch terminates onto a motor neuron or a spinal interneuron, mediating a simple reflex to the muscle (first source

of input to the motor system). The other branch terminates onto an ascending interneuron, which projects into the cerebral cortex targeting a psychomotor or cognitive neuron, whose axon descends to influence also the output of primary motor neurons (second source of input to the motor system) (Swanson, 2011). Even if these are just outlines, his observations reflect the basic plan of every brain. In combination with Sherrington's electrophysiological analysis of reflexes (Sherrington, 1906), Cajal's conceptual framework and the search for recurrent patterns and motifs of connectivity has, to the present day, remained at the heart of circuit mapping at any level of analysis (Braganza and Beck, 2018; Milo, 2002; Sporns and Kötter, 2004).

1.3 All the small things

Over the ensuing decades, nervous system complexity, density and tool availability have strongly dictated the type of experimental system and analysis that could be used to assemble comprehensive circuit maps (circuit dissection), such as a focus on a particular organism, behavior or type of neuron. In this regard, the work on smaller and more easily accessible nervous systems of invertebrates provided fundamental insights into neuronal function (Bullock and Horridge, 1965; Katz et al., 2013) and "the generality of cellular, synaptic, and network properties between invertebrate and vertebrate nervous systems" (Gelperin, 2019) **(Fig 1.2)**.

For example, the very first action potentials were recorded intracellularly in biophysical studies of the squid giant axon by Hodgkin and Huxley. Their groundbreaking mathematical model explaining the general electrical mechanisms underlying the generation and propagation of nerve impulses in both invertebrates and vertebrates is still being used today (Hodgkin and Huxley, 1952, 1939). These basic concepts also had a significant impact on modern computational and neural network science (Häusser, 2000; Seymour, 2012).

Since the 1960s, the study of simple forms of reflex circuits and behaviors in invertebrates shaped our understanding of the cellular and molecular mechanisms of learning and memory. The gill-withdrawal reflex in the sea slug *Aplysia*, with an underlying neural circuit of around 40 precisely wired neurons, exhibits habituation, sensitization, and classical conditioning - three of the most elementary forms of learning, which change the behavior of

the animal based on changes in the strength and effectiveness of synaptic connections between neurons (Kandel, 2001).

Studies on the functional organization of motor systems controlling rhythmic movements like the neural circuits generating the locust flight motor pattern, swimming in *Tritonia* or gastric mill movements in crustaceans, to name but a few, are great examples for invertebrate research that led to the idea of central pattern generators (CPGs) (Bucher et al., 2015; Burrows, 1975; Getting et al., 1980; Selverston et al., 1976). These neuronal circuits, when activated, produce rhythmic motor patterns that underlie behaviors like walking, swimming, breathing, flying and feeding independent of any sensory or descending inputs that carry specific timing information. However, sensory feedback loops can be critical to shape the period, phase and amplitude of the CPG's signals and to generate meaningful motor patterns and movements (Friesen, 2009; Grillner, 2009; Lang, 2009; Marder and Bucher, 2001; Nichols, 2009; Stein, 2014).

Another level of flexibility and plasticity comes with neuromodulation. Work on the stomatogastric nervous system of crustaceans, containing one of the most investigated neuronal circuits with just around 30 neurons, demonstrated the important role of different neuropeptides in modulation of motor pattern generation (Harris-Warrick et al., 1992; Marder et al., 1997; Marder and Weimann, 1992). The basic effects of neuromodulators on CPGs include alteration of cell-intrinsic properties and quantitative and qualitative modulation of synaptic interactions between neurons within a given network (Dickinson, 2006), which "adds considerable flexibility and computational power to neural circuits, enabling them to be multifunctional constructs" (McCormick and Nusbaum, 2014).

All these approaches, mostly based on systematic electrophysiological recordings and sparse labeling techniques to visualize the neurons by light microscopy, are invaluable for today's neuroscience and produced very detailed but still sparse and incomplete connectomes. The difficulty in neuronal circuit mapping results from the small size of neuronal processes and tremendously high number of synapses. The packing density of neural tissue reaches up to 100 thousand neurons with more than 700 million synapses per cubic millimeter in mammals (Braitenberg and Schüz, 1998). In the 1950s, the development of transmission electron microscopy (TEM), and new methods for nervous tissue preparation made

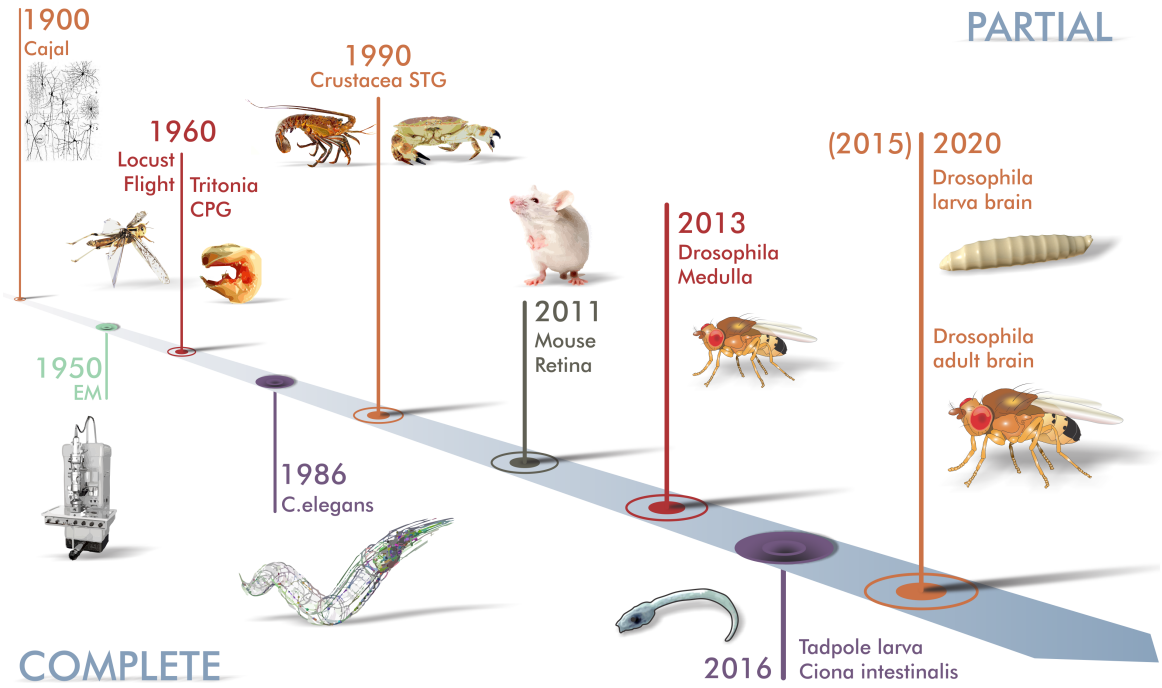

FIGURE 1.2. History of connectomics. Timeline of selected achievements in the field of connectomics with focus on invertebrate research.

it possible to image and analyze sufficiently large volumes of neuronal tissue at nanometer resolution. The nervous system of the roundworm (nematode) *Caenorhabditis elegans*, comprising 302 neurons, was the first to be reconstructed in near entirety at the level of synapses and gap junctions (Albertson and Thompson, 1976; White et al., 1986, 1976) and represents the first comprehensive map of an adaptive and integrative processing network that transforms sensory stimuli into coordinated motor activity. John White's data was reanalyzed and updated on several occasions and has been an invaluable resource in understanding how behaviors are coded within neuronal circuits (Cook et al., 2019; Jarrell et al., 2012; Mulcahy et al., 2018; Sawin et al., 2000; Varshney et al., 2011; Zhen and Samuel, 2015). Further, it has since informed many theoretical and analytical studies on network organization and contributed to the development of computational models and generally applicable circuit motifs (Fornito et al., 2016; Sporns, 2011; Szigeti et al., 2014; Towlson et al., 2013; Yan et al., 2017). Thus, one might say that White's 'the mind of a worm' was the birth of modern connectomics (Emmons, 2015).

To this day, the only other reported synaptic connectome of an entire nervous system is that of the tadpole larva of the ascidian *Ciona intestinalis* (Ryan et al., 2018, 2017, 2016), our closest living 'invertebrate' relative (Delsuc et al., 2006). These tadpoles have a basic

'vertebrate' body plan (Mikhailov and Gilbert, 2002) and their CNS, with only 177 neurons and 6618 synapses, shows strong conservations with the CNS of vertebrates.

1.4 Connectome constraints

Reaching completeness is the new holy grail in neuroanatomy. However, no vertebrate nanoscale studies achieved that goal so far. The problem arises from the combination of size and complexity of vertebrate nervous systems and the high resolution required to trace small structures, such as dendrites and synaptic vesicles (Lichtman and Denk, 2011). Further, modern connectomics is highly time-consuming and produces 'big data' (Helmstaedter, 2013; Lichtman et al., 2014). Even a salt grain sized cube (1 mm^3) of the mouse neocortex, sliced in 10,300 sections, picked up on moving tape and scanned at a resolution of 4 x 4 x 30 nm took 3 months of image data acquisition and is about 100 terabytes of data (Kasthuri et al., 2015). A whole human brain with an estimated data size of 2 Billion terabytes represents a problem that is still unsolvable at the moment (Morgan and Lichtman, 2017). The so far largest vertebrate connectome at synaptic resolution is from the mouse retina Inner Plexiform Layer covering just a very small column of the retina with 950 neurons. However, this connectivity map revealed cell types, circuit motifs and mechanism underlying motion detection and other aspects of visual function (Briggman et al., 2011; Helmstaedter et al., 2013).

There are other impeding factors that challenge connectomic efforts. Neurons, synapses and other cell processes have to be reconstructed from the imaging data to extract a neuron to neuron connectivity graph, which is anything but simple and a time-consuming process therefore termed as the "reconstruction problem" or "analysis gap" (Helmstaedter, 2013). This can be done manually by humans, what guarantees a very accurate reconstruction but, at the same time, very long processing times (years) and painstaking work for the annotator. Another approach involves automated algorithms, ensuring very short reconstruction times, but with a high susceptibility to errors, on the cost of accuracy. For example, falsely merging two neurons renders their reconstruction and consequently their connectivity useless.

In addition, it is important to recognize that an EM based connectome is merely showing a snapshot of the connectivity in any given nervous system. There are several shortcomings

associated with the conceptual link of structure and function. For example, synapses can strengthen, weaken or be silent. The distribution of ion channels and types of neurotransmitters expressed by a neuron can't be revealed by a connectivity map. Furthermore, hormonal and paracrine effects and the behavioral state of an organism enable neural circuits to be multifunctional (Bargmann and Marder, 2013; Morgan and Lichtman, 2017, 2013).

Nevertheless, the field of connectomics has undergone rapid development in recent years as efforts have been stepped up to improve sectioning, imaging, reconstruction and computational technologies (Denk and Horstmann, 2004; Hayworth et al., 2015; Januszewski et al., 2018; Knott et al., 2008; Xu et al., 2019, 2017). In combination with powerful genetic methods (Luo et al., 2018) it has become much more likely to overcome the challenges of mapping increasingly large nervous systems (Kornfeld and Denk, 2018; Lichtman and Denk, 2011; Schlegel et al., 2017; Zheng et al., 2018). Even if there are constrains to dense connectomic analysis, it will provide at least the exact number of neurons, all synaptic connections, the direction of information flow and any neuronal path arising therefrom in a given network by which one can predict how information is integrated and processed to select an action. "In exploring densely reconstructed networks, we will be able to deal with diversity in the connectivity of neurons not as noise to be averaged out, but as the principal phenomena to be understood" (Morgan and Lichtman, 2017).

1.5 Why the fly

To understand how elemental computations are performed in the brain, it is essential to have access to the structure, connectivity, genetics and the function of the neurons involved. The fruit fly *Drosophila melanogaster* has been used in research for more than 100 years and serves as a powerful model system meeting all requirements for studying the neuronal basis of behaviors (Bellen et al., 2010). The small central nervous system of *Drosophila* consists of ~100,000 cells in adults (Simpson, 2009) and only ~10,000 cells in the larva (Dumstrei et al., 2003). These tiny brains, operating on the same fundamental principles as their mammalian counterparts, are complex enough to mediate a wide range of elaborate behaviors, yet small enough to be imaged at nanometer resolution in their entirety, and allow single-cell structure-function analyses. In contrast to vertebrates, the morphology and connectivity of neurons in invertebrates is highly stereotyped across individuals which means that circuits and functions mapped in one individual will likely apply to other

animals (Gerhard et al., 2017; Spindler and Hartenstein, 2010). Circuit mapping is supported by a rich repertoire of established behavioral assays, electrophysiology and genetic tools, for example Gal4 lines (Brand and Perrimon, 1993), which can be used to genetically target, label and manipulate specific cell types (Venken et al., 2011) and dissect the function and organization of the fly nervous system.

One powerful example for circuit mapping in *Drosophila* and connectomes in general is the reconstruction of the fruit fly optic medulla. Although covering just a partial module, containing 379 neurons and 8637 chemical synaptic contacts, this connectome answered a 60 year old question about the existence and cellular implementation of an elementary motion detector (EMD) in the visual system (Plaza et al., 2014; Takemura et al., 2013). The EMD, a theoretical model (Hassenstein and Reichardt, 1956) explaining the minimal computations required to perceive movement from the activity of photoreceptors, was discovered as an anatomical circuit motif in the optical lobe of the fly with amazing parallels to the mouse retina (Borst and Helmstaedter, 2015; Helmstaedter et al., 2013).

Now, the largest brain map on synaptic level has been constructed from the adult *Drosophila* brain (Scheffer et al., 2020). Without focusing on specific circuits and networks, the FlyEM project and collaborators at Google generated a dense reconstruction of a portion of the central brain, roughly a third of the fly brain, containing 25,000 neurons with around 20 million chemical synapses. The special features of this effort are a stream of advances in imaging technology to maintain an isotropic resolution of 4 x 4 x 4 nm^3 while expanding the image volume to 3 x 10^7 μm^3 (Xu et al., 2019), deep-learning algorithms for automated segmentation of the image data (Januszewski et al., 2018) and a free-to-use policy for the data[3]. The researchers hope that this data will help to elucidate the networks of memory formation, motor control and sleep.

1.6 The larval mind

The brain of the *Drosophila* larva is ten-fold smaller in neuron number than adult flies, but still capable of fundamental behavioral and cognitive faculties, including various forms of taxis and kinesis beyond feeding and locomotion (Almeida-Carvalho et al., 2017). In 2012,

[3] https://www.janelia.org/project-team/flyem

the larva became the center of one of the most promising connectomics efforts. A whole brain EM volume of a first instar (L1) larva was compiled (4850 50-nm-slices, 3.5 x 3.5 nm resolution) and made available to the research community for manual neuron reconstruction and synapse annotation (Ohyama et al., 2015) **(Fig 1.2)**. The effort to produce a complete wiring diagram of the larval brain is an international collaborative initiative of more than 15 labs and 50 researchers. To date, around 80% of the dataset has been reconstructed and has already led to a wide range of high quality publications covering olfaction (Berck et al., 2016), learning and memory (Eichler et al., 2017; Eschbach et al., 2020), visual circuits (Larderet et al., 2017), sensorimotor circuits for feeding (Miroschnikow et al., 2018) and locomotion (Fushiki et al., 2016; Jovanic et al., 2016; Ohyama et al., 2015; Zwart et al., 2016), neuroanatomy (Schneider-Mizell et al., 2016), neurotransmission (Schlegel et al., 2016) and neurodevelopment (Andrade et al., 2019). Recent studies have also demonstrated the possibility of extracting single-cell transcriptomic data from entire brains of *Drosophila* larvae (Brunet Avalos et al., 2019; Cocanougher et al., 2019) which may ensure the seamless link between molecular function and nano-scale connectome structure. In summary, all of this underlines the suitability of *Drosophila* and especially the larva to be the next animal with a fully reconstructed connectome.

This thesis, whose contents have been partially published in (Miroschnikow et al., 2018), investigates the architecture of sensorimotor circuits underlying feeding behavior in the brainstem of larval *Drosophila* using the same EM volume described above.

1.7 Movement is life

"To move things is all that mankind can do, and for this the sole executant is a muscle, whether it be whispering a syllable or felling a forest."

- Charles S. Sherrington, 1924 (Eccles and Gibson, 1979)

The final common pathways of nearly all organism nervous system activity are the motor outputs (Sherrington, 1906), which can be broadly defined into those carried out by the muscles to produce movements and by the glands for secretion (Shepherd, 1987). Regardless of whether voluntary or not, these actions are selected, controlled and modulated at short and long timescales by different levels of parallel processing through a network of sensory and interneurons, learning and memory, as well as many other internal and

external variables to achieve desired behaviors (Hoke et al., 2017; Huston and Jayaraman, 2011). We have accumulated a substantial amount of concepts and knowledge on sensorimotor integration and action selection (Flanders, 2011; Grillner et al., 2005; Hooper and Büschges, 2017; Huston and Jayaraman, 2011; Todorov, 2004; Wolpert and Ghahramani, 2000). However, the generation of adaptive behaviors is still not well understood and the underlying neural networks, modules and brain regions are often treated as an arrangement of several black boxes. Given all the possible neuronal paths which can be traversed from sensory receptors to muscles - in form of simple reflex arcs, memory circuits or some other complex multisynaptic circuits in the brain - one major open question is how one neural path is selected from multiple possible paths to produce a desired output (Grillner et al., 2005).

1.8 The architecture of larval feeding

The neuronal networks that control food intake and energy homeostasis in *Drosophila* represent an attractive platform for neuroanatomical analysis of sensorimotor pathways. In general, feeding is one of the most fundamental and universal activities of animals. However, the transformation of food into nutrients and energy for an organism's body to operate, grow and survive is anything but simple and requires a plethora of actions from different anatomical and neuronal systems. Diverse factors like visual cues, smell, taste, texture, temperature of the food source up to rhythmic and stereotyped movements of different parts of the feeding apparatus during the consummatory act involve complex and interrelated neuronal circuits (Barlow, 2009; Rolls, 2005; Shepherd, 2011; Steuer and Guertin, 2019). The same holds for the parallel integration of internal signals, like nutritional and hormonal state generated before or after consumption (Friedman, 2019; Pool and Scott, 2014). Feeding can be seen as a sequence of behaviors in which every phase requires different levels of coordination (Bels and Whishaw, 2019; Stradmeyer, 1989).

This also applies to the instinctive and constant food intake behavior of the *Drosophila* larva which includes foraging to a potential food source, integration of multimodal sensory information from different external and internal sensory organs, central processing, decisions to feed or not to feed, which can be also dependent on nutritional state, humoral state and previous experience of the animal, to ultimately select and coordinate a sequence of motor programs and feeding structures to take up the food and transport it from the

pharynx into the esophagus (Apostolopoulou et al., 2015; Gerber et al., 2009; Green et al., 1983; Schoofs et al., 2014a, 2010; Zinke et al., 1999).

1.9 Three different motor systems underlie larval feeding behavior

Analogous to the three phases of deglutition in mammals, larval food intake can be structured into the oral, the pharyngeal and the esophageal phase (Matsuo and Palmer, 2009; Spearman et al., 2014). Prior to the oral phase, foraging movements of the head and the mouth hooks shove food into the mouth opening. After entering the cibarium (oral cavity in mammals), food is pumped into the pharynx by a series of contractions of the cibarial dilator muscles (CDM). After formation, a small portion of the food (bolus) is propelled into the esophagus and subsequently transported into the midgut (Schoofs et al., 2010; Zinke et al., 1999) **(Fig 1.3)**. The muscles responsible for the feeding cycle are innervated by three distinct pharyngeal nerves originating from the subesophageal zone (SEZ), a region analogous to the vertebrate brainstem (Ghysen, 2003) **(Fig 1.4; Fig 1.5)**. The prothoracic accessory nerve (PaN) innervates two dorsal protractor muscles ($Pro_{do}A$ and $Pro_{do}B$) responsible for head reaching and tilting. The maxillary nerve (MxN) innervates four different muscles groups: the mouth hook elevators and depressors (MHE, MHD) moving the mouth hooks up and down; the labial retractor (LR) pulling back the labium; the salivary gland ductus opener (SGDO) affecting salivation. The antennal nerve comprises the axons of pharyngeal motor neurons (PMNs) innervating the CDM driving pharyngeal pumping. It should be noted that head tilt and mouth hook movements are used for feeding and locomotion, whereas the muscles innervated by the AN are primarily utilized for feeding. The motor neurons and CPGs for the rhythmic feeding patterns are localized in the SEZ (Hückesfeld et al., 2015). The motor programs underlying feeding have been studied by extracellular nerve recordings of the pharyngeal nerves in semi intact larvae (Schoofs et al., 2010). (see **Fig 1.4** for a detailed description of all motor outputs and their routes to the periphery)

Along with the above mentioned motor outputs representing the somatic motor system that controls striated, voluntary or somatic muscles, the SEZ has additional modulatory output neurons corresponding to the autonomic motor system controlling pharyngeal muscles and visceral organs (Swanson, 2011) **(Fig 1.3)**. These neurons express serotonin, a major neuromodulator involved in regulating feeding and energy homeostasis in

invertebrates (Tecott, 2007) and vertebrates (Donovan and Tecott, 2013). The Se0, a cluster of four serotonergic cells, sends its axons through the antennal nerve and innervates the enteric nervous system including the foregut, midgut and the ring gland (Huser et al., 2012; Schoofs et al., 2014b; Shimada-Niwa and Niwa, 2014). A recent study demonstrated that serotonin is capable to modulate and set the motor rhythm frequency of pharyngeal pumping based on its release (Schoofs et al., 2018).

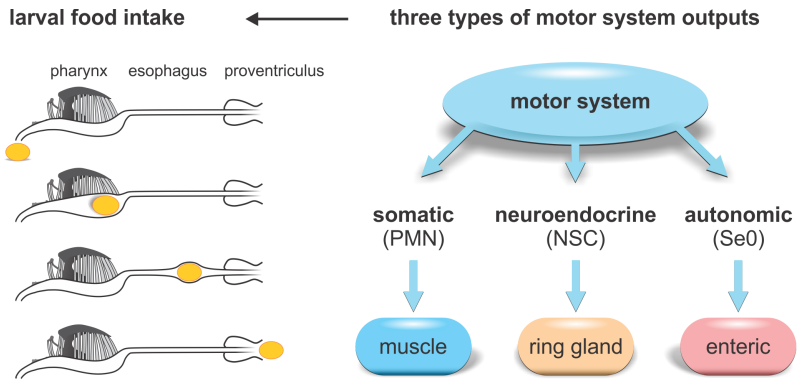

FIGURE 1.3. Food intake in *Drosophila* larvae and organization of the feeding motor system. Left: Sequential diagram of larval food intake shows how a food portion (yellow) is carried through the different regions of the foregut (Zinke et al., 1999). Right: Basic plan of the motor system as proposed by Swanson (Swanson, 2011). Three different types of motor system outputs (somatic, neuroendocrine and autonomic) correlated to the feeding retaled output neurons (pharyngeal motor neurons, PMN; neurosecretory cells, NSC; serotonergtic modulatory neurons, Se0) and their targets. Figure modified from Miroschnikow et al. 2020.

Finally, there is a third class of CNS output neurons, the neuroendocrine (Swanson, 2011) represented by the neuroendocrine cells controlling the ring gland (Siegmund and Korge, 2001), the major endocrine organ of *Drosophila* larvae analogous to the pituitary gland (De Velasco et al., 2004). Previously, three morphological similar clusters, collectively termed median neurosecretory cells (mNSCs) have been reconstructed in the larval EM project (Schlegel et al., 2016). These cells, expressing the neuropeptides Dilps (*Drosophila* insulin-like peptides), DH44 (diuretic hormone, a corticotropin-releasing hormone homolog) and DMS (Dromyosuppressin), receive direct input from sensory neurons and connect the SEZ to the ring gland. Similar to mammals, two of these peptides have been implicated in the control of feeding behavior. For example, increased insulin signaling in the nervous system decreases larval food intake (Wu et al., 2005), whereas deletion of Dilps causes growth defects and metabolic abnormalities like elevated circulating sugar levels in

the hemolymph (Zhang et al., 2009). In *Drosophila* adults, Dh44 expressing neurons have been shown to act as nutrient sensors for sugars (Dus et al., 2015), directly sense dietary amino acids and promote food consumption (Yang et al., 2018). The role of Dh44 in regulating larval food intake is not known.

The three described motor systems are under constant influence of different external and internal inputs that represent behavioral state, sensory cues and cognitive influences that originate from various parts of the body, e.g., from the chemosensory organs, humoral signals from the gut and hemolymph, or from higher brain centers.

1.10 Sensory projections underlying feeding behavior

Several studies suggested anatomical and functional parallels between the subesophageal zone in insects and the brainstem in vertebrates in the control of feeding (Schoofs et al., 2014a; Scott, 2018; Yapici et al., 2016). In general, the brainstem is responsible for automatic functions such as control of heart rate, breathing and other vital activities. Further, the brainstem serves a critical role in regulating food intake according to energy needs by integrating neuronal and hormonal information and bidirectionally communicating with other brains regions such as the hypothalamus (D'Agostino et al., 2016). In particular, the medulla oblongata houses a number of topographically distinct sensory and motor nuclei of the cranial nerves VII, IX, X, XI and XII innervating different muscles, structures and glands of the foregut including facial muscles, tongue, pharynx, larynx, as well as supplying the sense of taste. For example, the VIIth cranial nerve (facial nerve) carries taste sensory information from anterior 2/3 of the tongue, and innervates the salivary glands, and lip and facial muscles. The IXth cranial nerve (glossopharyngeal nerve) receives taste inputs from the posterior 1/3 of the tongue, and innervates the salivary glands and pharynx muscles. The Xth cranial nerve (vagus nerve) receives a majority of the sensory inputs from the enteric nervous system of the gut, and innervates pharynx and esophagus muscles. The XIth cranial nerve (spinal accessory nerve) and the XIIth cranial nerve (hypoglossal nerve) are thought to carry strictly motor information which innervate the pharynx and neck muscles, and the tongue muscles (Cordes, 2001; Simon et al., 2006).

Analogous to the cranial nerves, the three pharyngeal nerves of the *Drosophila* larva carry, in addition to the motor outputs, also sensory information from a variety of external,

pharyngeal and internal sensory organs from the head and the foregut. Several studies investigated the neuronal and functional organization of these sensory systems in detail (Apostolopoulou et al., 2015; Berck et al., 2016; Colomb et al., 2007; Kwon et al., 2011; Singh and Singh, 1984; Vosshall and Stocker, 2007). For example, the external organs include four pairs of chemosensory organs located on the tip of the larval head: the dorsal organ (DO), the terminal organ (TO) and the ventral organ (VO) and the labial organ (LBO). The DO has mainly olfactory function and houses olfactory receptor neurons sending their axons via the antennal nerve to the brain (Oppliger et al., 2000). The axon terminals converge in the deutocerebrum forming a glomerular structure called antennal lobe. The TO and VO are mainly dedicated to taste detection and project via the maxillary nerve to the SEZ. The pharyngeal taste organs include four pairs of chemosensory organs located in the pharynx: the dorsal (DPS), the ventral (VPS) and the posterior (PPS) pharyngeal sensilla, and the dorsal pharyngeal organ (DPO). The sensory neurons of the DPS, DPO and PPS enter the SEZ via the antennal nerve, the VPS via the maxillary nerve.

Similar to the vagal route (Xth cranial nerve) in mammals, a side branch of the antennal nerve also connects the enteric nervous system to the larval brainstem. The function and neuroanatomy of the ENS with the associated foregut structures has been investigated in dipteran larvae (Spieß et al., 2008). The internal sensory neurons are located in the proventricular ganglion (PVG), the hypocerebral ganglion (HCG) and the esophageal ganglion (EG) (see **Fig 1.4** for a detailed description of all sensory organs and their nerve routes to the SEZ).

Each of the above described external and pharyngeal gustatory sense organs has been shown to express a variety of gustatory receptor genes, ionotropic receptor genes, pickpocket genes and transient receptor potential channels (Apostolopoulou et al., 2015). Whereby the gustatory receptor gene family is likely the most common. In *Drosophila*, 68 gustatory receptors (GRs) are encoded by 60 gustatory receptor genes (Clyne, 2000; Scott et al., 2001). GRs are involved in the detection of sweet and bitter tastants (Chen and Dahanukar, 2020), CO_2 (Jones et al., 2007), pheromones (Watanabe et al., 2011), and even light (Xiang et al., 2010). A comprehensive analysis of expression patterns of 67 GR-Gal4 lines described the expression of 43 GRs in the larva, 39 of them in the larval gustatory system, and allowed the construction of a receptor-to-neuron map (Apostolopoulou et al., 2015; Kwon et al., 2011). The expression of GRs is not only restricted to external and

pharyngeal taste organs. Similar to the mammalian gastrointestinal tract, which have been proposed to detect nutrients and non-nutrients at several locations through taste receptors (Mei, 1978; Raka et al., 2019; Williams et al., 2016), the enteric nervous system including the gut in *Drosophila* expresses 15 GRs (Park and Kwon, 2011) which may be involved in detection of post-ingestive gustatory signals. The analysis of enteric GR-expression in the larva is still incomplete. However, some studies showed expression of GRs in the enteric nervous system. For example, Gr43a, probably the main sugar receptor in larvae, is expressed in the proventriculus (Mishra et al., 2013). Another study suggested members of the GR subfamily 28 (Gr28a), expressed in both external and enteric chemosensory neurons as molecular receptors necessary for cellular and appetitive behavioral responses to ribonucleosides and RNA (Mishra et al., 2018).

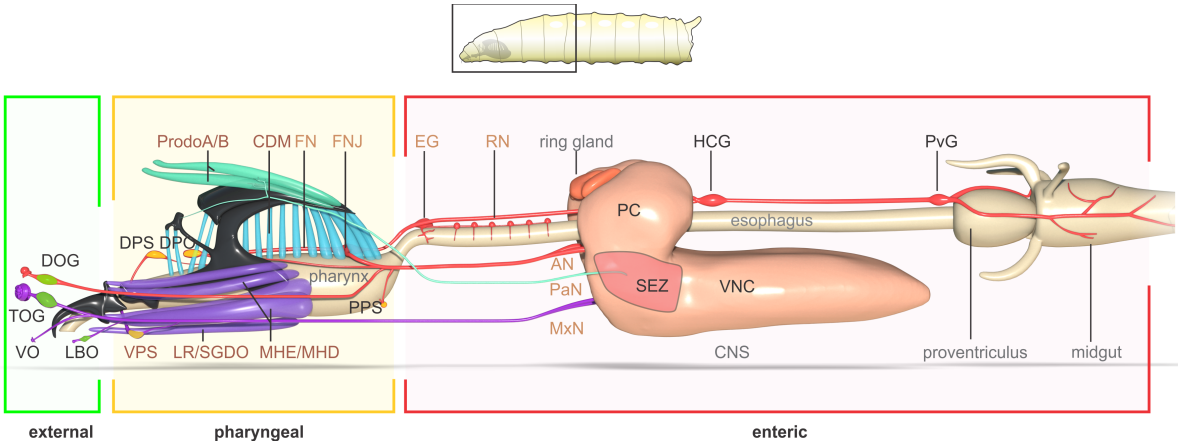

FIGURE 1.4. Anatomy of the pharyngeal nerves. The cephalic, pharyngeal and enteric sensory system of the *Drosophila* larval head (lateral view): Sensory neurons of the dorsal organ ganglion (DOG), dorsal pharyngeal sensilla (DPS), dorsal pharyngeal organ (DPO) and posterior pharyngeal sensilla (PPS) project to the subesophageal zone (SEZ) via the antennal nerve (AN). Sensory neurons of the enteric nervous system, including the frontal nerve (FN) and recurrent nerve (RN), esophageal ganglion (EG), hypocerebral ganglion (HCG) and proventricular ganglion (PvG), fuse together with the AN shortly after the frontal nerve junction (FNJ). The terminal organ ganglion (TOG), ventral organ (VO), labial organ (LBO) and ventral pharyngeal sensilla (VPS) project to the SEZ via the maxillary nerve (MxN). The prothoracic accessory nerve (PaN) contains sensory pathways from dorsal head region and enters the brain between the tritocerebrum and ventral ganglion.

The Feeding related muscle system: The motor neurons of the antennal nerve (PMNs) innervate the cibarial dilator muscles (CDM) through the frontal nerve. The mouth hook elevator (MHE), mouth hook depressor (MHD), salivary gland ductus opener (SGDO) and labial retractor (LR) are innervated by side branches of the maxillary nerve. The dorsal protractor ($Pro_{do}A$) is innervated by the prothoracic accessory nerve.

1.11 Larval 'brainstem' connectivity

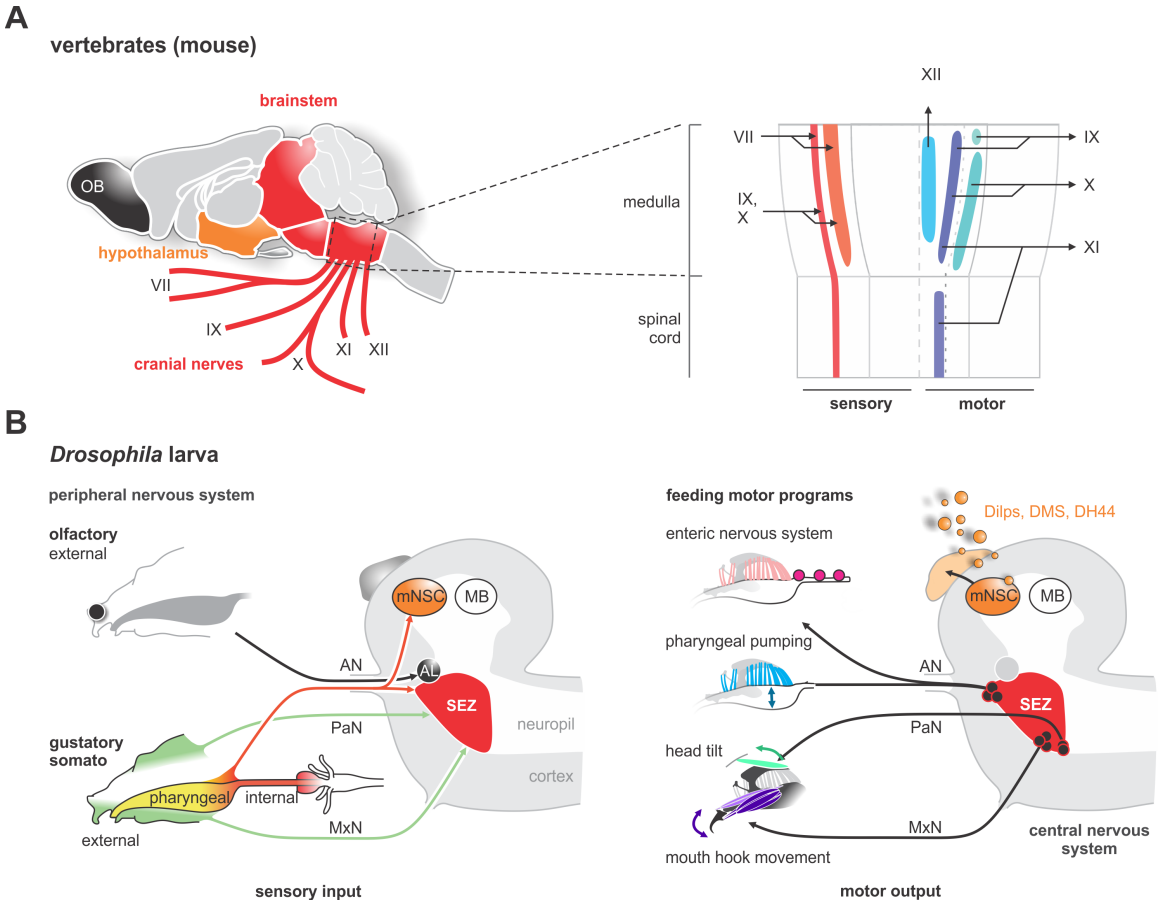

FIGURE 1.5. Vertebrate brain stem and *Drosophila* larva subesophageal zone. (A) Left: schematic diagram shows a lateral view of an adult mouse brain and the broad organization of different cranial nerves targeting the medulla of the brainstem. Right: Topographical chart of the medulla and part of the spinal cord shows innervation by sensory neurons and cell bodies of motor neurons in a cross section of the ventral view. Sensory nuclei are shown to the left, whereas motor nuclei are shown to the right. **(B)** Left: Schematic overview of external, pharyngeal and internal sensory systems targeting the subesophageal zone (SEZ), median neurosecretory cells (mNSCs) and the antennal lobe (AL) in *Drosophila*. Right: Schematic overview of central output neurons targeting feeding related muscles and the enteric nervous system. mNSCs target neuroendocrine organ (ring gland) and the periphery, by releasing neuropeptides such as Dilps, DMS, DH44. The mushroom body (MB), a learning and memory center, serves as landmark. Figure modified from Miroschnikow et al., 2018.

The SEZ is the common projection target of the described sensory afferents in the central nervous system. It serves as a multisensory hub relaying information to neurons that are associated with feeding and locomotion (Kendroud et al., 2017; Schoofs et al., 2018; Tastekin et al., 2015), and to higher brain centers like the protocerebrum (Schlegel et al.,

2016) and the mushroom body (Eichler et al., 2017; Heisenberg et al., 1985), an associative center in insect brains. Although there is broad knowledge at the morphological level on the organs underlying larval feeding behavior and physiology, as well as on the nerves innervating them in the periphery (Schoofs et al., 2014b, 2010), the central connectivity of the afferent and efferent neurons within these nerves are largely unknown. At the same time, advances in the *Drosophila* larva EM project offers an opportunity to elucidate an animals' feeding system on a brain-wide scale and at synaptic resolution.

Schlegel et al. 2016 performed an integrated analysis of fast synaptic and neuropeptide receptor connections for an identified cluster of 20 interneurons that express the neuropeptide encoding gene *hugin*. Hugin neuropeptide regulates food intake behavior in *Drosophila* (Schoofs et al., 2014a) and is a homolog of the mammalian neuropeptide neuromedin U, which has been shown to be involved in feeding in rodents (Melcher et al., 2006). A class of hugin neurons (huginPC), which responds to bitter gustatory cues (Hückesfeld et al., 2016) and suppresses pharyngeal pumping and food intake when activated (Schoofs et al., 2014a), receives direct synaptic inputs from a specific group of sensory neurons, and in turn, makes monosynaptic contacts to mNSCs (Schlegel et al., 2016). The EM based study not only provided a starting point for a combined approach to studying synaptic and neuropeptidergic circuits (Diao et al., 2017; Williams et al., 2017), but a basis for a comprehensive mapping of the sensory and output neurons that innervate the major feeding and endocrine organs.

1.12 Methods to investigate neuroanatomy

Correlating neuronal cell structure and function is decisive to obtain reliable and meaningful connectivity graphs but cannot be achieved without identifying single cell types. Since Cajal to the present days, broad classifications can be attained based on neuron morphology (e.g. size, soma position, axonal projection, and branching patterns). This is based on the assumption that the location and structure of a neuron is defined by its inputs and targets, and therefore a direct reflection of the neuron's underlying connectivity. This strategy is appropriate for determining cell categories such as sensory neurons, interneurons, projection and motor neurons, however can only be used to a certain extent.

To further characterize connectivity, neurons can be classified according to biochemical properties, such as expressed neurotransmitters, proteins and genes. Immunohisto-

chemistry is a suitable tool to recognize, inter alia, reference structures like characteristic areas of the neuropil or axon fascicles (Hartenstein et al., 2015). For example, the *Drosophila* gene futsch, which encodes a microtubule-associated protein recognized by the monoclonal antibody 22C10 can be used to visualize neurons axonal projections (Hummel et al., 2000).

Another approach is the use of binary expression systems like the Gal4-UAS system which are commonly utilized in *Drosophila* to target gene expression and express effectors/reporters in defined cell populations (Brand and Perrimon, 1993; Duffy, 2002). The Gal4 protein, derived from the yeast *Saccharomyces cerevisiae* (Giniger et al., 1985), is the transcriptional activator in this system and lacks endogenous targets within insects. The *upstream activation sequence* (UAS) is a Gal4 protein specific enhancer. These two components are maintained as separate transgenic lines of flies. For example, sensory neurons with gustatory function express specific gustatory receptors (GR) genes under the control of regulatory elements, which in turn can be used to generate transgenic and tissue-specific GR-Gal4 “driver” lines. The GR-Gal4 driver lines can be crossed to an UAS “responder” line which carries a transgene of interest, for example a green fluorescent protein (GFP) placed downstream of the Gal4 upstream activating sequence. In the resulting progeny (GR-Gal4 → UAS-GFP) all GR expressing cells are fluorescent due to the additional expression of GFP.

In the meantime, innumerable Gal4 driver and UAS responder lines have been generated, analyzed and are available in public repositories (e.g. Bloomington stock center, VDRC) representing an invaluable resource to target and identify specific cell populations, down to the single cell level.

1.13 Aims of the thesis

Little is known about central circuits, their elemental architecture and synaptic connectivity forming the neuronal basis for food intake and metabolic homeostasis. Therefore, the aim of the work described in this thesis was to use recent advances in whole brain EM imaging and reconstruction to provide a comprehensive synaptic map of sensory and output neurons that underlie feeding behavior in *Drosophila* larva.

Sensory systems and their central projections are typically organized by topographic maps of receptor arrays. For the subesophageal zone (SEZ), a multi-modal sensory integration center, it is not entirely clear whether such a topographic map exists. One aim of this thesis was to investigate whether the SEZ can be divided into smaller and likely functionally different compartments based on sensory projection and receptor expression.

Sensory information is integrated and processed to ultimately generate useful motor actions. This is in parts done via second-order neurons within the SEZ and projection neurons connecting the SEZ with higher brain centers. The second aim of this thesis was it therefore to investigate circuit motifs these interneurons are part of and how they relate to sensory integration and motor control.

The insect mushroom body (MB) is principally involved in the formation and recall of associative memories. It is well known for receiving olfactory inputs but not to what extent gustatory input reaches the MB. Furthermore, it remains unclear if and how output of the MB is integrated into feeding circuits. Hence, the third aim of this thesis was to investigate connections between feeding circuits and the MB.

Finally, this study aimed to produce a connectivity map of the *Drosophila* larval SEZ which will serve as a framework for further investigation of sensorimotor pathways and help to get insights into neuronal mechanisms of action selection to drive instinctive behaviors.

1.14 Declaration

Substantial contents of this work have been published in

Miroschnikow A, Schlegel P, Schoofs A, Hückesfeld S, Li F, Schneider-Mizell CM, Fetter RD, Truman JW, Cardona A, Pankratz MJ. 2018.
Convergence of monosynaptic and polysynaptic sensory paths onto common motor outputs in a *Drosophila* feeding connectome. *Elife* **7**. doi: 10.7554/eLife.40247

and reviewed in

Miroschnikow A, Schlegel P, Pankratz MJ. 2020.
Making Feeding Decisions in the *Drosophila* Nervous System. Curr Biol 30: R831–R840. doi: 10.1016/j.cub.2020.06.036

All analyzes and experiments were performed by A. Miroschnikow in the laboratory of M.J. Pankratz (LIMES Institute Bonn, University of Bonn, Germany) unless explicitly stated otherwise. All figures and description of results are created by A. Miroschnikow. The project (reconstruction) was performed in collaboration with the laboratory of A. Cardona (HHMI Janelia Research Campus, Ashburn, USA).

CHAPTER 2

MATERIALS

2.1 Flies

The following GAL4 driver and UAS effector lines were used (**Table 2.1**):

Name	Genotype	Source
Gr10a-GAL4	w[*]; wg[Sp-1]/CyO; P{w[+mC]=Gr10a-GAL4.3.7}2	Bloomington #57597
Gr22b-GAL4	w[*]; P{w[+mC]=Gr22b-GAL4.5.8}7/CyO; Dr[1]/TM3, Sb[1]	Bloomington #57604
Gr22e-GAL4	w[*]; wg[Sp-1]/CyO; P{w[+mC]=Gr22e-GAL4.2.5}2	Bloomington #57608
Gr23a-GAL4	w[*]; wg[Sp-1]/CyO; P{w[+mC]=Gr23a-GAL4.3.5}1	Bloomington #57611
Gr28a-GAL4	w[*]; P{w[+mC]=Gr28a-GAL4.T}G; Dr[1]/TM3, Sb[1]	Bloomington #57614
	w[*]; wg[Sp-1]/CyO; P{w[+mC]=Gr28a-GAL4.T}E1/TM3,Sb[1]	and #57613
Gr28b-GAL4	w[*];P{CaSpeR-AUG-GAL4=Gr28b-GAL4}/CyO; TM2/TM6B,Tb	Scott et al. 2001
Gr28b.a-GAL4	w[*]; wg[Sp-1]/CyO; P{w[+mC]=Gr28b.a-GAL4.3}5	Bloomington #57615
Gr28b.e-GAL	w[*]; P{w[+mC]=Gr28b.e-GAL4.4.245}2; Dr[1]/TM3, Sb[1]	Bloomington #57621
Gr2a-GAL4	w[*]; wg[Sp-1]/CyO; P{w[+mC]=Gr2a-GAL4.2.2}1D	Bloomington #57589
Gr32a-GAL4	w[*]; wg[Sp-1]/CyO; P{w[+mC]=Gr32a-GAL4.3.7.PW}1L	Bloomington #57622
Gr33a-GAL4	w[*]; wg[Sp-1]/CyO; P{w[+mC]=Gr33a-GAL4.4.7}17	Bloomington #57624
Gr39a.a-GAL4	w[*];wg[Sp-1]/CyO; P{w[+mC]=Gr39a.a-GAL4.3.4}7/TM3,Sb[1]	Bloomington #57631
Gr39a.b-GAL4	w[*]; wg[Sp-1]/CyO; P{w[+mC]=Gr39a.b-GAL4.1}1D	Bloomington #57632
Gr39a.d-GAL4	w[*]; P{w[+mC]=Gr39a.d-GAL4.1.7}1/CyO; Dr[1]/TM3, Sb[1]	Bloomington #57634
Gr39b-GAL4	w[*]; wg[Sp-1]/CyO; P{w[+mC]=Gr39b-GAL4.4.4}2	Bloomington #57635
Gr43a-GAL4	w[*]; P{w[+mC]=Gr43a-GAL4.0.5}9; Dr[1]/TM3, Sb[1]	Bloomington #57636
	w[*]; wg[Sp-1]/CyO; P{w[+mC]=Gr43a-GAL4.5.3}17	and #57637

Gr43a^{GAL4} KI	Gr43a[GAL4-knockin]	Miyamoto et al. 2012
Gr57a-GAL4	w[*]; wg[Sp-1]/CyO; P{w[+mC]=Gr57a-GAL4.6}8D/TM3,$Sb_{[1]}$	Bloomington #57642
Gr58b-GAL4	w[*]; wg[Sp-1]/CyO; P{w[+mC]=Gr58c-GAL4.1.1}1	Bloomington #57646
Gr59a-GAL4	w[*]; wg[Sp-1]/CyO; P{w[+mC]=Gr59a-GAL4.1.5}2/TM3,$Sb_{[1]}$	Bloomington #57648
Gr59d-GAL4	w[*]; wg[Sp-1]/CyO; P{w[+mC]=Gr59d-GAL4.4.1}1L	Bloomington #57652
Gr63a-GAL4	w[*]; P{w[+mC]=Gr63a-GAL4.0.8}5; Dr[1]/TM3, Sb[1]	Bloomington #57660
Gr66a-GAL4	w[*];P{CaSpeR-AUG-GAL4=Gr66a-GAL4}/CyO; TM2/TM6B,Tb	Scott et al. 2001
Gr68a-GAL4	[*]; P{w[+mC]=Gr68a-GAL4.1.8}2; Dr[1]/TM3, Sb[1]	Bloomington #57671
Gr77a-GAL4	w[*]; wg[Sp-1]/CyO; P{w[+mC]=Gr77a-GAL4.4}1L	Bloomington #57672
Gr93a-GAL4	w[*]; wg[Sp-1]/CyO; P{w[+mC]=Gr93a-GAL4.5}2DD	Bloomington #57679
Gr93b-GAL4	w[*]; wg[Sp-1]/CyO; P{w[+mC]=Gr93b-GAL4.5.3}1	Bloomington #57680
Gr93c-GAL4	w[*]; P{w[+mC]=Gr93c-GAL4.3.8}3; Dr[1]/TM3, Sb[1]	Bloomington #57681
Gr93d-GAL4	w[*]; P{w[+mC]=Gr93d-GAL4.2.4}11; Dr[1]/TM3, Sb[1]	Bloomington #57684
Gr94a-GAL4	w[*]; P{w[+mC]=Gr94a-GAL4.3.7}10; Dr[1]/TM3, Sb[1]	Bloomington #57686
Orco-GAL4	P{w[+mC]=Orco-GAL4.C}142t52.1, w[*]	Bloomington #23909
pebbled-GAL4	w[*],P{GawB=peb-GAL4}	(Corl et al., 2009)
UAS-GFP	w[*]; P{y[+t7.7] w[+mC]=10XUAS-mCD8::GFP}attP2	Bloomington #32184

Table 2.1: List of fly strains

2.2 Fly Care

All flies and larvae were raised and kept in plastic vials filled with standard fly food (**Table 2.2**). They were stored at 18°C or 25°C and 50% to 60% relative air humidity. Flies and larvae at 18°C were kept under a natural day and night cycle, flies and larvae at 25°C were kept under a 12/12-hour light/dark cycle.

For antibody stainings, 4h egg collections were made on apple juice agar plates containing a spot of yeast-water paste. After 48h, larvae were transferred into food vials containing standard fly food. All larvae used for stainings were 98 +/- 2 h old.

2.3 Buffers and Media

The following buffers and media were used (**Table 2.2**):

Name	**Composition**
Mowiol	12ml glycerin; 9.6g Mowiol40-88; 24ml H_2O; 48ml 0.2M TrisHCl; pH 8.5
Paraformaldehyde 4%	5ml 37% paraformaldehyde, 45ml PBS 1x

Phosphate-buffered saline (PBS)	80g NaCl; 2g KCL; 2.4g KH_2PO_4; 18.1g Na_2HPO_4;
PBS 10x	topped of with ddH_2O to 1l; pH 7.4
PBS 1x	900 ml ddH_2O; 100 ml PBS 10x
PBS-T 1%	1% Triton X-100 in PBS 1x
Poly-L-lysine	0.1% (w/v) in H_2O
Standard Fly Food	18l ddH_2O, 1.5l golden syrup, 1223g corn flour, 248g beer yeast, 130g thread agar, 30g 10% nipagin dissolved in 300ml 100 % EtOH

Table 2.2: List of buffers and media

2.4 Reagents

The following reagents were used (**Table 2.3**):

Name	Abbreviation	Source
Beer yeast		Gewürzmühle Brecht, Eggenstein
Corn flour		Broicher Mühle, Bedorf
Ethanol	EtOH	Carl Roth, Karlsruhe
Glycerin		Carl Roth, Karlsruhe
Goat serum		Life Technologies, Darmstadt
Golden syrup		Grafschafter Krautfabrik, Meckenheim
Methyl-4-Hydroxybenzoat	Nipagin	Sigma-Aldrich Chemie, Steinheim
Mounting medium	DPX	Sigma-Aldrich Chemie, Steinheim
Mowiol40-88		Sigma-Aldrich Chemie, Steinheim
Paraformaldehyde 37%		Carl Roth, Karlsruhe
Poly-L-lysine 0.1%	Polylysine	Sigma-Aldrich Chemie, Steinheim
Potassium chloride	KCl	Carl Roth, Karlsruhe
Potassium dihydrogen phosphate	KH_2PO_4	Carl Roth, Karlsruhe
Sodium chloride	NaCl	Carl Roth, Karlsruhe
Sodium dihydrogen phosphate	Na_2HPO_4	Carl Roth, Karlsruhe
Tris(hydroxymethyl)aminomethan	TrisHCl	Carl Roth, Karlsruhe
Triton X-100		Carl Roth, Karlsruhe
Xylene	Xylene cyanol	Sigma-Aldrich Chemie, Steinheim

Table 2.3: List of reagents

2.5 Antibodies

The following antibodies were used (**Table 2.4**):

Name	Host	Dilution	Source
α-22C10	mouse	1:500	Developmental Studies Hybridoma Bank
α-fasciclin2	mouse	1:500	Developmental Studies Hybridoma Bank
α-GFP	rabbit	1:500	Abcam plc
α-GFP-FITC	goat	1:500	Abcam plc
α-mouse-AF568	goat	1:500	ThermoFisher
α-rabbit-AF488	goat	1:500	ThermoFisher

Table 2.4: List of antibodies

2.6 Consumables

The following consumables were used (**Table 2.5**):

Description	Article	Source
Cover slides	20x20mm	Carl Roth, Karlsruhe
	24x24mm	
Elastosil silicon rubber	RT 601A/B	Wacker Silicones
Foam plug	∅ 28mm	Kunststoffteile Klühspieß
	∅ 36mm	
	∅ 50mm	
Glass slides	76x26mm	Carl Roth, Karlsruhe
Petri dish	∅ 60 x 15mm	Sarstedt
	∅ 92 x 16 mm	
Pipette tips	0.2 – 10 μl	Corning, NY
	1 – 200 μl	
	100 – 1000 μl	
Plastic vials	∅ 28mm	Greiner Bio-One
	∅ 36mm	
	∅ 50mm	
Reaction tube	1.5 ml	Eppendorf
	2.0 ml	
Tungsten wire	∅ 33.45 mm	Osram
	∅ 40.80 mm	
	∅ 65.60 mm	

	∅ 77.42 mm	
	∅ 94.11 mm	

Table 2.5: List of consumables

2.7 Hardware

The following hardware was used (**Table 2.6**):

Description	Model	Source
Binocular	Stemi 2000	Zeiss, Jena
Confocal microscope	LSM 780	Zeiss, Jena
Forceps	Dumont	Fine Science Tools, Heidelberg
Hot plate stirrer	RH Basic2	Ika, Staufen
Light source	EasyLED TSL + MC750	Schott
Micro pipettes	Pipetman P	Gilson
Micro scissors	FST 15000-00 fine	Fine Science Tools, Heidelberg
pH meter	HI 221	Hanna Instruments, Smithfield RI
Rotation wheel	Stuart SB3	Stuart

Table 2.6: List of hardware

2.8 Software

The following software was used (**Table 2.7**):

Name	Version	Source
Blender3D	2.79b	Blender Foundation
CATMAID	2018.04.15	Saalfeld et al. 2009
CATMAID-to-Blender	6.2.0	https://github.com/schlegelp/CATMAID-to-Blender
Corel Draw	X7	Corel Cooperation
Excel	Excel for Mac v15.39	Microsoft Cooperation, USA
JupyterLab	1.0.2	Jupyter; www.jupyter.org
Gephi	0.9.2	www.gephi.org
Mendeley	1.19.4	Elsevier, Inc.
PyMaid	0.105	https://github.com/schlegelp/PyMaid
Python	2.7/3.5/3.6/3.7	Python Software Foundation
SigmaPlot	12	Systat Software
Zen	11.0	Zeiss

Table 2.7: List of software

CHAPTER 3

The following description of methods was modified from Miroschnikow et al., 2018.

METHODS

3.1 Neuronal reconstruction

All reconstructions were based on an ssTEM (serial section transmission electron microscope) data set of a complete nervous system of a 6-h-old [iso] CantonS G1 x w1118 larva as described in (Ohyama et al., 2015). Using a modified version of the web-based software CATMAID (Saalfeld et al., 2009) neurons' skeletons were reconstructed and synapses annotated following the methods described in (Ohyama et al., 2015) and (Schneider-Mizell et al., 2016).

Sensory and motor neurons were identified by reconstructing all axons in the antennal nerve, maxillary nerve and the prothoracic accessory nerve. Further, neurons with their soma and synaptic contacts in the brain and projections through one of the three pharyngeal nerves have been identified as motor neurons and serotonergic output neurons. Neurons with their soma in the brain but neither synaptic contacts nor dendritic branches were identified as pioneer neurons.

All annotated synapses represent fast, chemical synapses equivalent to previously de-

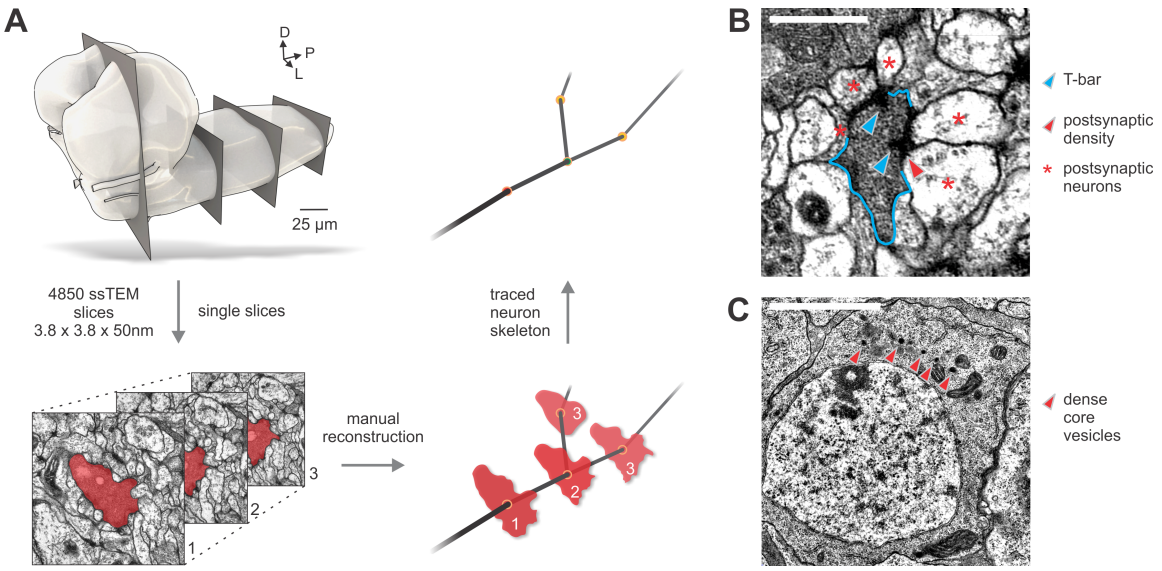

FIGURE 3.1. Neuronal reconstruction and synapse annotation. (A) 3D rendering of the ssTEM volume used for the reconstruction all neurons presented in this study. Neuron profiles (1, 2, 3, …, n) were followed in the EM sections. Neuron skeletons are determined by tracing the center of n neuron profiles of a given neuron. **(B)** Identified presynaptic sites in a sensory neuron. Profile of sensory neuron is outlined (blue). Opening in outline indicates synaptic site. T-bars and postsynaptic densities are marked (arrowheads). Scale bar represents 0.5 μm **(C)** Soma of a pharyngeal motor neuron. Dense core vesicles (DCVs) are marked (arrowheads). Scale bar represents 2μm.

scribed typical criteria: presynaptic vesicles, pre- (e.g. T-bars) and postsynaptic (postsynaptic density) membrane specializations (Prokop and Meinertzhagen, 2006) **(Fig 3.1)**.

Dense core vesicles (DCVs), the package units of neuropeptides, were traceable in the EM images as their protein content makes them electron- dense. DCVs were manually counted in somata of pharyngeal motor neurons (PMNs) and serotonergic output neurons (Se0) **(Fig 4.2)**.

A PDF neuron atlas showing the morphology and connectivity of all reconstructed neurons is available via https://doi.org/10.7554/eLife.40247.042.

An adjacency matrix with the complete connectivity of all neurons used in this study is available via https://doi.org/10.7554/eLife.40247.044.

3.2 Morphology similarity score

To neuron morphologies **(Fig 4.1; Fig 4.2; Fig 4.3; Fig 4.4; Fig 4.5; Fig 4.20; Fig 4.22),** a morphology similarity score described by Kohl et al. 2013 were used. Briefly, reconstructions of neurons are converted to "dotprops", 3d positions with an associated tangent vector: for each dotprop from a query neuron, the closest point on a target neuron was determined and scored by distance and the absolute dot product of their two tangent vectors. The total similarity score is the average score over all point pairs between query neuron Q and target neuron T:

$$S(Q,T) = \frac{1}{n}\sum_{i=1}^{n}\sqrt{\left|q_i \cdot t_j\right| e^{-\frac{d_{ij}^2}{2\sigma^2}}}$$

where n is the number of points in the query neuron, d_ij is the distance between point i in the query neuron and its nearest neighbor, point j, in the target neuron and q_i and t_j are the tangent vectors at these points. σ determines how close in space points must be to be considered similar. For calculations, σ of 2 um was used.

Similarity score algorithm was implemented in a Blender plugin by Philipp Schlegel (https://github.com/schlegelp/CATMAID-to-Blender).

3.3 Synapse similarity score

To calculate similarity of synapse placement between two neurons, the synapse similarity score was calculated **(Fig 4.3; Fig 4.6 – 4.10; Fig 4.22; Fig 4.28):**

$$f(i_s, j_k) = e^{\frac{-d_{sk}^2}{2\sigma^2}} e^{\frac{|n(i_s)-n(j_k)|}{n(i_s)+n(j_k)}}$$

With the overall synapse overall synapse similarity score for neurons i and j being the average of $f(i_s, j_k)$ over all synapses s of i. Synapse k being the closest synapse of neuron j to synapse s [same sign (pre-/post-synapse) only]. d_{sk} being the linear distance between synapses s and k. Variable σ determines which distance between s and k is considered as close. $n(j_k)$ and $n(i_s)$ are defined as the number of synapses of neuron j/i that are within a radius

ω of synapse k and s, respectively (same sign only). This ensures that in case of a strong disparity between $n(i_s)$ and $n(j_k)$, $f(i_s, j_k)$ will be close to zero even if distance d_{sk} is very small. Values used: $\sigma = \omega = 2000$ nm.

Similarity score algorithm was implemented in a Blender plugin by Philipp Schlegel (https://github.com/schlegelp/CATMAID-to-Blender).

3.4 Normalized connectivity similarity score

To compare connectivity between neurons **(Fig 4.3)**, a modified version of the similarity score described by Jarrell et al., 2012 was used:

$$f(A_{ik}, A_{jk}) = \min(A_{ik}, A_{jk}) - C_1 \max(A_{ik}, A_{jk})\, e^{-C_2 \min(A_{ik}, A_{jk})}$$

With the overall connectivity similarity score for vertices i and j in adjacency matrix A being the sum of $f(A_{ik}, A_{jk})$ over all connected partners k. C_1 and C_2 are variables that determine how similar two vertices have to be and how negatively a dissimilarity is punished. Values used were: $C_1 = 0.5$ and $C_2 = 1$. To simplify graphical representation, we normalized the overall similarity score to the minimal (sum of $-C_1 \max(A_{ik}, A_{jk})$ over all k) and maximal (sum of $\max(A_{ik}, A_{jk})$ over all k) achievable values, so that the similarity score remained between 0 and 1. Self-connections (A_{ii}, A_{jj}) and A_{ij} connections were ignored.

Normalized connectivity similarity score algorithm was implemented in a Blender plugin by Philipp Schlegel (https://github.com/schlegelp/CATMAID-to-Blender).

3.5 Clustering

Clusters for dendrograms were created based on the mean distance between elements of each cluster using the average linkage clustering method. Clusters were formed at scores of 0.06 for synapse similarity score to provide the broadest possible groups **(Fig 4.6 - 4.10)**.

Clustering algorithm was implemented in a Blender plugin by Philipp Schlegel (https://github.com/schlegelp/CATMAID-to-Blender).

3.6 Percentage of synaptic connections

Percentage of synaptic connections was calculated by counting the number of synapses that constitute between neuron A and a given set of pre- or postsynaptic partners divided by the total number of either incoming our outgoing synaptic connections of neuron A.

For presynaptic sites, each postsynaptic neurite counted as a single synaptic connection **(Fig 4.22; Fig 4.24; Fig 4.28; Fig 4.29; Fig 4.32; Fig 4.37)**.

3.7 Ranking index

Ranking index was calculated by counting the number of synapses that constitute between neuron A and a given target neuron B divided by the highest number of synapses among all incoming synaptic connections of target neuron B **(Fig 4.3 – 4.34; 4.36)**.

3.8 Neuronal representation

Neurons were rendered with Blender3D (ww.blender.org) and edited in Corel Draw X7 (www.corel.com). A script for a CATMAID-to-Blender interface is on Github (https://github.com/schlegelp/CATMAID-to-Blender)

3.9 Graphs

Graphs were generated using Excel for Mac v15.39 (www.microsoft.com), Sigma Plot 12.0 (www.sigmaplot.com), Gephi 0.9.2 (www.gephi.org) and edited in Corel Draw X7.

3.10 Immunohistochemistry

Dissected larval brains with attached CPS and intact pharyngeal nerves were fixed for 1 hr in paraformaldehyde (4%) in PBS, rinsed with PBS-T and blocked in PBS-T containing 5% normal goat serum. For antibody stainings of Gr-GAL4>10xUAS-mCD8::GFP primary antibody were conjugated goat anti-GFP (1:500, Abcam, ab6662), mouse anti-fasciclin2 (1:500, DSHB) and mouse anti-22C10 (1:500, DSHB) and the secondary antibody was anti-

mouse Alexa Flour 568 (1:500, Invitrogen).

Brains were rinsed with PBS-T and mounted in Mowiol (Roth, 0713). For antibody stainings of Gr43a-GAL4>10xUAS-mCD8::GFP primary antibody were rabbit anti-GFP (1:500, Abcam, ab6556), mouse anti-fasciclin2 (1:500, DSHB) and mouse anti-22C10 (1:500, DSHB) and the secondary antibody were anti-rabbit Alexa Flour 488 (1:500, Invitrogen) and anti-mouse Alexa Flour 568 (1:500, Invitrogen). Brains were rinsed with PBS-T and dehydrated through an ethanol-xylene series and mounted in DPX. Imaging was carried out using a Zeiss LSM 780 confocal microscope with a 25x objective (Zeiss).

CHAPTER 4

The following description of result and figures were modified from Miroschnikow et al., 2018.

RESULTS

4.1 Reconstruction of the pharyngeal nerves

All axons within the three pharyngeal nerves were reconstructed using a complete serial section EM volume of the central nervous system (CNS) of a first instar larva (Ohyama et al., 2015) **(Fig 4.1 – 4.5)**. 349 neurons with no soma and blind endings in the CNS were identified as sensory neurons. To investigate subgroups of sensory neurons, all neurons were hierarchically clustered based on morphology similarity score. The fact that the antennal nerve (AN) and maxillary nerve (MxN) each are fusions of different axon bundles that arise during embryonic development (Hartenstein et al., 2017; Kendroud et al., 2017) **(Appendix, Tab A.1)** is reflected by the sensory neuron axon bundling in the cross sections at the nerve entry sites to the CNS. The AN and MxN each have three distinct axon bundles (B1, B2, B3) which show regionalizations of their target areas in the brain. The prothoracic accessory nerve (PaN) has one sensory neuron bundle targeting a distinct area in the posterior end of the subesophageal zone (SEZ) (**Fig 4.1 A,B**). The AN has two sensory projections per side that extend into the protocerebrum, whereas 30 percent of the MxN sensory projections extend into the ventral nerve cord. With an average length of 110 micrometers pharyngeal sensory neurons add up to a total cable length of 37.3 millimeters. Four AN sensory neurons with projections to the protocerebrum exceed

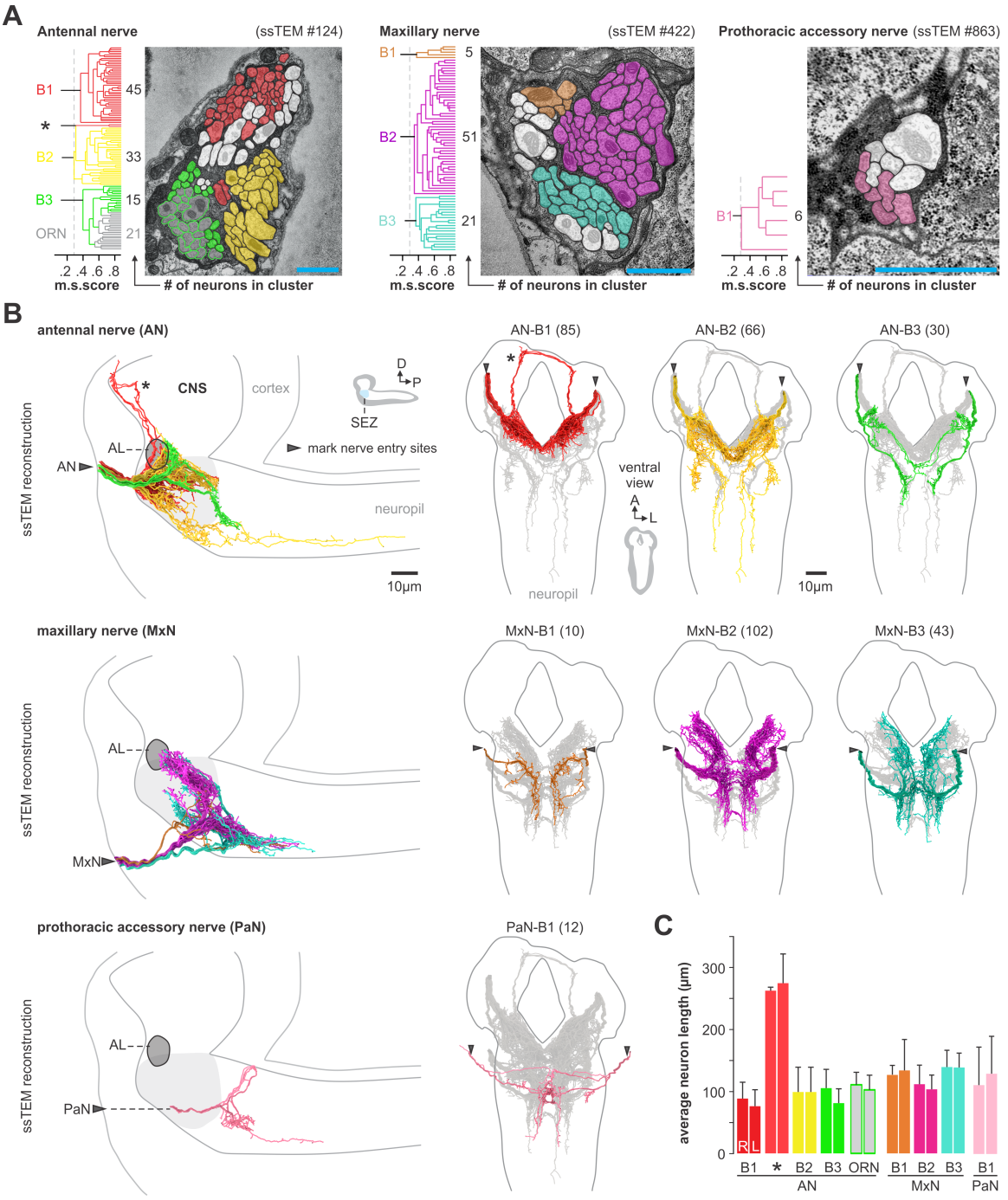

FIGURE 4.1. EM reconstruction of the pharyngeal nerve sensory neurons. (A) Sensory neurons were identified by reconstructing all neurons in the three pharyngeal nerves. Hierarchical morphology similarity score (m.s.score) was calculated for all sensory neurons of the antennal nerve (AN), maxillary nerve (MxN), prothoracic accessory nerve (PaN). The previously described olfactory receptor neurons (ORNs) (Berck et al., 2016) were included in AN clustering. Clustering revealed three distinct sensory neuron axon bundles (B1, B2, B3) within the AN and MxN. Dendrograms represent neurons of the right side and are colored based on morphology similarity score. Asterisk marks two sensory neurons per hemiside with projections to the protocerebrum. The olfactory receptor neurons (ORN) targeting the antennal lobe (AL) are part of AN-B3. Numbers represents number of sensory neurons in cluster.

ssTEM cross sections show right nerve entry sites of the three pharyngeal nerves. Neuron profiles of all neurons are colored based on morphology similarity score. **(B)** EM reconstruction of pharyngeal sensory input (left panels, lateral view). Arrow marks nerve entry site. Antennal lobe (AL) is shown as a reference. ORNs are not shown. EM reconstruction of each AN, MxN and PaN axon bundle (right panels, ventral view). Numbers represent total numbers of sensory neurons of axon bundles of the right and left side. **(C)** Quantification of the total sensory neuron length. Asterisk marks two sensory neurons per hemiside with projections to the protocerebrum. Whiskers represent standard deviation.

the average neuron length by a factor of 2.5 (**Fig 4.1 C**).

For output neurons, 29 neurons per side with somata and synpatic inputs in the CNS were identified as motor and modulatory neurons. To investigate specific subclusters of output neurons, all neurons were hierarchically clustered based on morphology similarity score. The AN output neurons consist of 14 pharyngeal motor neurons (PMNs) and a special class of four serotonergic modulatory neurons (the Se0 cluster) that project to the entire enteric nervous system (Huser et al., 2012; Schoofs et al., 2014b; Shimada-Niwa and Niwa, 2014) (**Fig 4.2, Fig 4.3**). The PMNs can be further subdivided into two morphological classes (PMN A, PMN B) according the relative position of their denritic fields **(Fig 4.2 B)**. Unexpectedly, seven PMNs were found to have a large number of presynaptic sites. During the process of reconstruction, dense core vesicles (DCVs), the packing units of neuropeptides were counted in the somas. Compared to the other AN output neurons, PMN 5 and 6 on both hemisides show high quantities of DCVs.

The four serotonergic neurons can be further divided into one that projects anteriorly to the pharynx (Se0ph), and three that project posteriorly towards the enteric nervous system (Se0ens) (see **Fig 4.3** for detailed analysis of the Se0 cluster).

The maxillary nerve comprises nine output neurons that can be separated morphologically into three distinct clusters. The mouth hook depressor (MHD) cluster, mouth hook elevator (MHE) cluster and the labial retractor (LR) and salivary gland ductus opener (SGDO) cluster (**Fig 4.4**). The three different clusters have been identified based on unpublished obervations of Andreas Schoofs (personal communication). The prothoracic accessory output neurons consist of two motor neurons (PaN motor) innervating the dorsal protractor (ProdoA) and two previously described huginPH neurons (**Fig 4.5**), although for the latter the peripheral target still unknown (Schlegel et al., 2016).

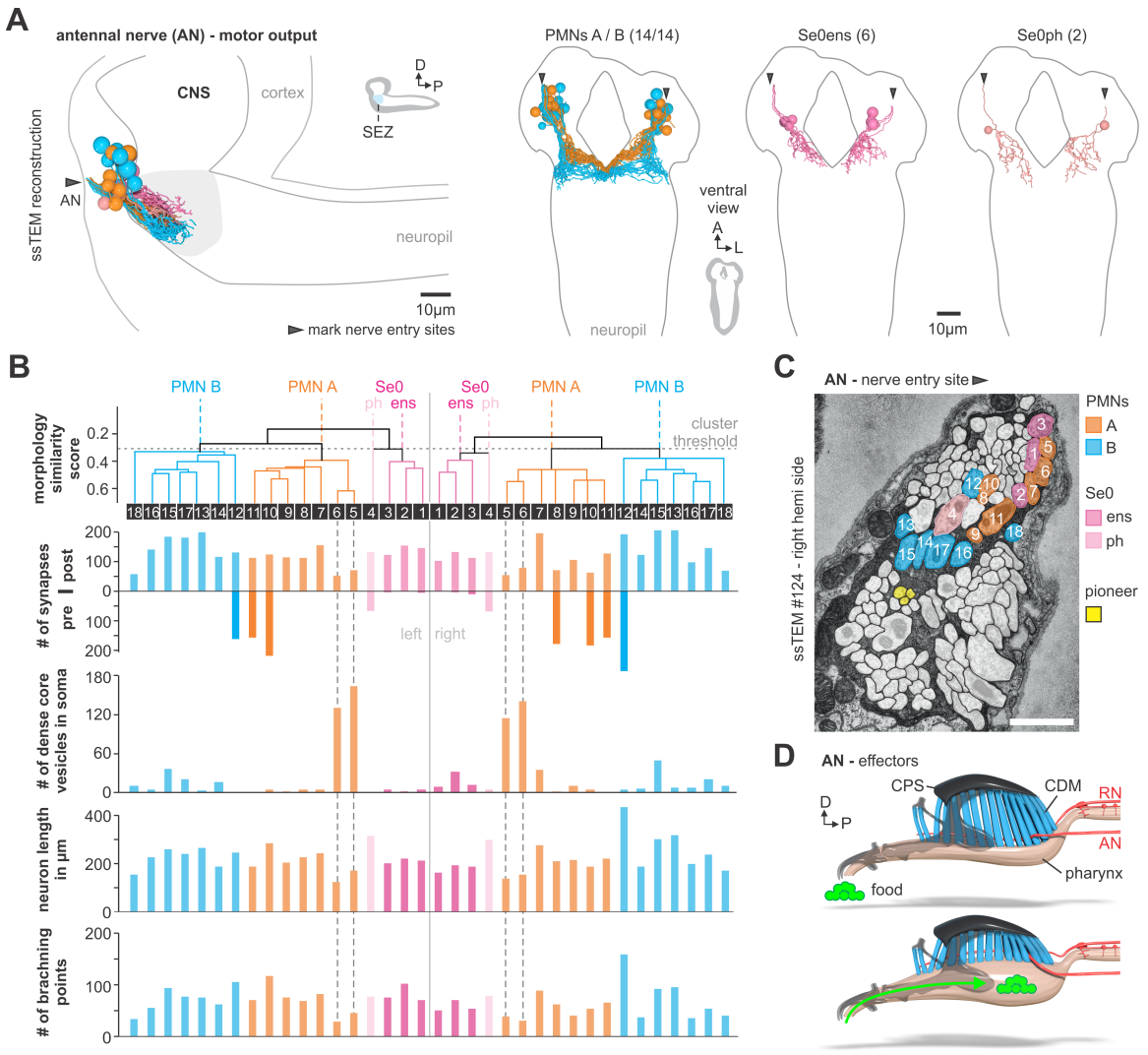

FIGURE 4.2. EM reconstruction of antennal nerve output neurons. (A) Output neurons were identified by reconstructing all neurons in the antennal nerve (AN) with somata in the CNS. Pioneer neurons are not shown. Neurons are colored based on their morphological class. Arrow marks nerve entry site. Numbers represent total numbers of each output neuron class of the right and left side. **(B)** Hierarchical morphology similarity score was calculated for all AN output neurons. Dendrograms represent neurons of the left and right side and are colored based on morphology similarity score. Quantification of number of pre- and postsynaptic sites, number of dense core vesicles in soma, raw cable length and number of branching points of each output neuron. **(C)** ssTEM cross section shows right nerve entry sites of the AN. Neuron profiles of all output neurons are colored and numbered based on morphology similarity score. **(D)** Effectors of antennal nerve (AN) motor output neurons. Pharyngeal motor (PMNs) and serotonergic output neurons (Se0ph) leave the CNS via the AN and innervate the cibarial dilator musculature (CDM) for pharyngeal pumping. Contraction of CDM leads to food ingestion. Cephalopharyngeal skeleton (CPS), recurrent nerve (RN). See **Fig 4.3** for identification and detailed description of Se0 cluster.

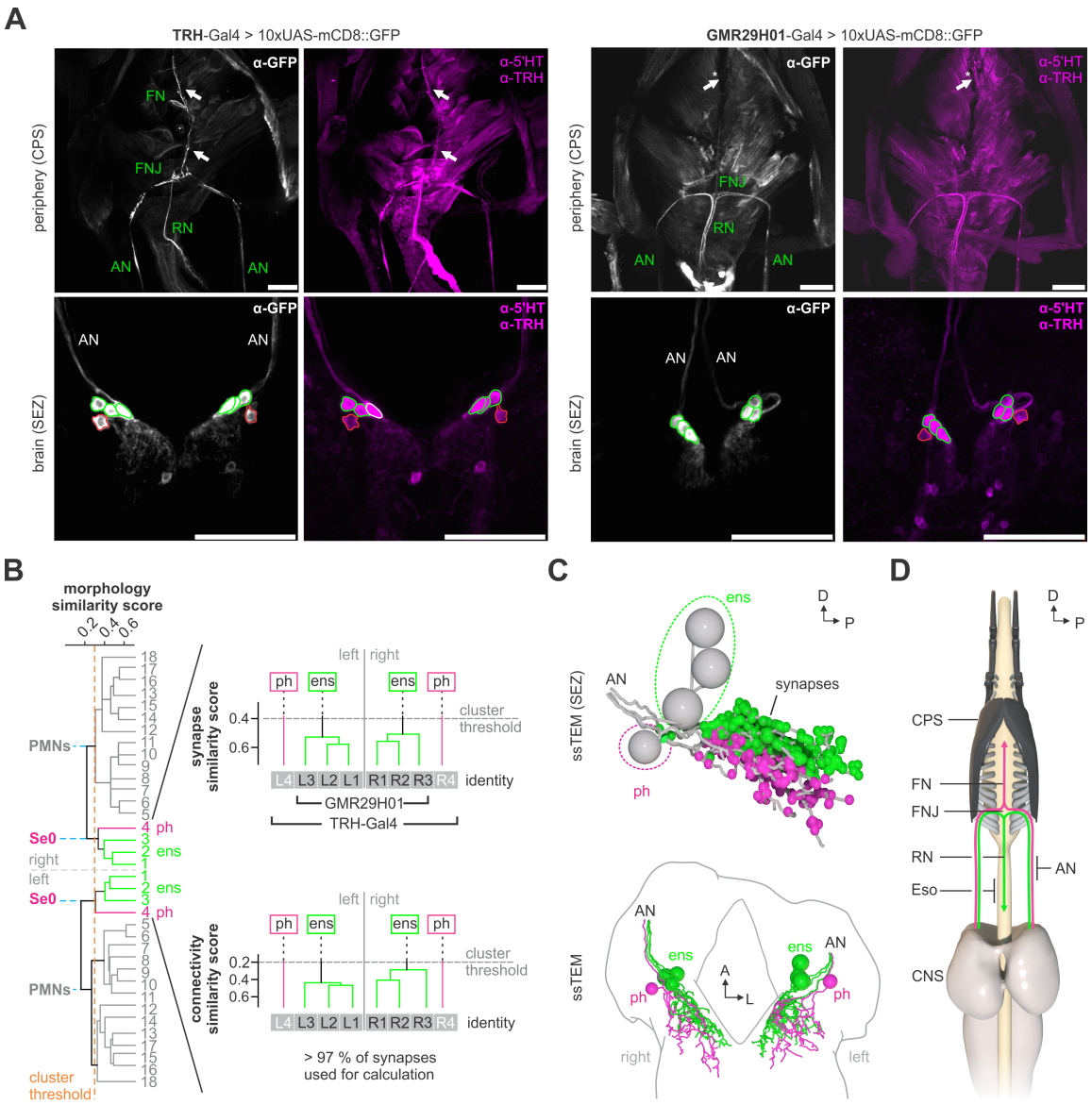

FIGURE 4.3. Identification of serotonergic output neurons (Se0) in the EM volume. (A) Analysis of serotonergic GAL4 lines. Expression of TRH and Serotonin in TRH-Gal4 and GMR29H01-Gal4 driving GFP. TRH-Gal4 shows expression in all 4 cells of the Se0 cluster. In contrast, GMR29H01-Gal4 shows expression in only 3 of the 4 Se0 cells. In comparison with the TRH-Gal4 line, GMR29H01 does not show expression in the frontal nerve (FN). Thus, the frontal nerve is innervated by Se0ph neurons. **(B)** All output neurons of the left and right antennal nerve (except seven pioneer neurons) are ordered by dendrogram of morphological similarity between each neuron. Dendrograms are split into pharyngeal motor neurons (PMNs) and serotonergic output neurons (Se0) (left panel). Synapse similarity score and connectivity similarity score of the Se0 cluster (right panel). Morphology, synapse and connectivity clustering revealed two subclusters within the Se0 cluster consistently across both hemi sides that match the 3 Se0ens and 1 Se0ph neurons. **(C)** Distribution of synaptic sites (upper panel) and EM reconstruction (lower panel) of the clustered Se0 neurons. **(D)** Summarizing representation of the Se0 projections in the periphery. Se0ph projects into the CDM via the frontal nerve (FN), whereas Se0ens projects to the enteric nervous system via the recurrent nerve (RN).

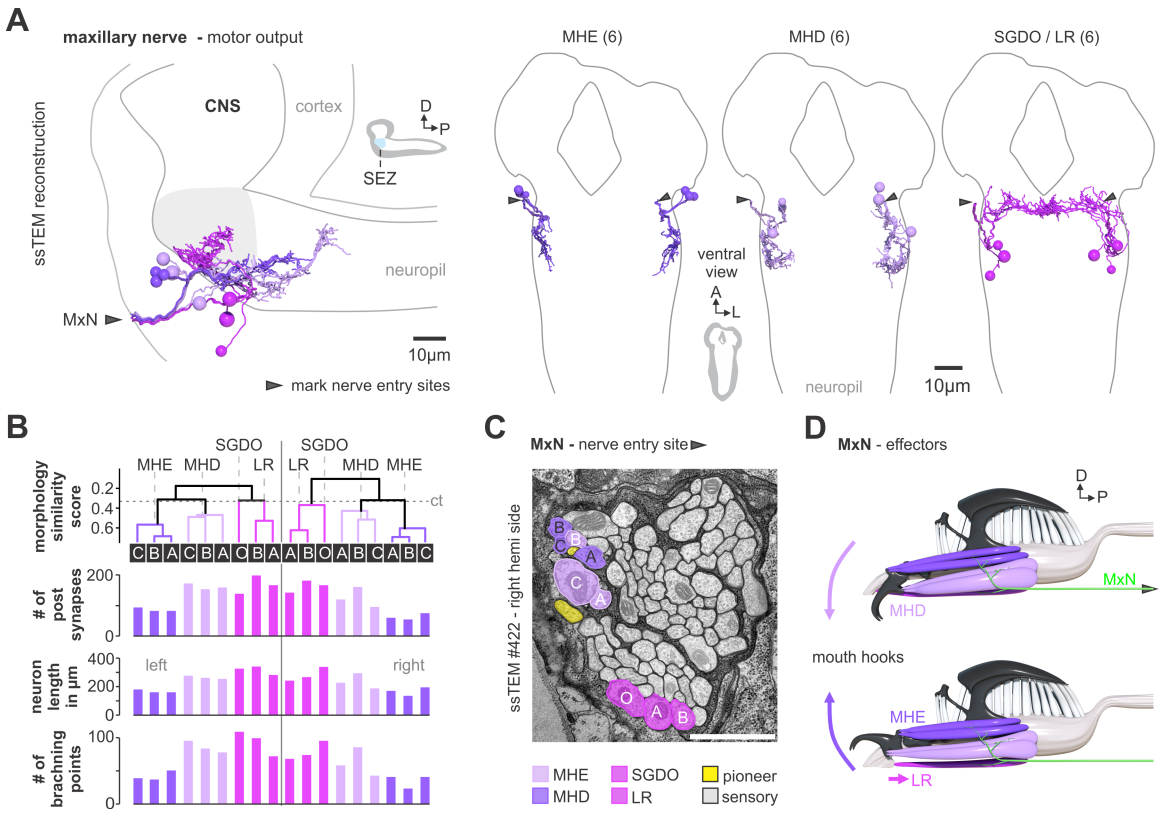

FIGURE 4.4. EM reconstruction of maxillary nerve output neurons. (A) Output neurons were identified by reconstructing all neurons in the maxillary nerve (MxN) with somata in the CNS. Pioneer neurons are not shown. Neurons are colored based on their morphological class. Arrow marks nerve entry site. Numbers represent total numbers of each output neuron class of the right and left side. **(B)** Hierarchical morphology similarity score was calculated for all MxN output neurons. Pioneer neurons were not included in clustering. Dendrograms represent neurons of the right side and are colored based on morphology similarity score. Quantification of number of pre- and postsynaptic sites, raw cable length and number of branching points of each output neuron. **(C)** ssTEM cross section shows right nerve entry sites of the MxN. Neuron profiles of all output neurons are colored and labeled based on morphology similarity score. **(D)** Effectors of MxN motor output neurons. MxN motor neurons leave the CNS via the MxN and innervate mouth hook elevator (MHE) and depressor (MHD), labial rectractor (LR) and salivary gland ductus opener (SGDO).

4.2 Topographical patterns of sensory and output synaptic compartments in the CNS

All pre- and postsynaptic sites of all reconstructed sensory neurons were annotated, resulting in a total amount of 74053 pre – and 337 postsynaptic sites. To investigate potential modality specific subregions in the brain, all sensory neurons were hierarchically clustered

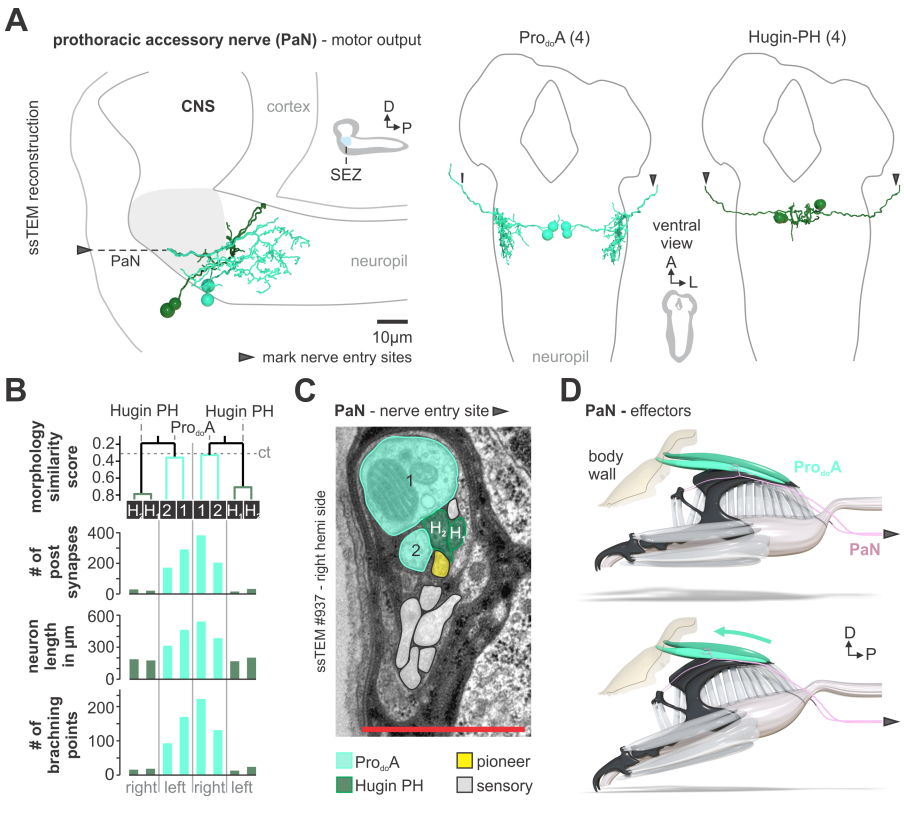

FIGURE 4.5. EM reconstruction of prothoracic accessory nerve output neurons. (A) Output neurons were identified by reconstructing all neurons in the prothoracic accessory nerve (PaN) with somata in the CNS. HuginPH are shown for comparison (Schlegel et al., 2016). Pioneer neurons are not shown. Neurons are colored based on their morphological class. Arrow marks nerve entry site. Numbers represent total numbers of each output neuron class of the right and left side. **(B)** Hierarchical morphology similarity score was calculated for all PaN output neurons. Pioneer neurons were not included in clustering. Dendrograms represent neurons of the right side and are colored based on morphology similarity score. Quantification of number of pre- and postsynaptic sites, raw cable length and number of branching points of each output neuron. **(C)** ssTEM cross section shows right nerve entry sites of the PaN. Neuron profiles of all output neurons are colored and labeled based on morphology similarity score. **(D)** Effectors of PaN output neurons. PaN motor neurons leave the CNS via the PaN and innervate the dorsol protractor (ProdoA) for head tilt movements.

based on synapse similarity score by computing the spatial overlap of synaptic sites between two neurons (**Fig 4.6 A**). The cluster cutoff was set to 0.06 to provide the broadest possible groups (**Fig 4.6 B)** which also was consistent with gustatory receptor expression patterns in the CNS (**Fig 4.12 – 4.18**) and connectivity patterns (**Fig 4.22, Fig. 4.24, Fig. 4.28**). This revealed seven topographically distinct compartments in the CNS (**Fig 4.6 C**). The anterior part of the Anterior Central sensory compartment (ACa), anterior part of the Anterior Ventral sensory compartment (AVa), posterior part of the Anterior Ventral sensory compartment (AVp), posterior part of the Anterior Central sensory compartment (ACp), anterior-lateral part of the Anterior Central sensory compartment (ACal), posterior-lateral part of the Anterior Central sensory compartment (ACpl) and Ventromedial sensory compartment

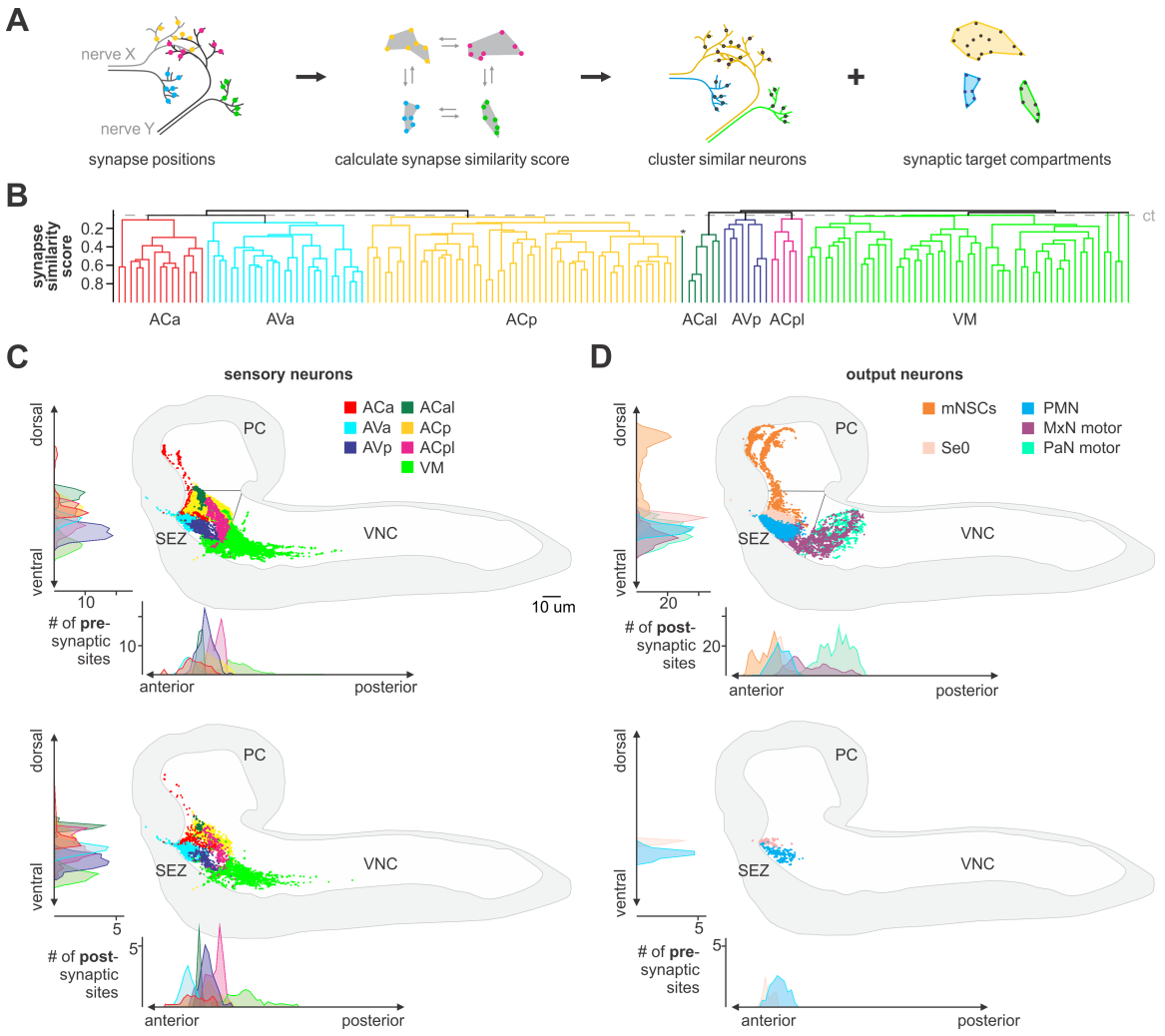

FIGURE 4.6. Spatially segregated central axon projections of sensory neurons. (A) Calculation of pairwise synapse similarity score for all non-olfactory sensory neurons of the antennal-, maxillary- and prothoracic accessory nerve. **(B)** Similarity of sensory neuron synapse placement. Hierarchical clustering based on synapse similarity score revealed seven distinct (non-overlapping) areas of sensory convergence within the SEZ: ACa, AVa, AVp, ACp, ACal, ACpl and VM. Convergence zones are targeted by varying numbers of sensory neurons but are consistent across hemispheres. Dendrogram shows left sensory neurons only. Asterisk marks one neuron which was manually moved from ACp (yellow) to ACal (dark green) to be consistent with the connectivity data. **(C)** Spatial distribution of synaptic sites for all sensory neuron clusters. Each dot represents a single synaptic site. Graphs show distribution along dorsal-ventral and anterior-posterior axis of the CNS. **(D)** Spatial distribution of synaptic sites for all neuroendocrine (mNSCs), serotonergic (Se0) and motor neuron (PMN, MxN motor, PaN motor) classes. Each dot represents a single synaptic site. Graphs show distribution along dorsal-ventral and anterior-posterior axis of the CNS.

(VM). These compartments differ in the number of sensory neurons as well as the identity of the pharyngeal nerves that give rise to them. For example, the ACa comprises 30 neurons

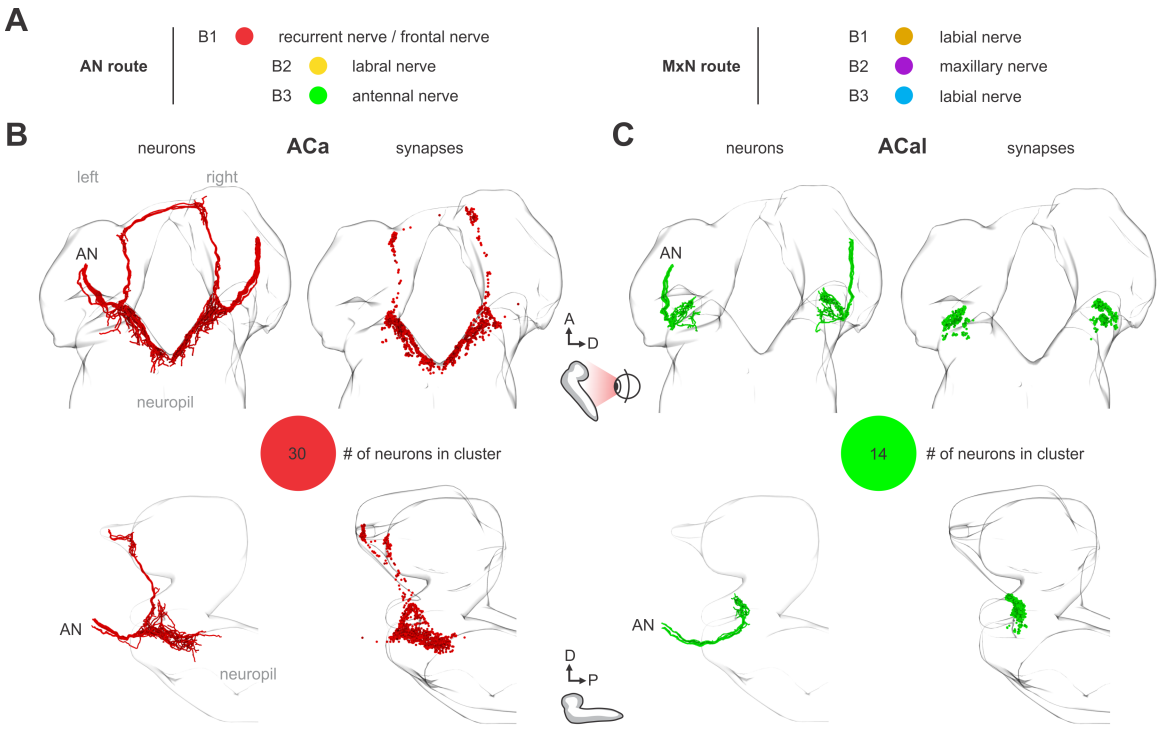

FIGURE 4.7. EM reconstruction of compartment forming sensory neurons and their synaptic sites I. (A) Peripheral origin of AN and MxN axon bundles of pharyngeal nerves and nerve branches. The recurrent nerve, the frontal nerve labral nerve and the antennal nerve enter the brain as single morphologically indistinguishable nerve collective (termed as a whole the antennal nerve). The maxillary nerve and labial nerve also enter the brain as morphologically indistinguishable nerve collective (termed as a whole the maxillary nerve). **(B, C)** ACa, ACal, EM reconstruction and distribution of synaptic sites of afferent neurons as clustered in **Fig 4.6**. Each dot represents a synaptic site. Neurons and synapses are colored based on their peripheral origin (nerve). Number in colored circle represents number of sensory neurons in cluster.

that are exclusively derived from the AN; by contrast, the VM comprises 102 neurons that derive from all three pharyngeal nerves (**Fig 4.7 – 4.9**).

For output neurons, all pre- and postsynaptic sites of all reconstructed motor and modulatory neurons of the three pharyngeal nerves were annotated, resulting in a total amount of 1471 pre – and 7856 postsynaptic sites. Interestingly, only the Se0ph neurons and a small group of seven PMNs showed presynaptic sites (**Fig 4.2 B; Fig 4.3 B; Fig 4.4 B; Fig 4.6 D**). For neuroendocrine output neurons, the previously reconstructed neurosecretory cell clusters of the pars intercerebralis (PI) were included and their postsynaptic sites are

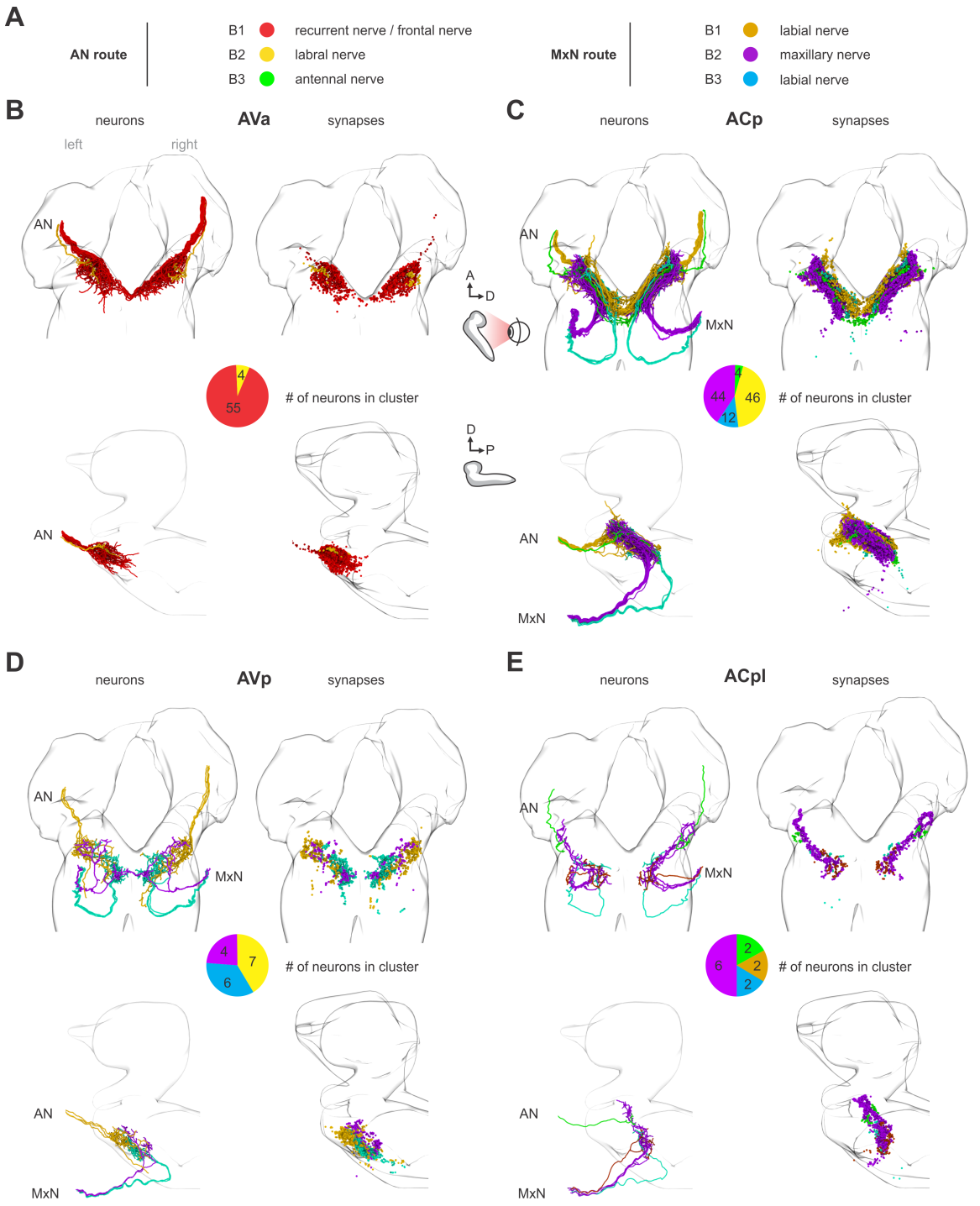

FIGURE 4.8. EM reconstruction of compartment forming sensory neurons and their synaptic sites II. (A) See **Fig 4.7** for nomenclature of the nerves. **(B, C, D, E)** AVa, ACp, AVp, ACpl, EM reconstruction and distribution of synaptic sites of afferent neurons as clustered in **Fig 4.6**. Each dot represents a synaptic site. Neurons and synapses are colored based on their peripheral origin (nerve). Number in colored circle represents number of sensory neurons in cluster. ACp and ACpl show convergence of 4 different neuronal paths (nerves).

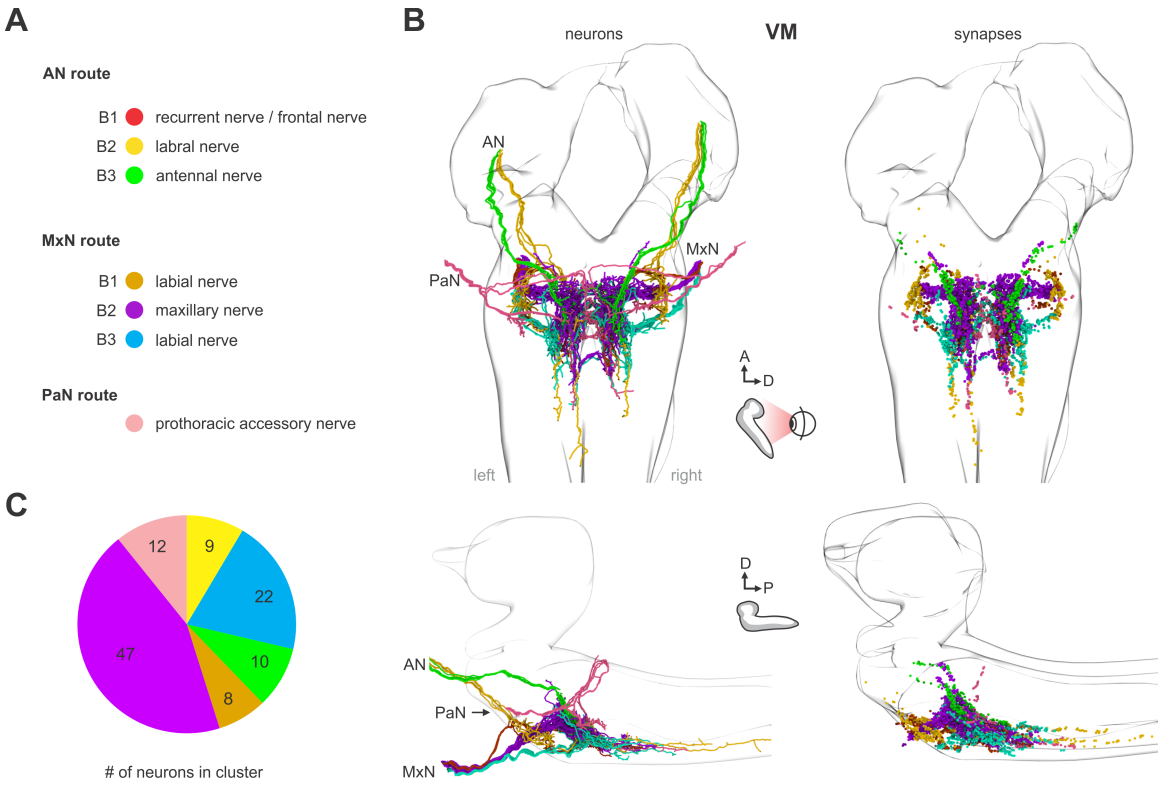

FIGURE 4.9. EM reconstruction of compartment forming sensory neurons and their synaptic sites III. (A) See **Fig 4.7** for nomenclature of the nerves. **(B, C)** VM, EM reconstruction and distribution of synaptic sites of afferent neurons as clustered in **Fig 4.6**. Each dot represents a synaptic site. Neurons and synapses are colored based on their peripheral origin (nerve). Number in colored circle represents number of sensory neurons in cluster. VM is the sensory compartment with the highest degree of convergence of different neuronal paths (nerves).

shown in **Fig 4.6 D**. These neurons innervate the major endocrine organ of *Drosophila* larvae (the ring gland) and express the neuropeptides Dilps (*Drosophila* insulin-like peptides), DH44 (diuretic hormone, a corticotropin releasing hormone homolog) and DMS (Dromyosuppressin), and receive monosynaptic inputs from the sensory system (**Fig 4.16**).

A summary of the pre- and postsynaptic compartments of the input and output neurons is shown in **Fig 4.10 - 4.11**. Taken together, these data define all sensory input convergence zones and output compartments of the three pharyngeal nerves underlying feeding motor program at synaptic resolution.

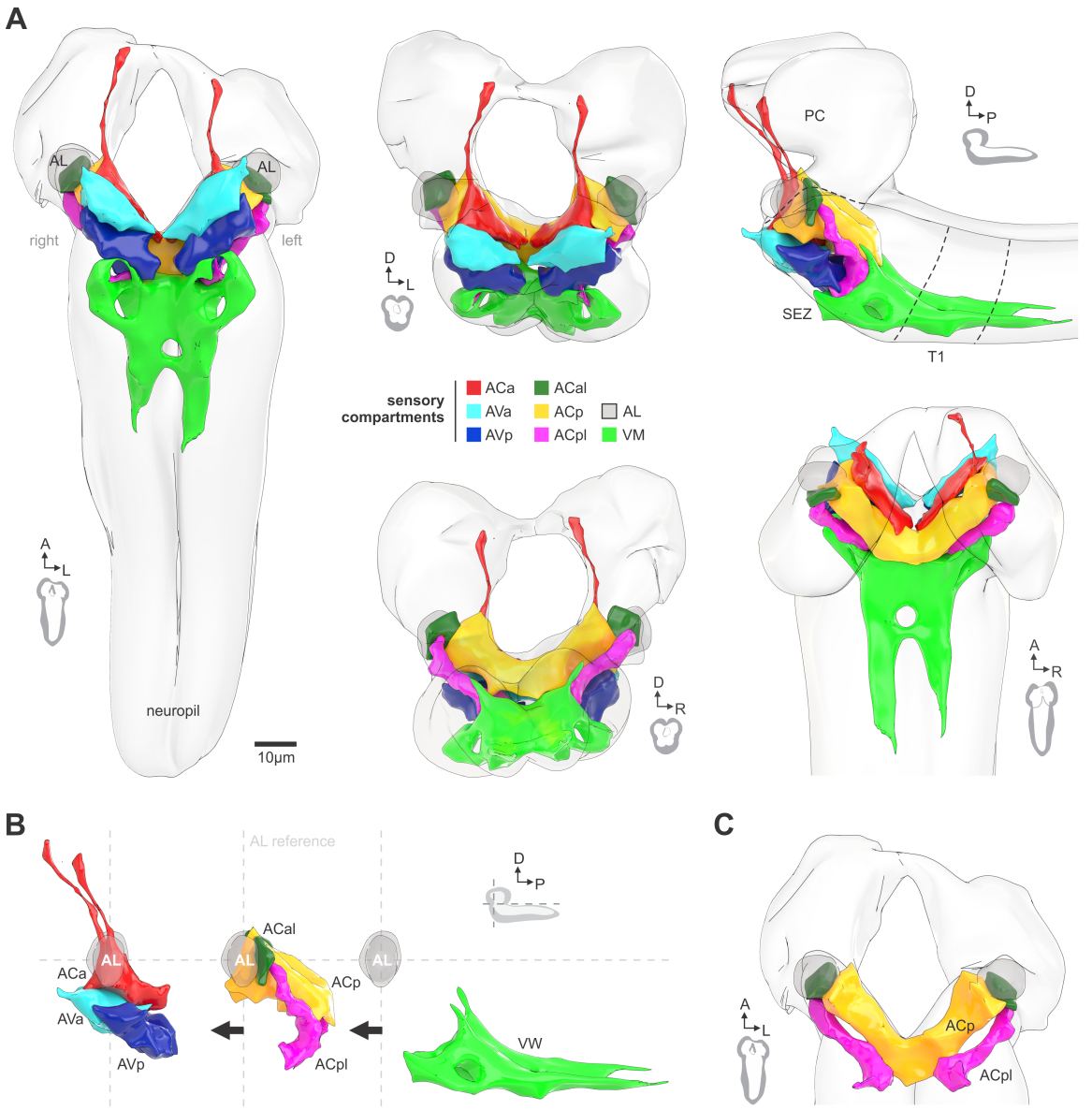

FIGURE 4.10. Sensory compartments. (A) Glomerular-like compartmentalization of the subesophageal zone (SEZ). Non-overlapping digital 3D models delineate compartments based on synapse similarity score. Protocerebrum (PC), first thoracic segment (T1). **(B)** Expanded view of partly intermeshed sensory compartments (digital 3D models), subgrouped into monosynaptic reflex module (ACa, AVa and AVp, see **Fig 4.24**), mushroom body module (AL, ACal, ACp and ACpl, see **Fig 4.28**) and somatosensory compartment (VM). **(C)** The ACpl (posterior lateral part of the Anterior Central sensory compartment) with 14 neurons which laterally flanks the ACp (primary gustatory center) delineate a so far undescribed sensory compartment in the larva (comparable to antenna-subesophageal tract "AST" in adults (Ito et al., 2014).

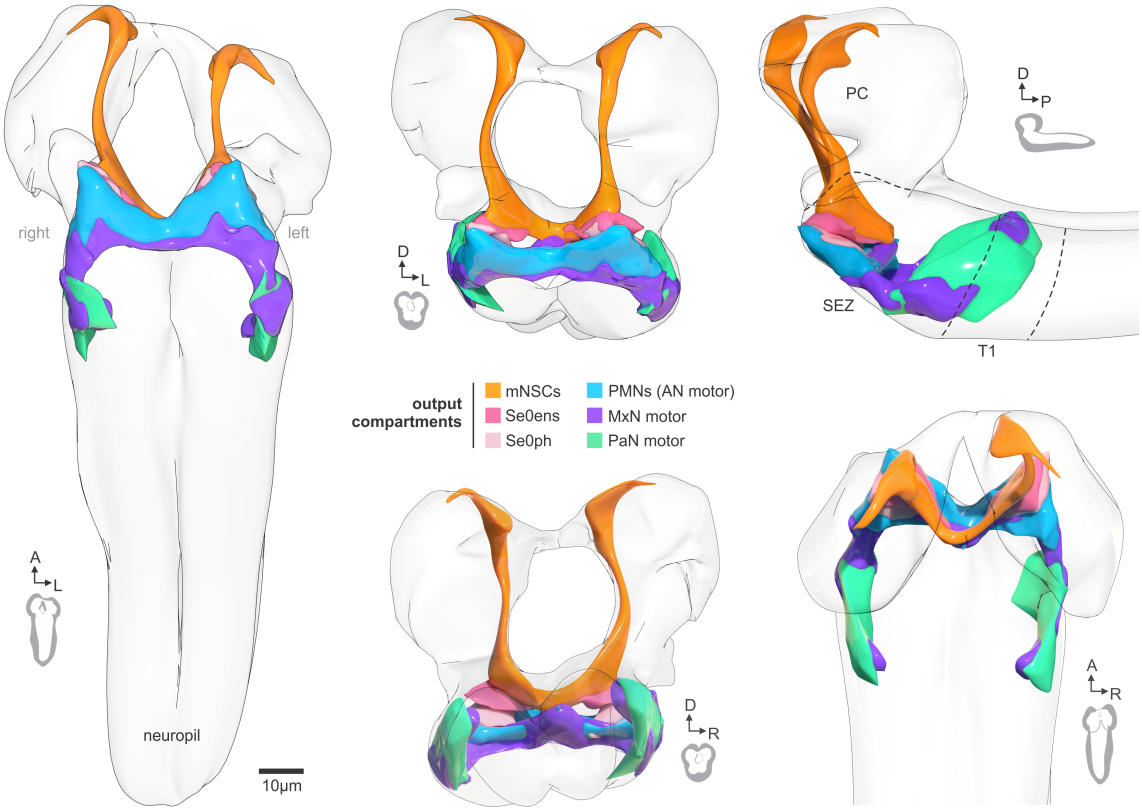

FIGURE 4.11. Output compartments. Digital 3D models of output neuron compartments based on synapse placement within the protocerebrum (PC), subesophageal zone (SEZ) and anterior half of prothoracic segment (T1).

4.3 Mapping peripheral origin of central sensory compartments

To investigate the peripheral origins of the sensory neurons that comprise the different synaptic compartments, 35 sensory receptor Gal4 lines were used to follow the projections from the sensory organs into the CNS (**Fig 4.12 - 4.19**). The mapping was backed by the fact that the pharyngeal nerves enter the SEZ in distinct axon bundles that can be observed in both light microscope and ssTEM sections (**Fig 4.19; Fig 4.20 A, B**). The AN and MxN each have three bundles which arise during embryonic development (Hartenstein et al., 2017; Kendroud et al., 2017) whereas the PaN has just one bundle. The well characterized projections from the external olfactory organ (DO) to the antennal lobe (AL), for example, use bundle 3 of the antennal nerve (AN-B3). The basic strategy, using two of the gustatory receptors (Gr28a and Gr43a) to follow sensory neuron projections from the periphery into the CNS is illustrated in **Fig 4.20**.

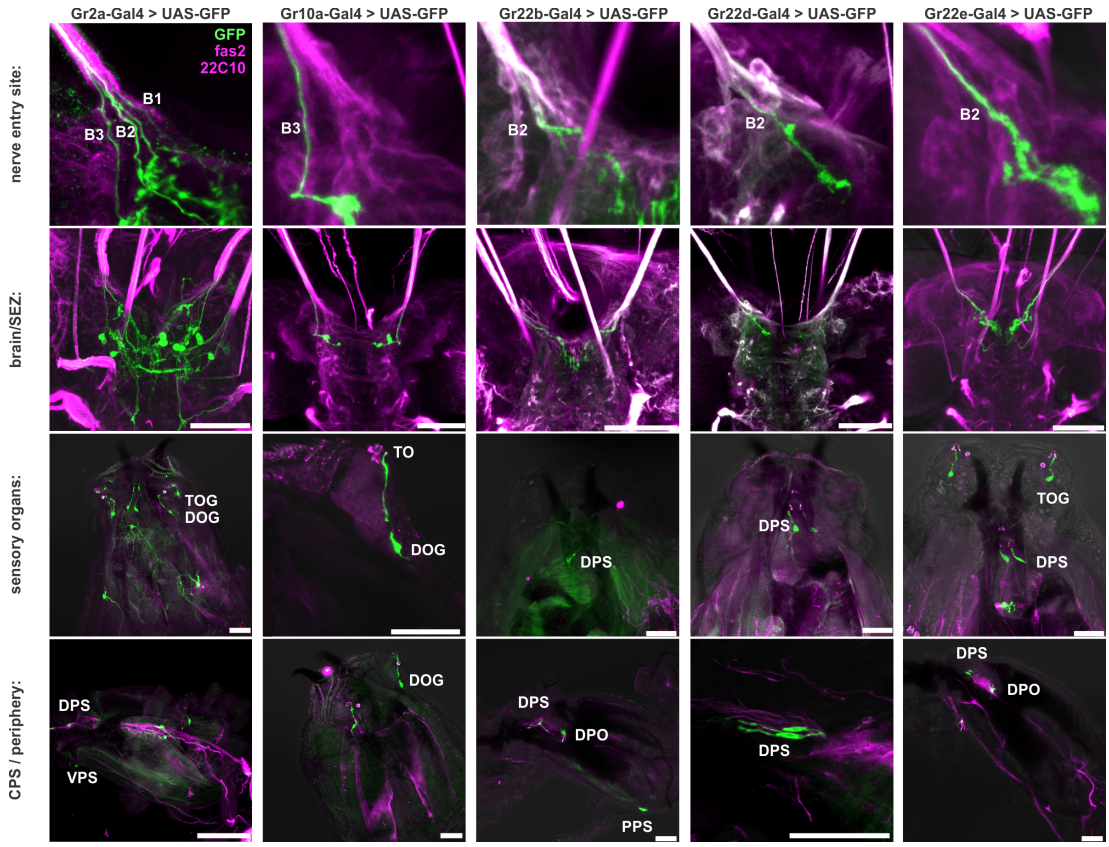

FIGURE 4.12. Gustatory receptor expression I. See **Fig 4.18** for description.

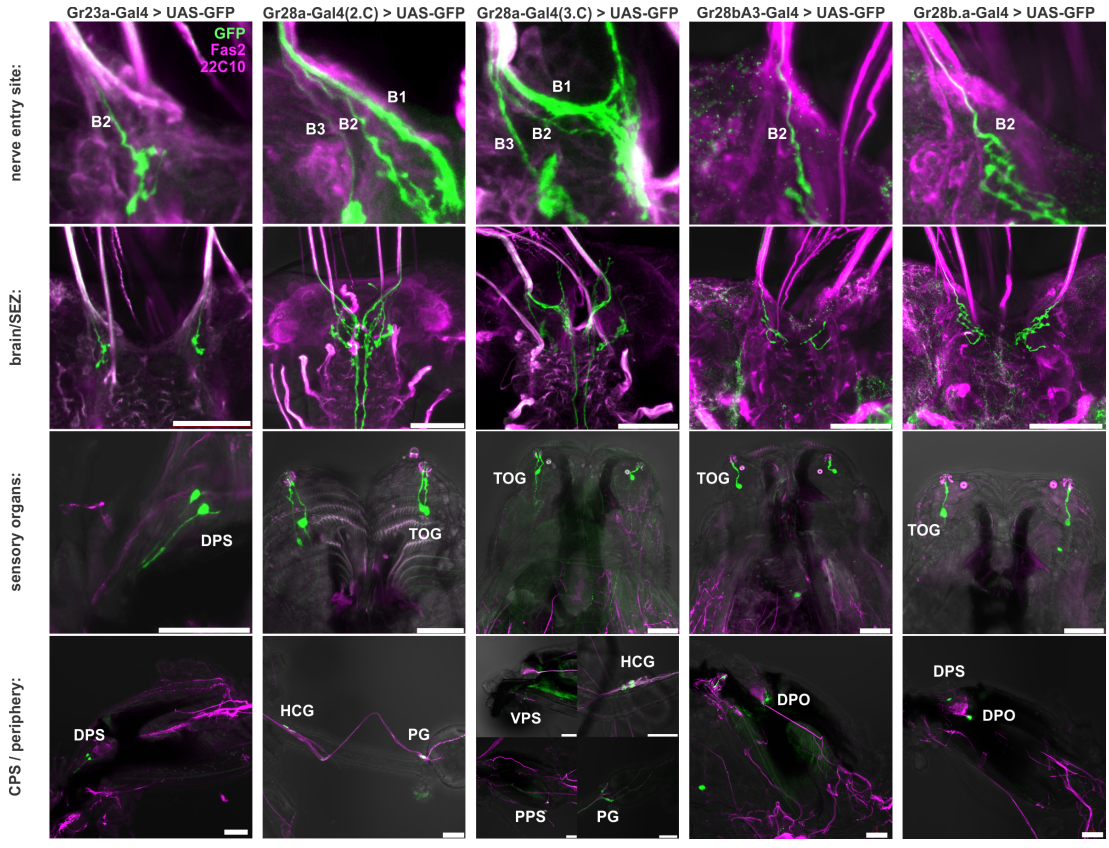

FIGURE 4.13. Gustatory receptor expression II. See **Fig 4.18** for description.

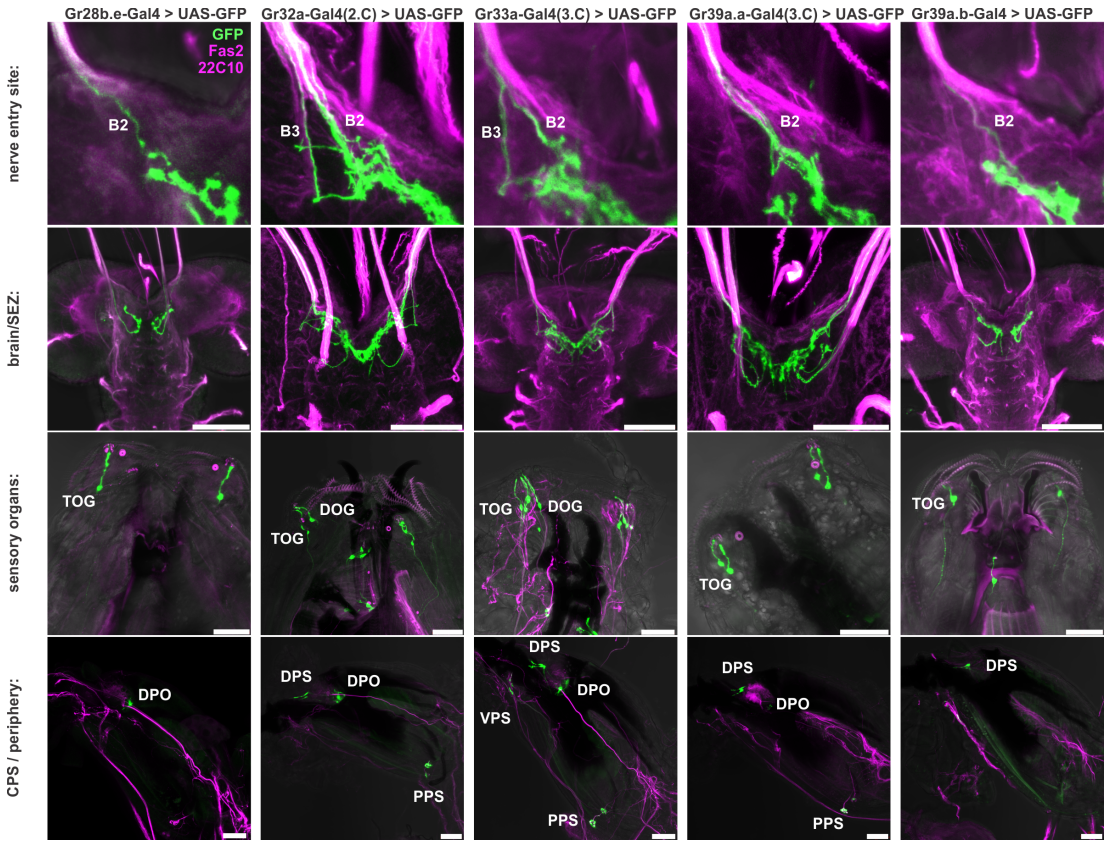

FIGURE 4.14. Gustatory receptor expression III. See **Fig 4.18** for description.

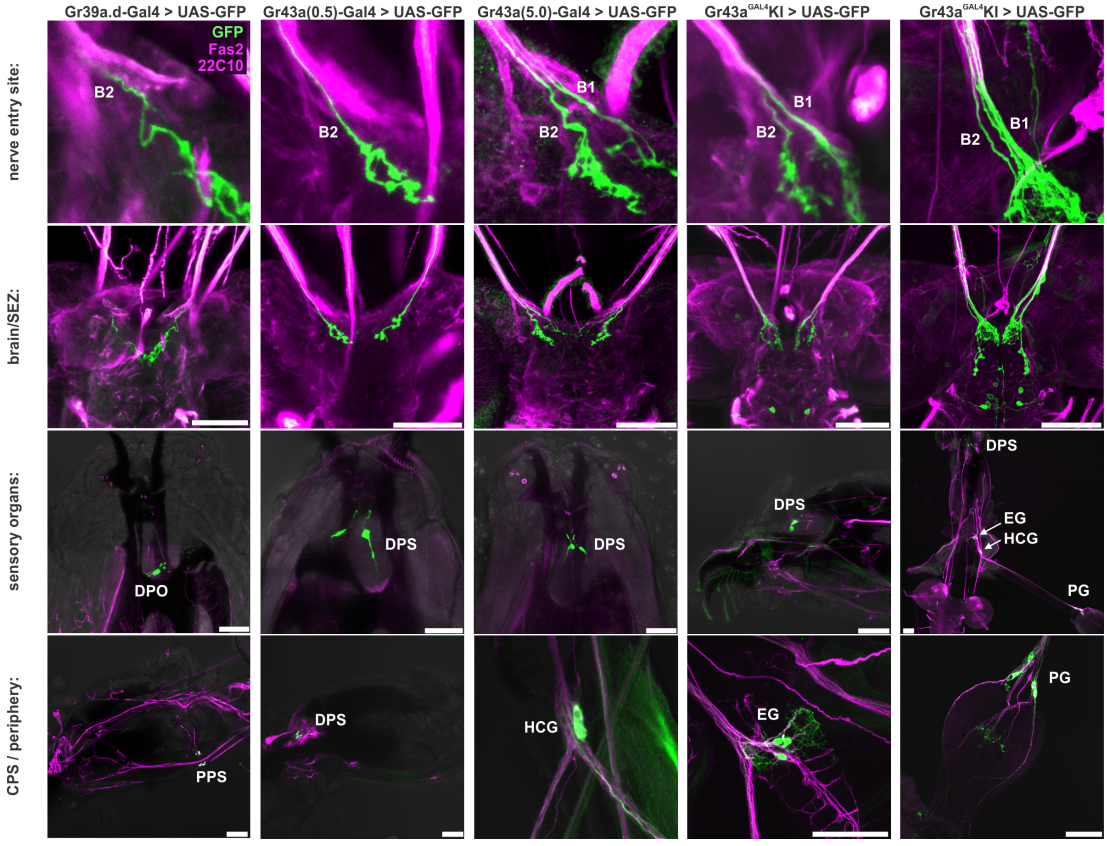

FIGURE 4.15. Gustatory receptor expression IV. See **Fig 4.18** for description.

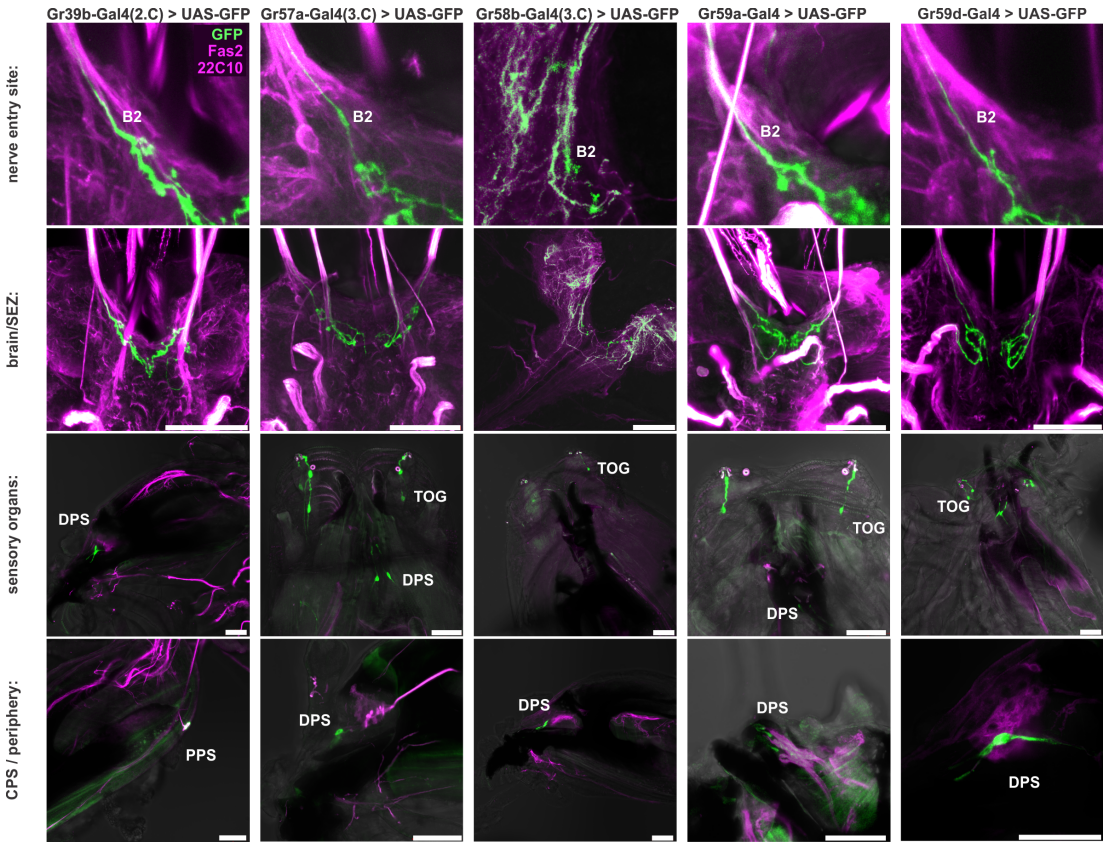

FIGURE 4.16. Gustatory receptor expression V. See **Fig 4.18** for description.

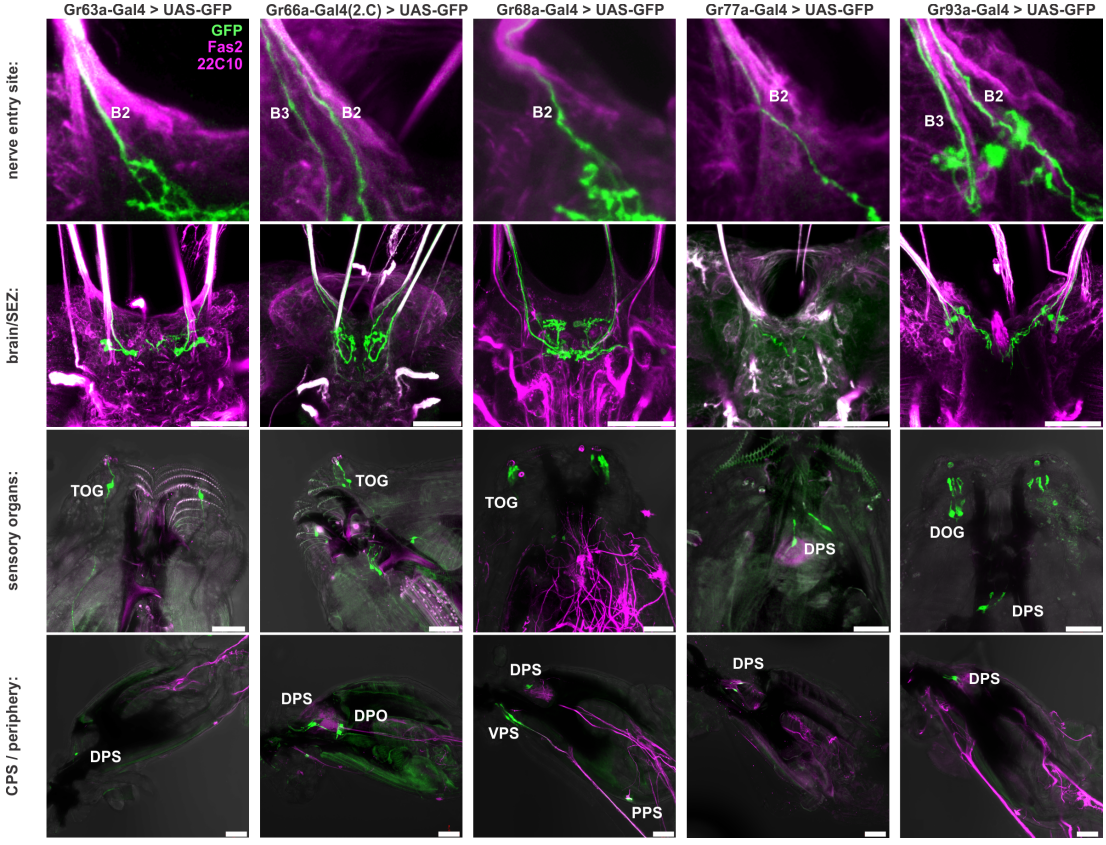

FIGURE 4.17. Gustatory receptor expression VI. See **Fig 4.18** for description.

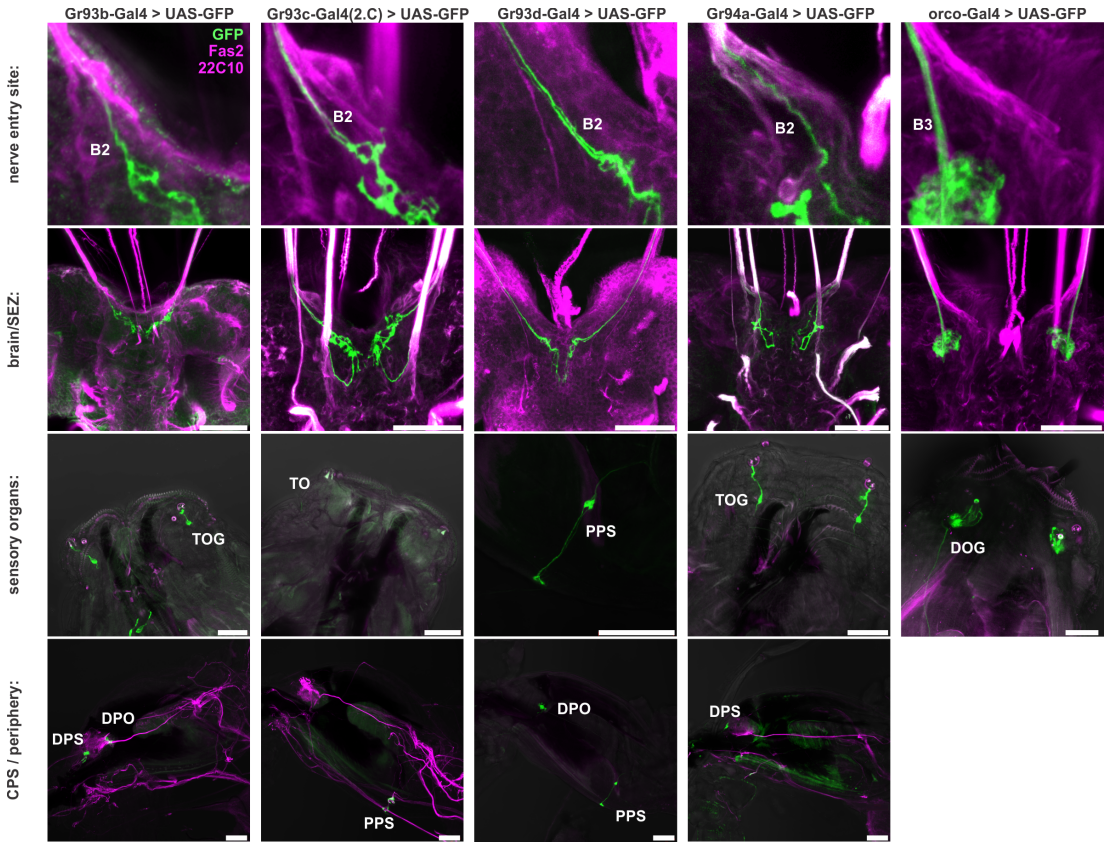

FIGURE 4.18. Gustatory receptor expression VII. Analysis of gustatory receptor GAL4 lines. Expression of 22C10 (Futsch) and Fas2 (Fasciclin 2) in Gr-Gal4 and orco-Gal4 (ORNs) driving GFP. Top row and all scale bars = 50μm.

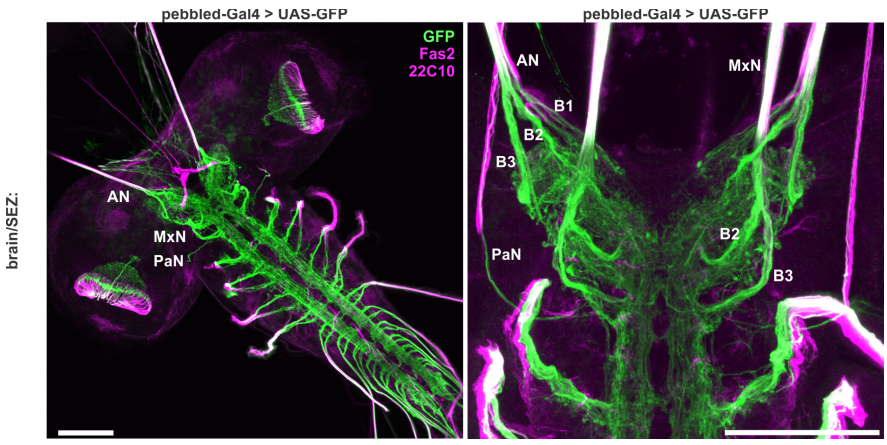

FIGURE 4.19. Sensory neuron expression. Expression of 22C10 and Fas2 in pebbled-Gal4 driving GFP. Pebbled-Gal4 was used as a pan-sensory neuronal marker to show expression in the brain. Scale bars = 50μm.

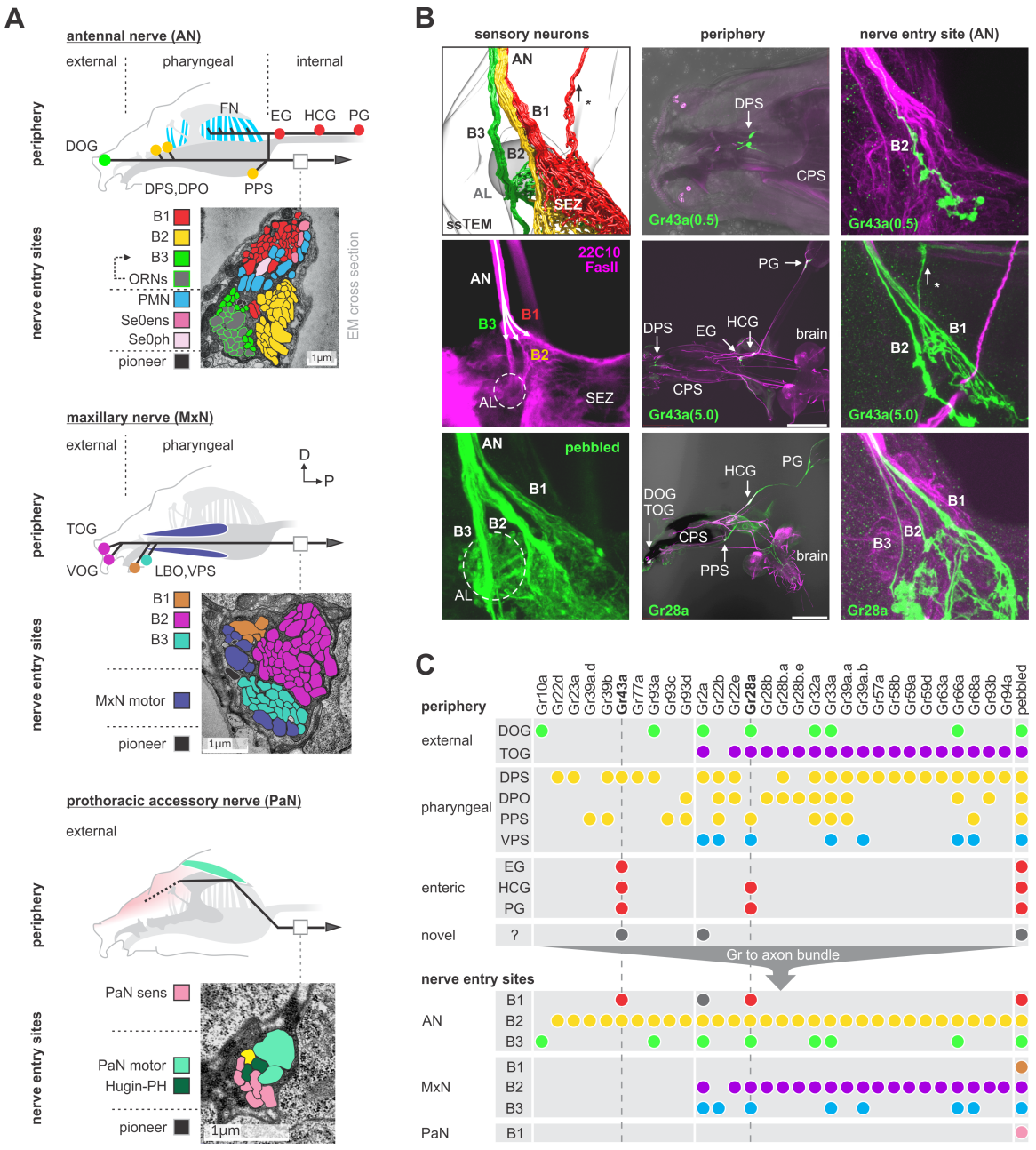

FIGURE 4.20. Mapping peripheral origin of sensory neurons. (A) Origins and targets of feeding related sensory and motor neurons. The AN comprises motor axons innervating the cibarial dilator muscles (blue striped region) and sensory axons from the dorsal organ ganglion (DOG), pharyngeal sensilla (DPS, DPO, PPS), frontal nerve (FN) and enteric nervous system (ENS). The MxN comprises motor axons innervating the mouth hook elevator and depressor (in purple), labial retractor and salivary gland ductus opener; and sensory axons from the terminal organ ganglion (TOG), ventral organ ganglion (VOG), labial organ (LBO) and pharyngeal sensilla (VPS). The PaN comprises motor axons innervating the dorsal protractor (in green), and sensory neurons with a hypothesized origin in the anterior pharyngeal region (in beige). EM cross section of the right AN, MxN and PaN at nerve entry site (lower panels). Neuronal profiles of all neurons are colored based on their morphological class and origin. **(B)** Mapping of Gr28a and Gr43a gustatory receptor neuron projection through distinct

bundles of the AN from the enteric nervous system. Pebbled-Gal4 was used as a pan-sensory neuronal marker to show expression in all 3 bundles of the AN. Asterisk marks sensory projections into the protocerebrum. Scale bars = 50μm. **(C)** Summary table of selected Gr expression patterns from the peripheral origin (sensory organs and ganglia), and their expression in respective nerve entry site. Note that Gr28a and Gr43a show expression in the ENS (EG, esophageal ganglion; HCG, hypocerebral ganglion; PG, proventricular ganglion), which results in projections through bundle 1 (B1).

For example, Gr43a(0.5)-Gal4 shows expression in one cell of a pharyngeal sensory organ (DPS) and bundle 2 of the antennal nerve (AN-B2). In comparison, Gr43a(5.0)-Gal4 shows expression in the DPS and in three ganglia of the enteric nervous system (EG, HCG and PG) which results in projections through bundle 2 (AN-B2) and bundle 1 (AN-B1) of the antennal nerve. This analysis, denoting the receptor line used and their expression in the sensory organs and axon bundles of each pharyngeal nerve, is collected in **Fig 4.20 C.** In summary, the antennal nerve comprises enteric, pharyngeal and external gustatory receptor neurons (GRNs) projecting through AN-B1, AN-B2 and AN-B3, respectively. For the maxillary nerve, pharyngeal GRNs project through MxN-B3 and external GRNs through MxN-B2. MxN-B1 and the PaN showed no GRN expression.

These results were then used to determine the peripheral origin of the seven synaptic compartments defined in **section 4.2**. This revealed a wide spectrum in compartment composition (**Fig 4.21 A**). For example, the ACa is derived 100% from the enteric nervous system, while the AVa is 93% enteric; these are the only two sensory compartments with enteric origin. As a comparison, the antennal lobe (AL) and the ACal are derived 100% from a single external sensory organ ganglion, the dorsal organ ganglion. The AVp and ACp stand out by their bigger part of pharyngeal sensory neurons, whereas three-thirds of all sensory neurons forming the ACpl and VM are of external origin.

Interestingly, the topographical location of the sensory compartments within the CNS broadly mirrors in a concentric manner the peripheral origins from which they derive: the inner-most enteric organs project to the anterior most region, the pharyngeal sensory organs project to the middle region, while the most external organs project to the outer-most region (**Figure 4.21 B**). Recent light microscopy study on the projections of somatosensory neurons onto the adult brain also showed topographically separate target areas in the brain (Tsubouchi et al., 2017).

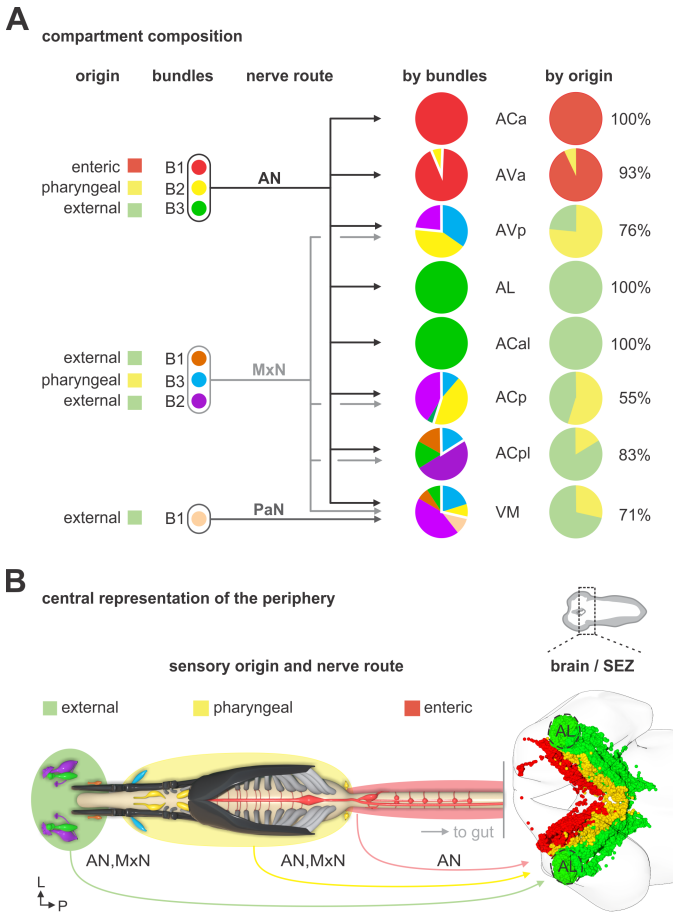

FIGURE 4.21. Organization of sensory projections. (A) Sensory compartment composition by peripheral origin. ACa, ACal and AL each derive from a single sensory origin. In contrast, AVa, AVp, ACp, ACpl and VM integrate several sensory origins. Percentage compartment composition is shown by nerve bundles and by origin (enteric, pharyngeal, external). Percentage numbers illustrate the greater part of origin. **(B)** Somatotopic arrangement of sensory neuron synapses in the brain and SEZ, showing a layered arrangement that mirrors the antero-posterior layout of innervated body structures. The internal layer (red) represents the enteric system.

4.4 Axo-axonic connections between sensory neurons

By reconstructing all central synapses of sensory neurons, an unexpectedly high number of axo-axonic connections was found between the sensory projections within the central nervous system (**Fig 4.22**). The majority of these inter-sensory connections were between neurons of the same synaptic target compartment, which underscores the clear-cut boundaries between the sensory compartments (**Fig 4.22 A, B**). This is in contrast to the well characterized olfactory receptor neurons (ORNs) that project onto the antennal lobe (AL) (**Fig 4.22 B, C**). For example, at a threshold of two synapses the AL has none, whereas 50% of the ACa neurons have above threshold inter-sensory connections. The complexity and sensory divergence at the inter-sensory level is illustrated in **Fig 4.22 C, D**. Around 70 % of all sensory neurons are involved in inter-sensory connections whereby the majority has 1-3 and ranging up to 12 downstream sensory neurons. Viewed from the total output connections of the sensory neurons, the percentage of inter-sensory synapses are small relative to

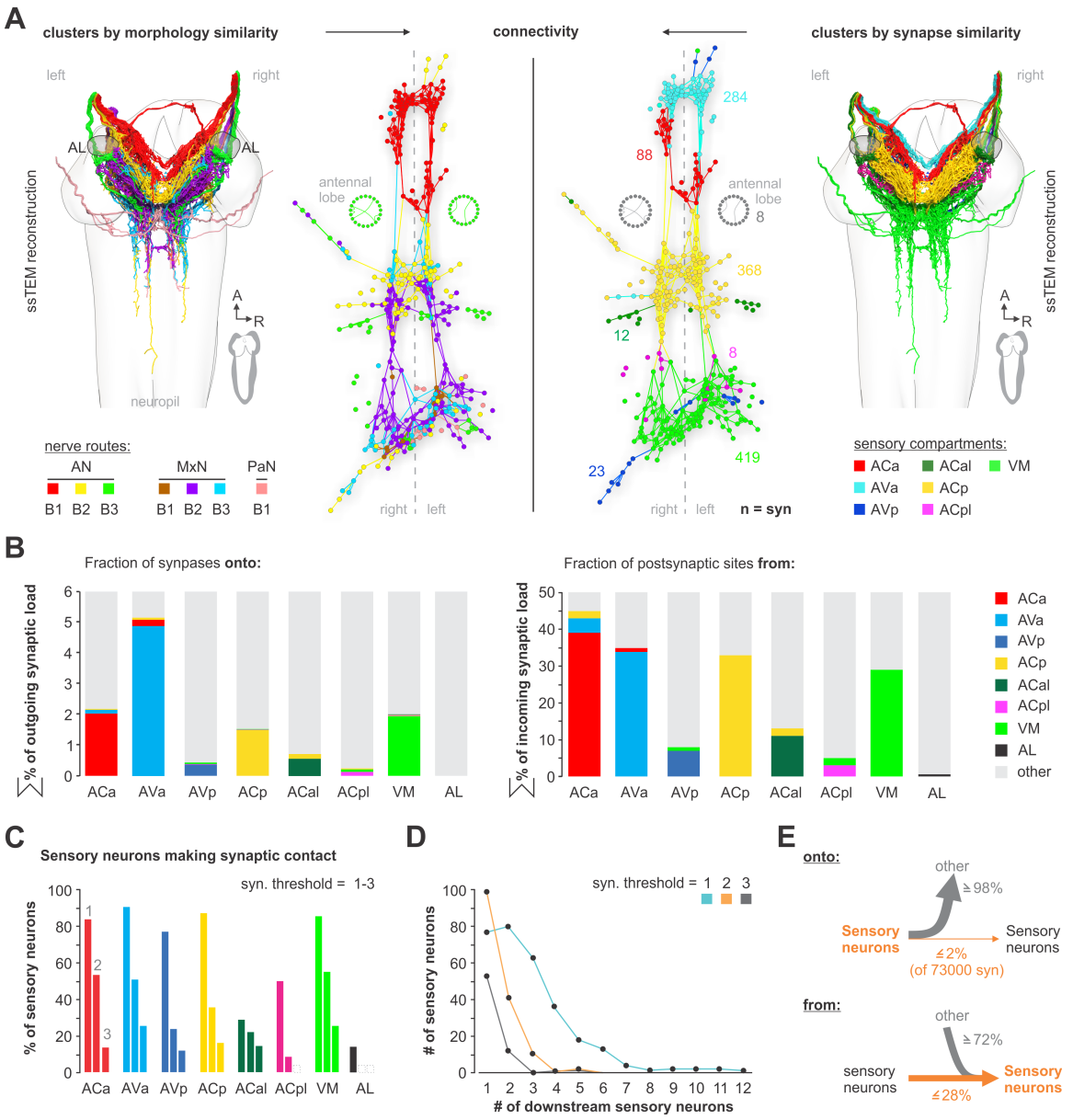

FIGURE 4.22. Sensory-sensory communication. **(A)** Left: EM reconstruction of pharyngeal sensory input colored based on peripheral origin (nerves, axon bundles. Middle panel: Comparative force directed connectivity graphs of all axo-axonic connections between sensory neurons colored based on peripheral origin (nerves) and broader identity (sensory compartments). Each node represents a single neuron. Note that sensory to sensory contacts are made mainly between sensory neurons of the same class, not between classes. Right: EM reconstruction of clustered sensory neurons. **(B)** Percentage of synapses of sensory neuron from and onto sensory neurons. **(C)** Percentage of sensory neurons of sensory compartments involved in intra compartment sensory connections, using a synaptic threshold of 1-3 synapses. Around 80% of all sensory neurons in ACa, AVa, AVp, ACp, and VM form intra sensory connections. ACal and ACpl have the lowest number of neurons and also show low number of intra sensory contacts. **(D)** Amount of monosynaptic downstream partners (sensory neurons) per sensory neuron, using a synaptic threshold of 1–3 synapses. **(E)** Summarizing representation of axo-axonic

contact input-to-output ratio viewed from the presynaptic neuron side (top) or from the postsynaptic neuron side (bottom).

the total sensory outputs (less than 2% of 74,000 synapses); however, viewed from the total input of the sensory neurons, around 28 percent of their total synaptic inputs originate from other sensory neurons (**Fig 4.22 B, E**). These connections are made both in an hierarchical manner as well as reciprocally, suggesting that sensory information processing is occurring already at an inter-sensory level in the brain (**Fig 4.23 A, B**). Within the compartments, the primary gustatory center (ACp) and the somato sensory center (VM) have inter-sensory connections even between neurons of different nerves (**Fig 4.23 C),** indicating integration of sensory information with likely similar modalities from different body regions at the sensory neuron level.

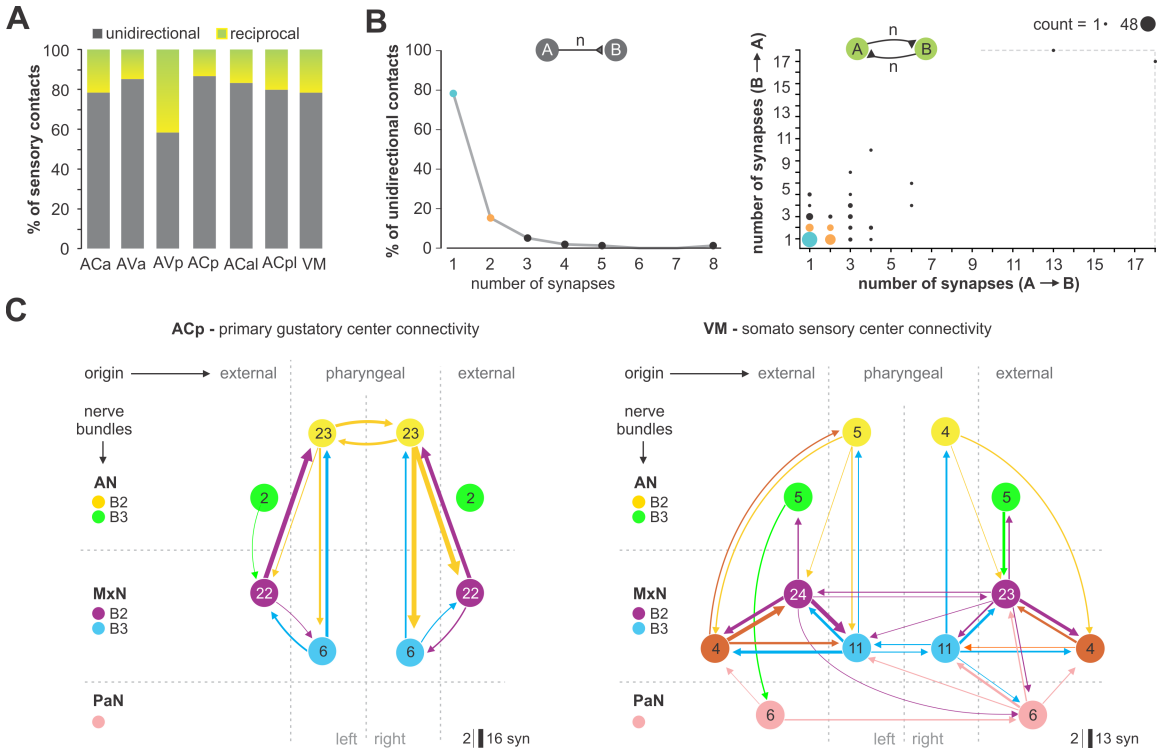

FIGURE 4.23. Connectivity principles of inter-sensory connections. (A) Percentage of neurons per sensory compartment showing hierarchical or reciprocal inter-sensory connections. Most of the sensory neurons are connected in a hierarchical manner. (B) Percentage of all unidirectional connections across all sensory clusters in relation to synaptic strength between two sensory neurons (left panel). Amount of reciprocal connection combinations between two sensory neurons (right panel). (C). Connectivity graph of all inter-sensory contacts of ACp and VM neurons using a synaptic threshold of 2. Sensory information with different peripheral origin (nerves, organs) is integrated at the sensory level. Node numbers indicate amount of sensory neurons.

4.5 Axo-dendritic connections from sensory to output neurons

Having annotated all central synapses of in- and output neurons, surprisingly the most basic element of circuit architecture was found: direct monosynaptic connections between input and output neurons (**Fig 4.24; Apendix, Fig A.1 - A.3**). The vast majority of the monosynaptic connections are made from anterior 3 of the 7 sensory compartments (ACa, AVa and AVp) (**Fig 4.24 B**): around 90% of the neurons in these three compartments make monosynaptic contacts whereby the majority has 1-3 and ranging up to 21 downstream output neurons (**Fig 4.24 C**). When viewed from the sensory neuron side, a small fraction of synapses (less than 5%) make monosynaptic contacts; however, when viewed from the output neuron side, the percentage of monosynaptic inputs they receive are substantial. For example, around 40% of all input synapses onto the serotonergic Se0 neurons, and between 10-25% of all mNSC input synapses, are from sensory neurons (**Fig 4.24 D, E**). In- and output compartments do not perfectly overlap. As a consequence, single input compartments make monosynaptic connections to neurons in overlapping output compartments, as one progresses from neuroendocrine (mNSCs), serotonergic neuromodulatory (Se0), and pharyngeal motor neurons (PMNs) (**Fig 4.25 – 4.26**): ACa inputs onto the neuroendocrine and Se0 neurons; AVa onto neuroendocrine, Se0 and PMNs; AVp onto Se0 and PMNs; VM onto MxN and PaN motor neurons. Thus, the monosynaptic connections essentially cover all output neurons in contiguous, overlapping domains. In addition, as one progresses from the inner to the outer somatotopic layers in the SEZ (see **Fig 4.21**), there is a graded contribution of connections having monosynaptic sensory-to-output contacts (highest being between the inner layers). In other words, the greatest number of monosynaptic connections occur between the enteric system and the neuroendocrine system, followed by the pharyngeal sensory neurons to the pharyngeal motor neurons, and least from external sensory neurons (**Fig 4.25 B, C**). For example, the olfactory projections from the external dorsal organ have no monosynaptic connections whatsoever to any output neuron. In this context, the Se0 serotonergic neurons appear to play a special role, as these have the greatest number of monosynaptic contacts from both the enteric system and the pharyngeal sensory neurons.

In sum, these results indicate that the monosynaptic connections between sensory and output neurons form a special class with which a core or an ‘elemental’ feeding circuit can be constructed (**Fig 4.27**).

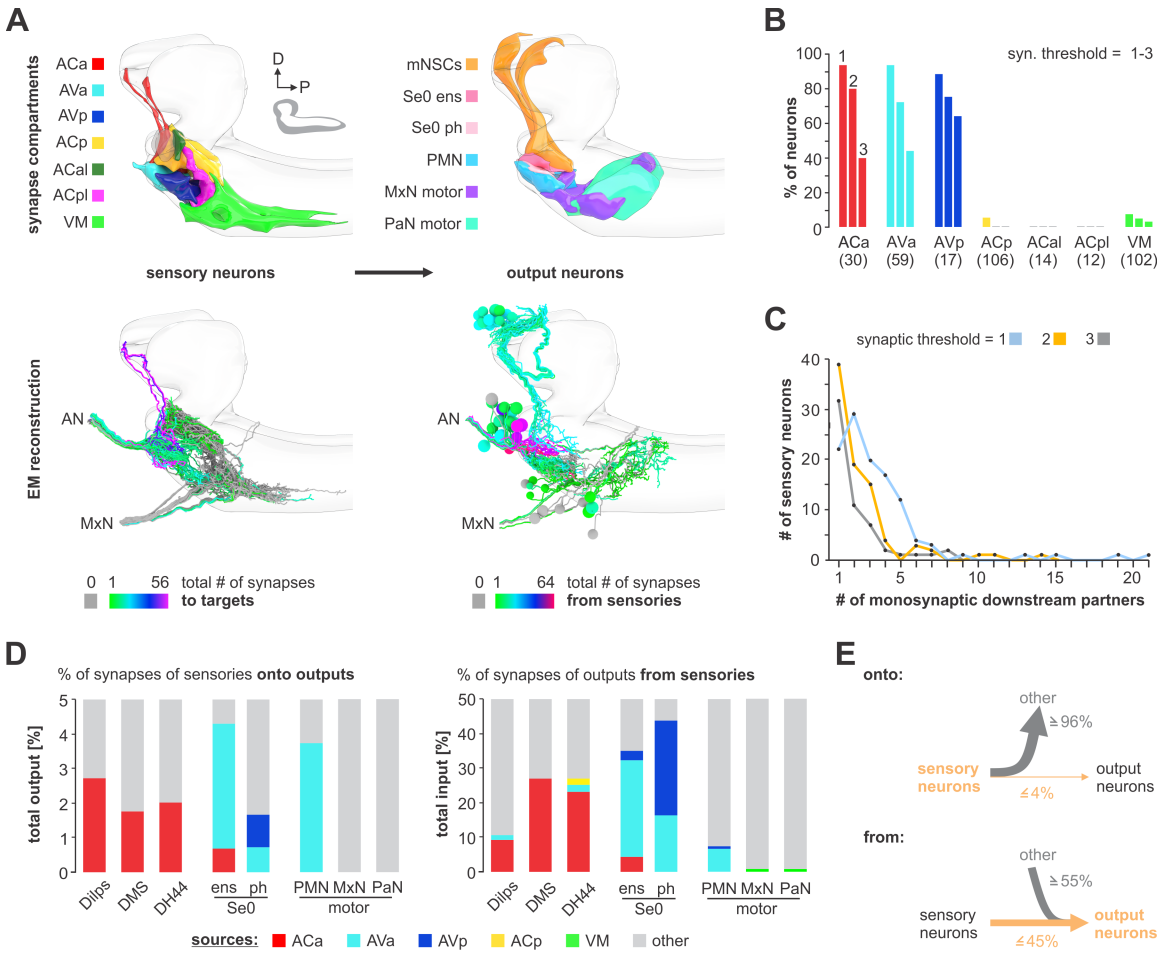

FIGURE 4.24. Monosynaptic circuits between sensory and output neurons. (A) Lateral 3D models of the presynaptic sensory compartments and postsynaptic terminals for each output neuron type (upper panel). EM reconstruction of respective neurons (lower panel). Left: sensory neurons are color-coded based on total number of synapses to their monosynaptic target. Right: output neurons are color-coded based on total number of synapses from sensory neurons. Lateral views show neurons of the right side. **(B)** Percentage of sensory neurons of the respective sensory compartment forming monosynaptic circuits, using a synaptic threshold of 1-3 synapses. About 90% of all sensory neurons of ACa, AVa, AVp are part of monosynaptic circuits; in contrast, ACp, ACal, ACpl and VM show little to none. **(C)** Amount of monosynaptic downstream partners per sensory neuron, using a synaptic threshold of 1-3 synapses. **(D)** Percentage of synapses of sensory neurons to monosynaptic targets (upper panel). Percentage of synapses of output neurons from sensory neurons (lower panel). **(E)** Summarizing representation of monosynaptic input-to-output ratio viewed from the sensory neuron side (onto) or from the output neuron side (from).

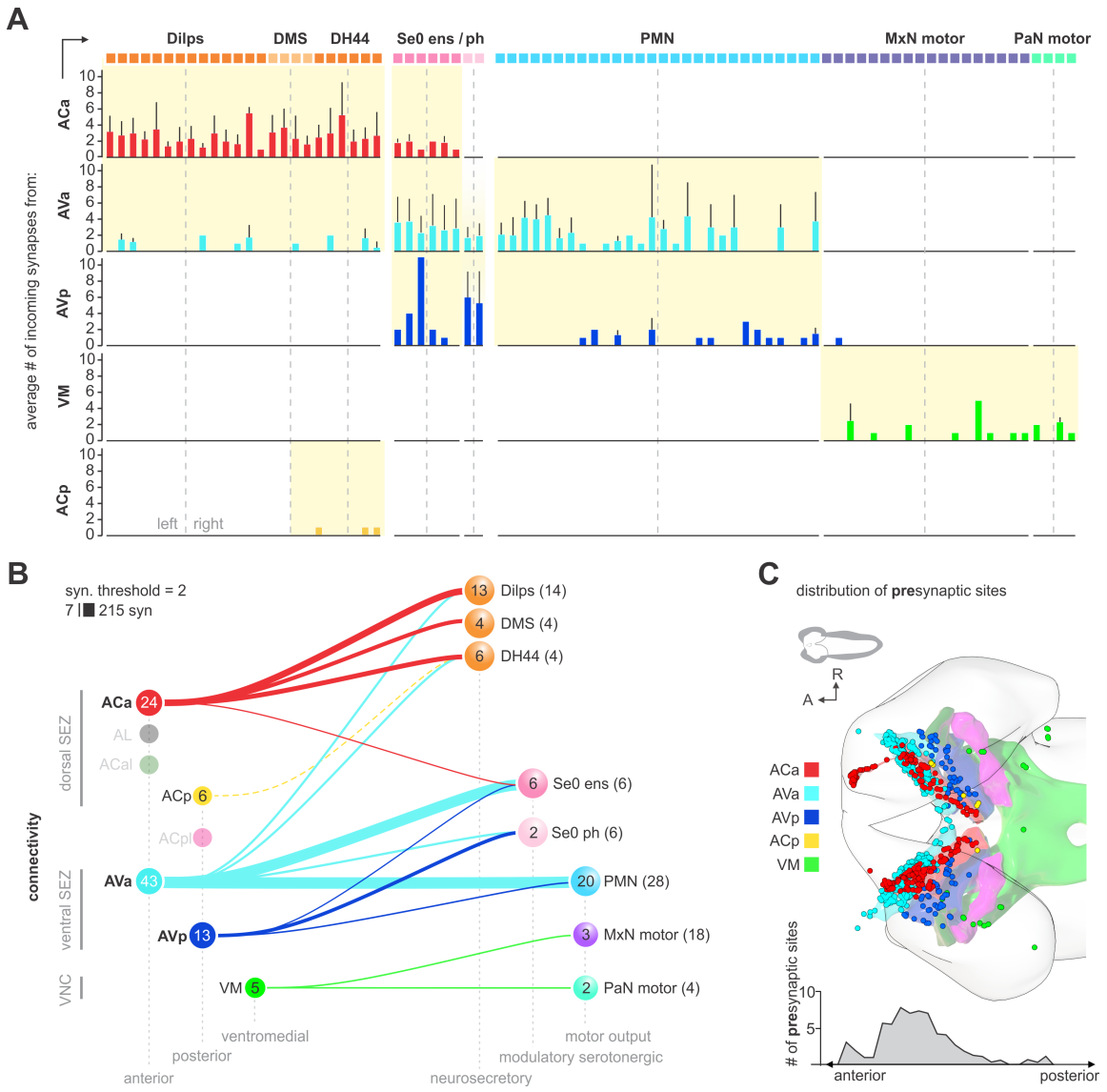

FIGURE 4.25. Monosynaptic connections in overlapping domains. (A) Connectivity between sensory neurons of different compartments (Aca, Ava, AVp, ACp and VM) and postsynaptic output targets. Each column represents an output target. Whiskers represent standard deviation. **(B)** Connectivity diagram of axo-dendritic connections between sensory and output neurons. Circles represent previously defined sensory and output compartments (**Section 4.2**). Sensory compartments with no monosynaptic reflex connections are faded. **(C)** Spatial distribution of presynaptic sites of all monosynaptic connections between sensory and output neurons. Each dot represents a single synaptic site. Graph shows distribution along anterior-posterior axis of the CNS.

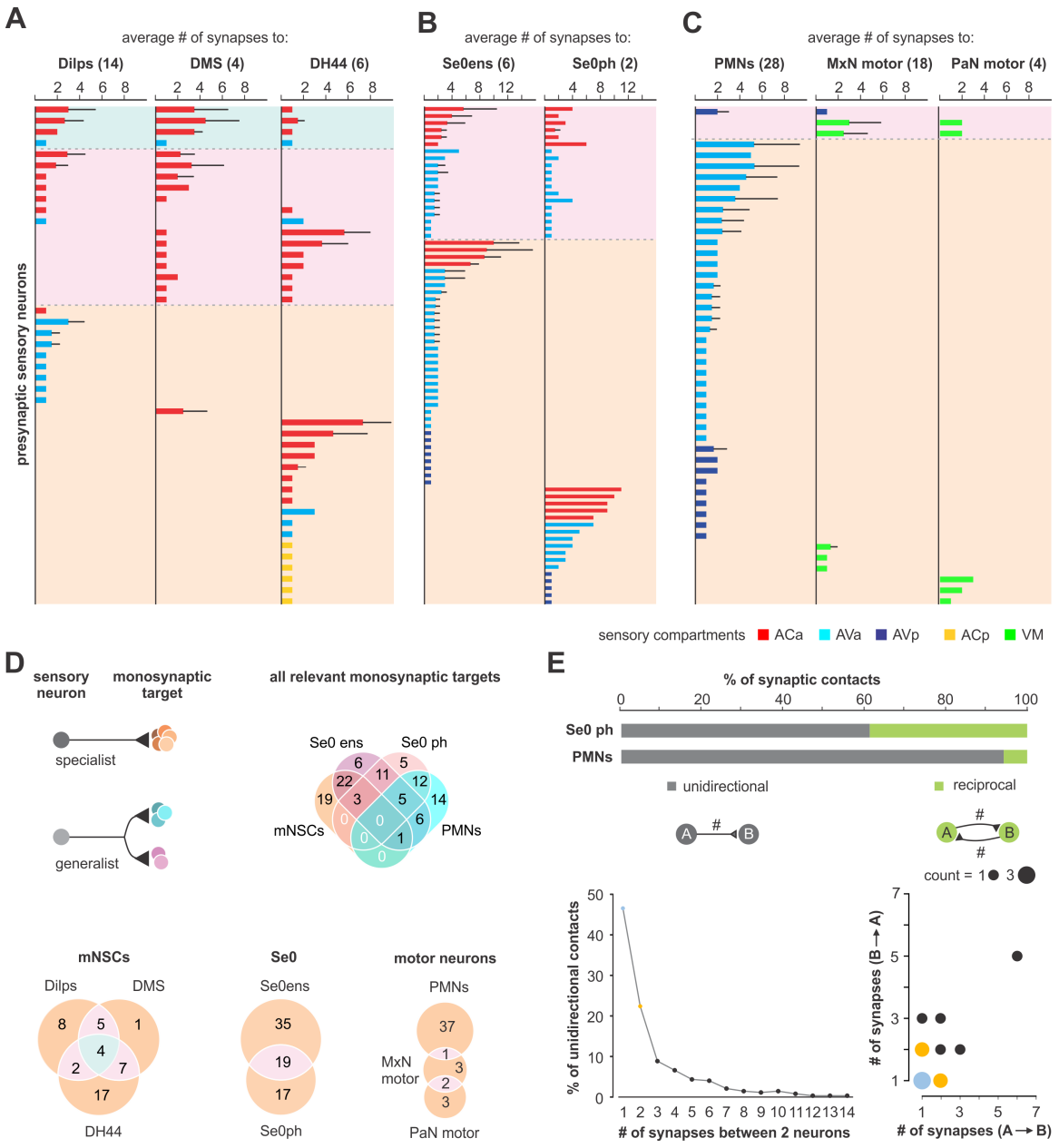

FIGURE 4.26. Connectivity principles of monosynaptic reflex connections. **(A,B,C)** Connectivity between presynaptic sensory neurons of mNSCs (Dilps, DMS, DH44), the Se0 Cluster (Se0ens, Se0ph) and feeding motor neurons (PMNs, MxN-, PaN motor neurons). Each line across the graphs represents a presynaptic partner (sensory neuron) of the output neurons. Whiskers represent standard deviation. **(D)** Specialists target exclusively one output group. Generalists diverge onto different output groups. Venn diagrams show overlap and difference between presynaptic sensory neurons of the different target groups. **(E)** Percentage of output neurons targeted in a hierarchical or reciprocal manner. Only Se0ph (2 cells) and a few pharyngeal motor neurons (7 cells) show presynaptic sites. Therefore, reciprocal contacts only occur in these cases (upper panel). Percentage of all unidirectional connections from all sensory neurons to a given output target, relative to the number of synapses between two neurons (left panel). Amount of reciprocal connection combinations from all sensory neurons to a given output target, or vice versa (right panel).

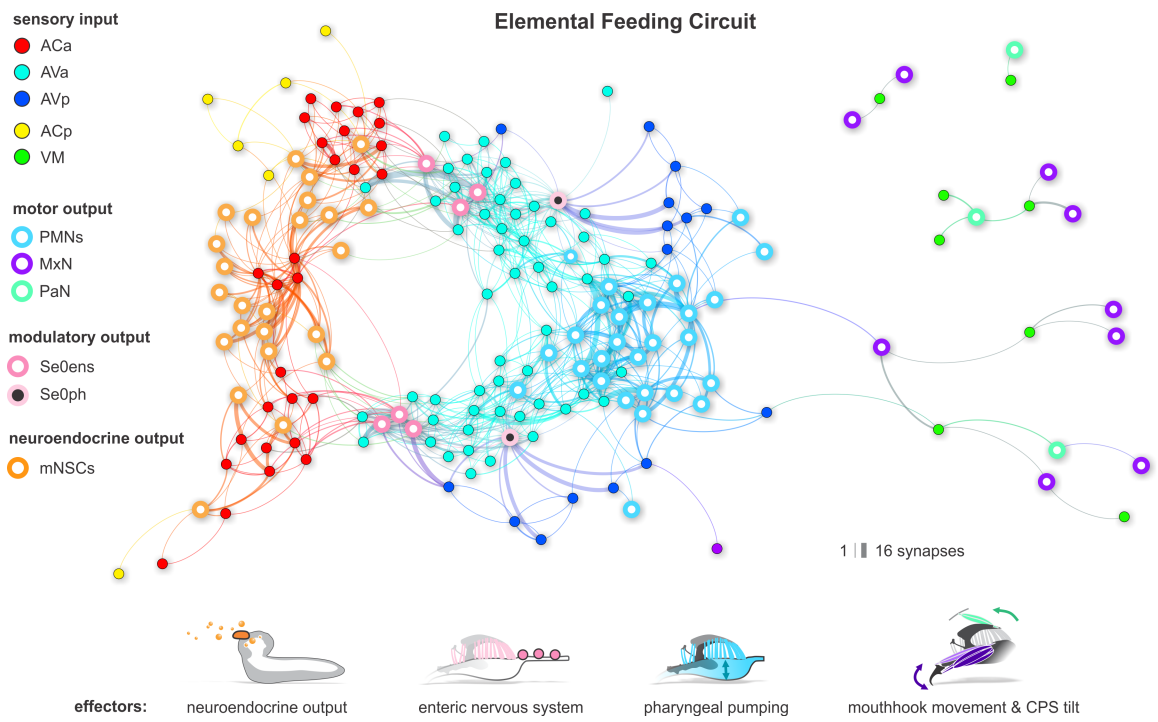

FIGURE 4.27. Elemental feeding circuit. Force-directed connectivity graph of all axo-dendritic connections between sensory neurons and output neurons. Each node represents a single neuron. Nodes are colored based on their broader identity (sensory compartment, motor, modulatory and neuroendocrine groups). Effectors of neurosecretory, modulatory and motor neurons (lower panel): mNSCs target the ring gland and release *Drosophila* insulin-like-peptides (Dilps), Dromyosuppressin (DMS) and diuretic hormone 44 (DH44); Pharyngeal motor and Se0ph neurons target the pharyngeal pump; Se0ens neurons target the enteric nervous system; MxN motor neurons control mouth hook movement, labial retraction and opening of the salivary gland ductus; PaN motor neurons tilt the whole CPS.

4.6 Multisynaptic connections to the mushroom body associative memory circuits

As a contrast to the direct input-to-output connections, this work additionally includes the connections to a higher brain center for learning and memory, the mushroom body (MB). Therefore, the previously described projection neurons to the MB calyx (Berck et al., 2016; Eichler et al., 2017) were analyzed for inputs from the sensory neurons identified here. Remarkably, the monosynaptic reflex circuits and the multisynaptic MB projections utilize an almost completely different set of sensory synaptic compartments (**Fig 4.28 A**). The three compartments that comprise the vast majority of the monosynaptic circuits (ACa, AVa and AVp) have no outputs onto the MB input projection neurons; rather, three new synaptic

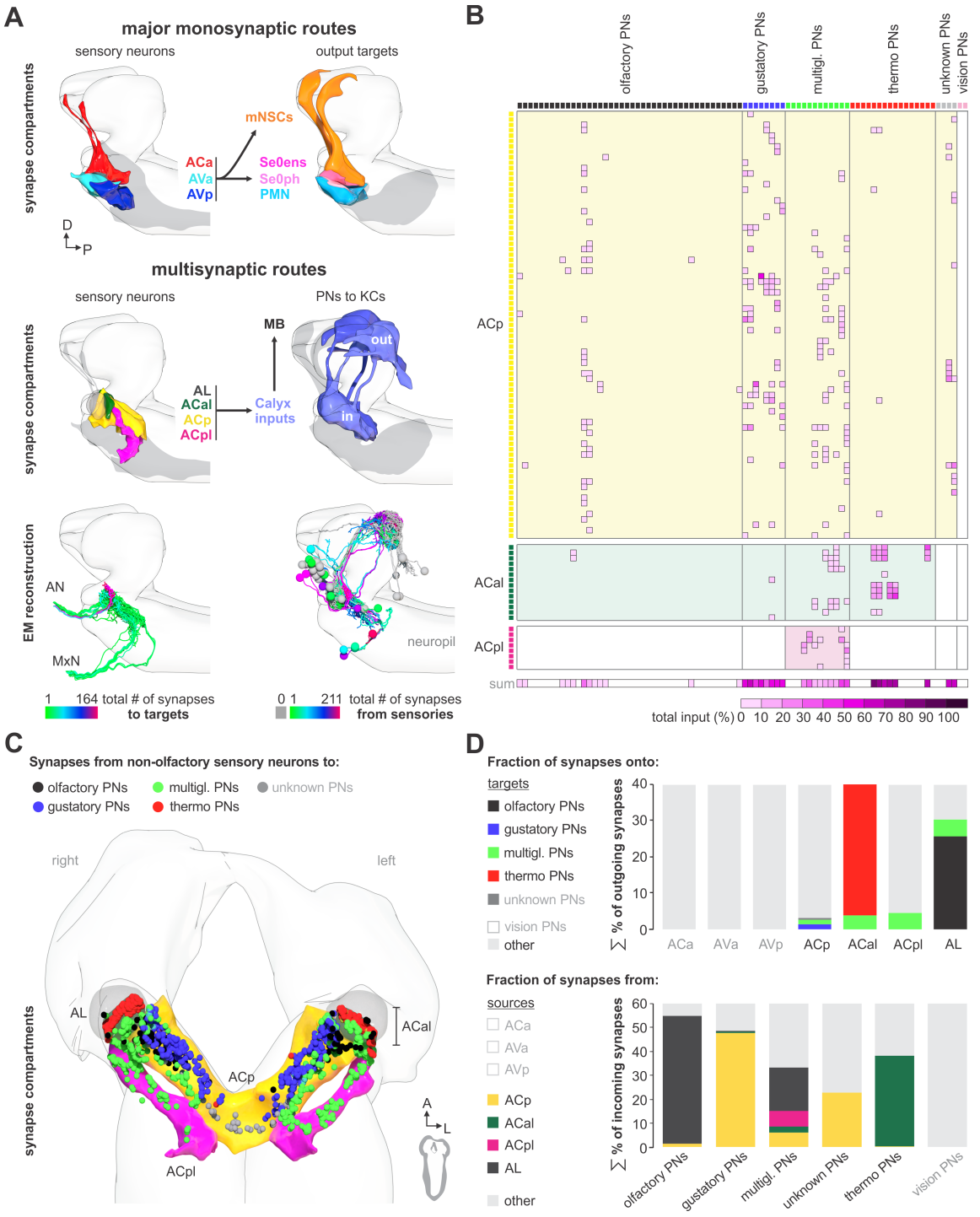

FIGURE 4.28. Multisynaptic sensory inputs onto mushroom body circuits. (A) Schematic of major monosynaptic routes (top panel). Connectivity between presynaptic sensory neurons (ACa, AVa and AVp) and postsynaptic outputs (mNSCs, Se0ens, Se0ph and PMNs). Schematic of multisynaptic routes to the mushroom body (middle panel). Connectivity between presynaptic sensory neurons (antennal lobe, ACal, ACp, ACpl) and postsynaptic projection neurons to the calyx (PNs to KCs). EM reconstruction of respective neurons (lower panel); Left: sensory neurons (olfactory receptor neurons are excluded) are color-coded based on total number of synapses to the projection neurons. Right: projection neurons are color-coded based on total number of synapses from sensory neurons. Lateral views show

neurons of the right brain hemisphere. **(B)** Adjacency matrix showing sensory-to-PN connectivity, color-coded by percentage of inputs on PN dendrites. Or35a-PN is essentially the only olfactory projection neuron that receives multisensory input from non-olfactory receptor neurons of the ACp (primary gustatory center). **(C)** Distribution of synapses from afferent non-olfactory sensory neurons onto projection neurons to the calyx in relation to synapse compartments (3D models). Each dot represents a synaptic site. Synapses are colored based on target neurons class (PNs to KCs). **(D)** Percentage of presynapses of sensory neurons to PNs (upper panel). Percentage of postsynapses of PNs from sensory neurons (lower panel).

compartments are utilized (ACp, ACal and ACpl) (**Fig 4.28 A,B**). Aside from the AL (from which over 20% of output synapses of the ORNs target the MB calyx via olfactory projection neurons), the most prominent synaptic compartment is the ACal, from which almost 40 % of the synapses output onto thermosensory projection neurons. Around 45 % of all incoming synapses onto the gustatory projection neurons derive from ACp (**Fig 4.28 D**). This is also consistent with the view that the ACp is the primary sensory compartment onto which the external and pharyngeal gustatory sensory organs project (Colomb et al., 2007; Hartenstein et al., 2017). The multiglomerular projection neurons receive synaptic input from four different sensory compartments (AL, ACal, ACp and ACpl) may therefore play an important role in multi-modal sensory information integration to the MB circuits.

For a comprehensive neuron atlas of all neurons of this study and their connectivity, see supplemental data of Miroschnikow et al., 2018.

4.7 Integration of polysynaptic connections onto monosynaptic circuits

The hugin neuropeptide (*Drosophila* neuromedin U homolog) circuit is a well described example for interneurons relaying gustatory information to the protocerebrum and the mNSCs in *Drosophila* larva (Hückesfeld et al., 2016; Schlegel et al., 2016). The present study examines the position of hugin protocerebrum neurons (huginPC) with respect to the monosynaptic reflex and multisynaptic MB memory circuits (**Section 4.5, 4.6**). Based on the work of Hückesfeld et al. 2016 and Schlegel et al. 2016a on mapping sensory inputs onto huginPC, most inputs were expected from the ACp, which is the primary gustatory sensory compartment (Colomb et al., 2007; Hartenstein et al., 2017). Strikingly, most of the huginPC neurons receive inputs from the sensory compartments ACa and AVa, which

are the two major monosynaptic compartments that originate from enteric regions (**Fig 4.29 A**). HuginPC and mNSCs share a set of presynaptic sensory neurons (**Fig 4.29 B**). In addition, huginPC neurons do receive different inputs from the external and pharyngeal organs (i.e., through sensory compartment ACp), but to a much smaller degree (**Fig 4.29 C**). Thus, unlike the MB circuit that utilizes a completely new set of sensory inputs, the huginPC circuit is associated with a feeding related monosynaptic circuit. Further, huginPC neurons are used as an alternative route for sensory-to-mNSC connections with enteric origin and integrate a completely new set of sensory neurons onto the mNSCs (**Fig 4.29 D**).

FIGURE 4.29. Connectivity between presynaptic sensory neurons of mNSCs and huginPC neurons.

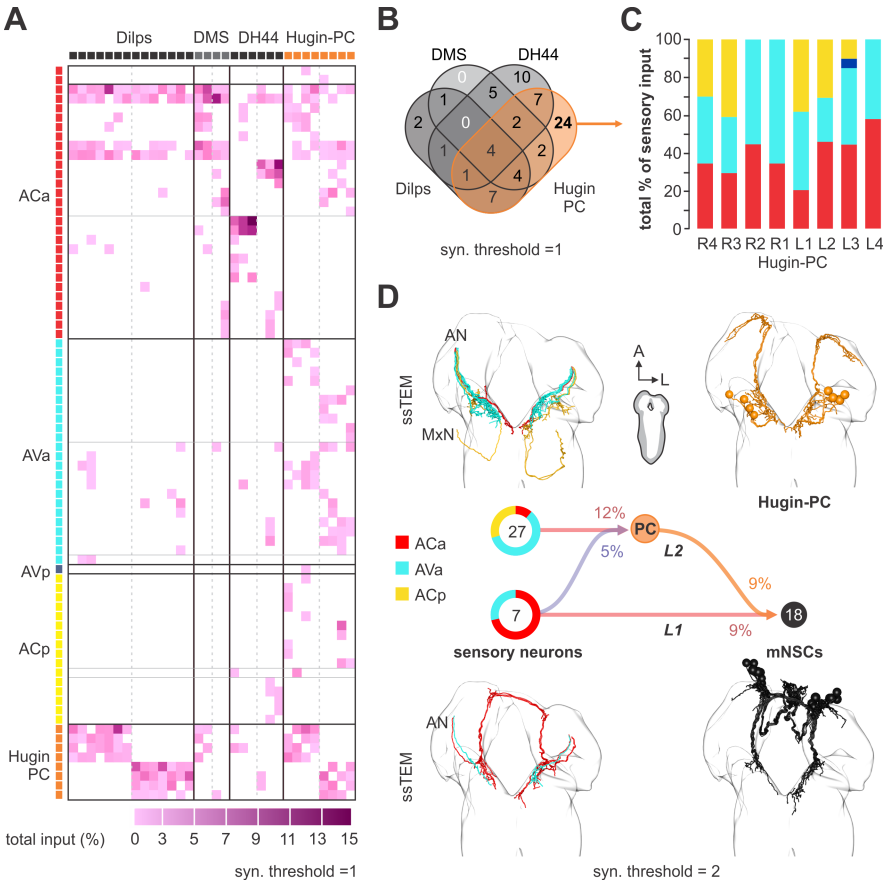

(A) Adjacency matrix showing sensory-to-mNSCs and huginPC connectivity, color-coded by percentage of inputs on mNSC and huginPC dendrites. Sensory neurons are ordered based on synapse similarity score (sensory compartments); they are listed based on their connectivity patterns to their targets. Dotted lines separate left and right targets. **(B)** Venn diagram shows overlaps and difference between presynaptic sensory neurons of the different target groups. **(C)** Sensory profile of each individual huginPC neuron. On average 80% of the total incoming synaptic load from sensory neurons made by enteric sensory neurons, and 20% by pharyngeal and external sensory neurons. **(D)** Summarizing representation of all seven monosynaptic sensory-to-mNSCs paths, which concurrently use huginPC neurons as an alternative route to target the mNSCs using a synaptic threshold of huginPC neurons receive sensory information from 27 other sensory neurons, thus integrating a completely different set of sensory neurons onto a basic reflex circuit. Figure shows EM reconstructions of respective neuron groups.

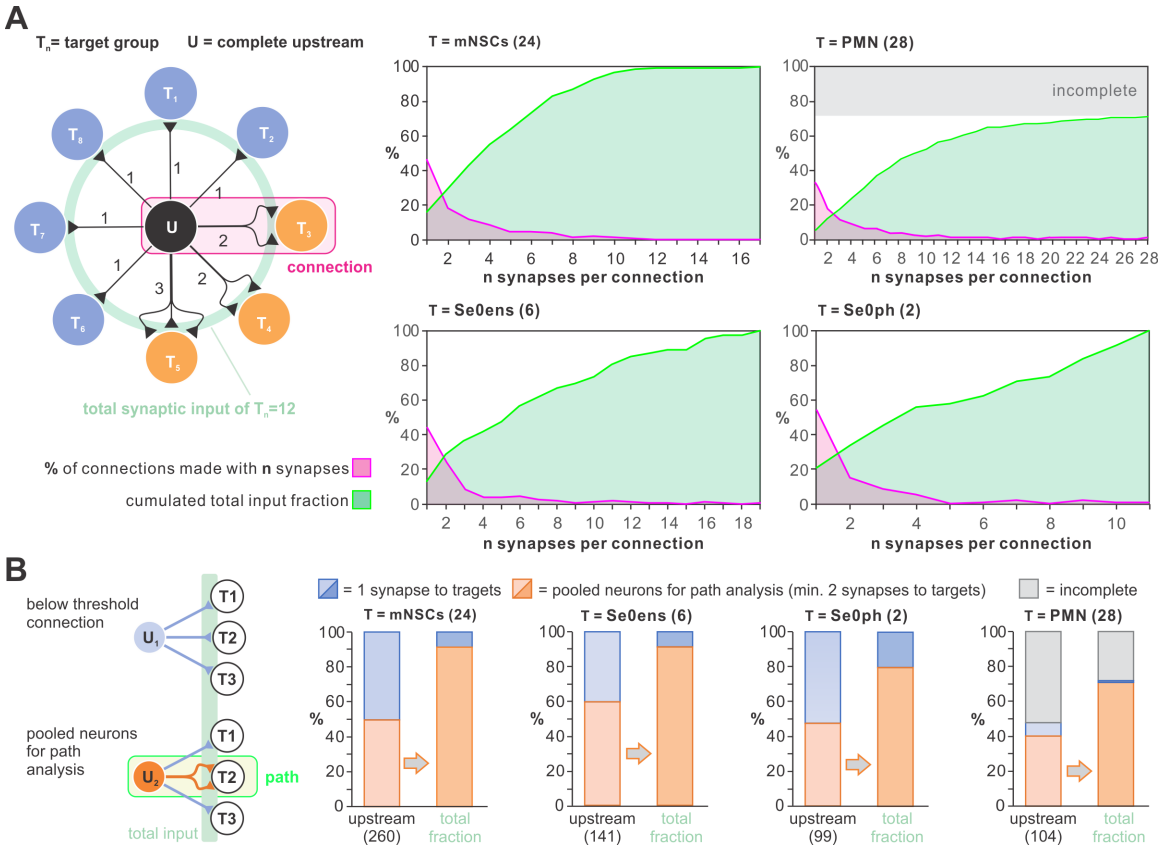

FIGURE 4.30. Completeness of the feeding connectome. (A) Left: Exemplary schematic connectome of a given target neuron group T and all their presynaptic neurons U. Neurons of U can make single or multiple connections to one or more neurons of T. A connection can consist of single or multiple synapses with up to 3 synapses. Right: Quantification of all synaptic connections to the different output neuron groups (mNSCs, Se0ens, Se0ph and PMNs). The contribution of the different connection types to the total synaptic input of the respective target group is shown as cumulated total input fraction. **(B)** Left: schematic illustrates the strategy how upstream neurons with min 2 synapses to the respective target neuron groups were selected and pooled for path analysis in **Section 4.7**. Pooled neurons consist of sensory neurons and interneurons.

These observations from the hugin neuropeptide circuit in interconnecting sensory and neuroendocrine outputs raise a broader question concerning the input-output connections: for any given pair of neurons comprising the monosynaptic reflex circuit, how many alternative polysynaptic paths exist and what could be the functional significance of such parallel pathways (Leonardo, 2005)? To answer these questions, it was necessary to primarily extend the dataset of reconstructed interneurons connecting sensory- to output neurons. Therefore, a map of all first order synaptic up- and downstream partners of the Se0 and PMN cluster was generated by Andreas Schoofs (personal communication) using a synaptic threshold of 2. Using the same synaptic threshold, all synaptic upstream partners of the

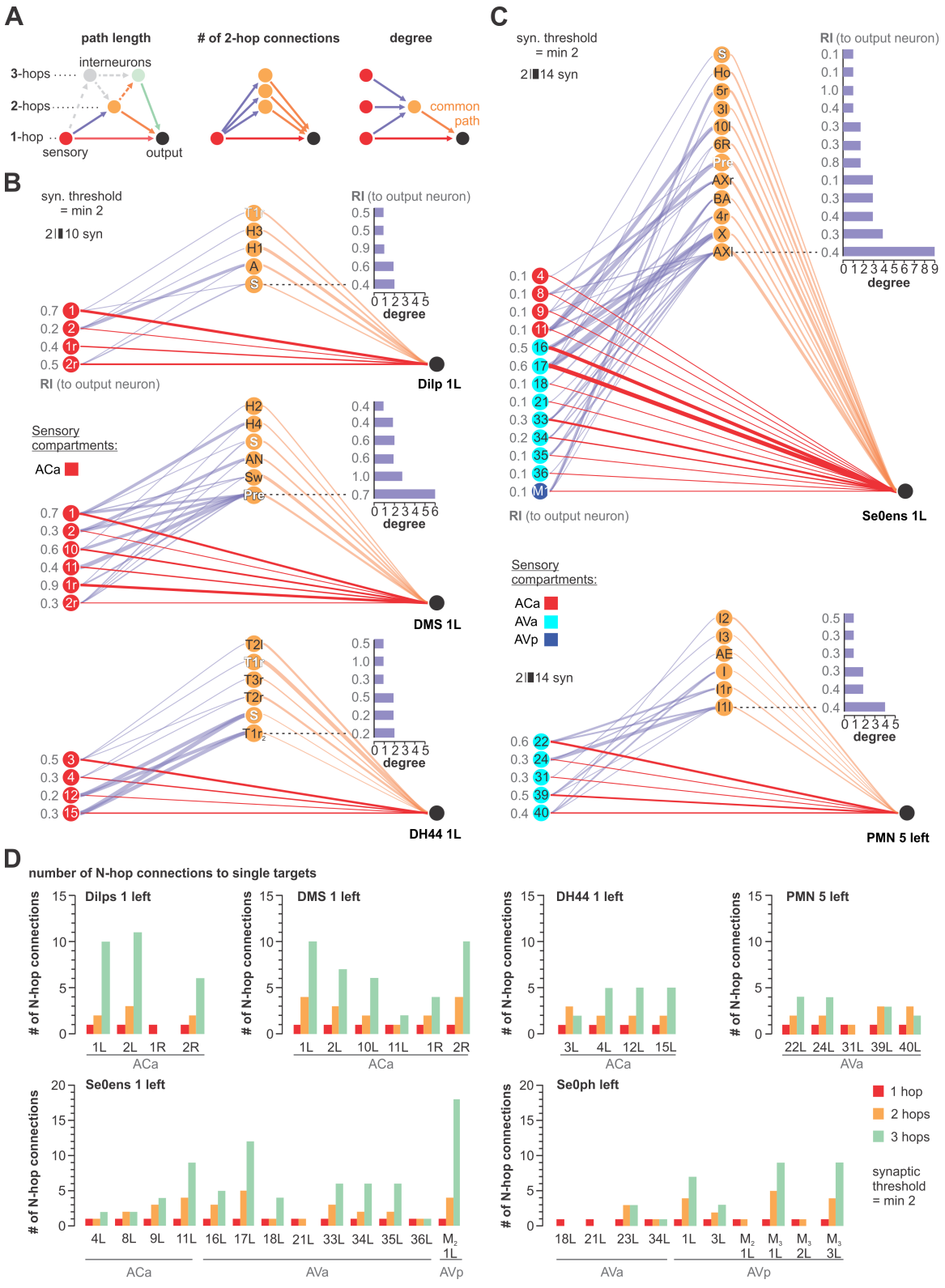

FIGURE 4.31. Parallel alternative pathways. (A) Path length: Illustration of direct (1-hop) sensory to output neuron connections and indirect (2-hop, 3-hop) paths which involve 1 or 2 interneurons to reach the same output neuron. 3-hop connections through interneurons which are not part of the direct upstream of the output neurons were not considered. Number of 2-hop connections: Illustration of sensory divergence, which defines the number of possible paths to reach the same target neuron

through different interneurons. Degree: Illustration of sensory convergence, which defines how often (degree) a common path is used by different sensory neurons to reach the same output neuron. **(B)** All 1- and 2-hop connections for one cell from each of the Dilp, DMS and DH44 clusters of neurosecretory output cells, using a synaptic threshold of 2. Ranking index (RI) shows the relative synaptic strength of every connection compared to the total synaptic input of the output neuron (1.0 represents the highest from all possible inputs to the output neuron). **(C)** All 1- and 2-hop connections for one cell from each of the Se0 and PMN clusters, using a synaptic threshold of 2. Ranking index (RI) shows the relative synaptic strength of every connection compared to the total synaptic input of the output neuron. **(D)** Quantification of alternative N-hop connections for each monosynaptic sensory-to-target connection. Paths are calculated for one cell from each of the output neuron clusters using a synaptic threshold of 2.

mNSCs reconstructed by (Schlegel et al., 2016) were added. In total, 363 neurons were analyzed to determine whether they are used as alternative routes for sensory-to-output connections (**Fig 4.30 B**).

The basic strategy is illustrated in **Fig 4.31 A**. In **Fig 4.31 B,C**, a target neuron from each Dilps, DMS, DH44, Se0ens and PMN cluster was selected, and all sensory neurons that make monosynaptic connections (1-hop) with at least two synapses were listed. Using the same threshold, all possible di-synaptic paths (2-hop) to reach the same target were mapped. The degree illustrates how often a particular interneuron is used for the different possible converging paths (‘degree’ of convergence). Further, the relative synaptic strengths of the connection among the various paths were calculated (‘ranking index’ of 1.0 represents highest synaptic strength from all possible to the output neuron). Several properties are revealed: (1) different sensory neurons make monosynaptic contacts to a common output target (2) each output neuron can be reached from a given sensory neuron by multiple routes through the use of different interneurons (3) a given interneuron can receive inputs from different sensory neurons to target the same output neuron; this would fit the definition of the ‘common path’ that Sherrington described (Sherrington, 1906). These observations hold true for the majority of examined monosynaptic sensory-output pairs (**Fig 4.31 D**). However, a correlation between the relative synaptic strength and the commonness of the respective paths (i.e., how often a path is used) could not be shown (**Fig 4.34 B**).

A potential functional consequence of such circuit architecture can be seen if all sensory inputs onto the interneurons are included. As an example, **Fig 4.32 A** shows ‘Dilp 1L’ as a

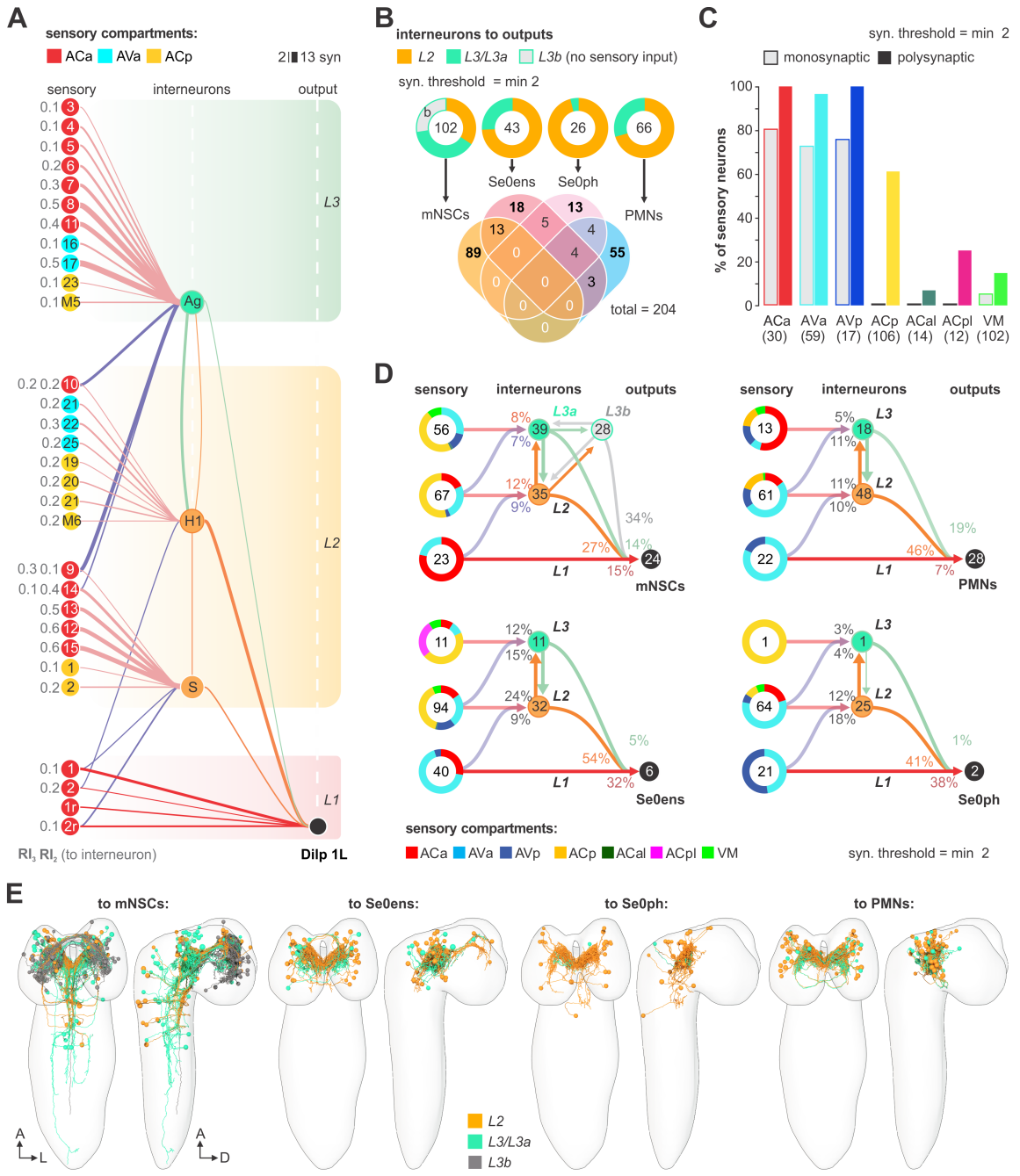

FIGURE 4.32. Integration of polysynaptic connections onto monosynaptic circuits. (A) Superimposition of selected 2- and 3-hop paths. Layer 1 (L1) shows a basic sensory-to-Dilp circuit. Layer 2 (L2) represents alternative paths through directly (2-hop) connected interneurons ('S' and 'H1/huginPC left 1') and their sensory inputs; using a synaptic threshold of 2. Both interneurons integrate a completely different set of sensory neurons from different sensory compartments to connect onto the basic sensory-to-Dilp circuit. Layer 3 (L3) represents paths through indirectly connected interneurons ('Ag') and their sensory inputs, using a synaptic threshold of 2. This interneuron receives sensory information from layer 2 and also integrates a completely different neurons onto the basic sensory-to-Dilp circuit. Ranking index (RI) shows relative synaptic strength of every sensory-to-output connection compared to the total synaptic input of the interneurons. RI_2 and RI_3 are the ranking indices for layer 2 and layer

3 interneurons, respectively. **(B)** Number of different interneurons to respective output neuron classes (mNSCs, Se0ens, Se0ph and PMNs), using a synaptic threshold of 2. Interneurons are divided into two groups. Layer 2 (L2) represents interneurons that act as alternative paths (2-hop). Layer 3 (L3) is divided into interneurons which receive monosynaptic sensory inputs (L3a) and those which do not receive monosynaptic input from any sensory neuron (L3b). Percentage (outer circle) represents proportion of L3, L3a and L3b interneurons per group. Venn diagram shows overlap and difference between presynaptic interneurons of the different target groups. **(C)** Percentage of sensory neurons of the respective sensory compartment forming monosynaptic circuits (monosynaptic) compared to percentage of sensory neurons integrated by L2 and L3 interneurons (polysynaptic), using a synaptic threshold of 2. **(D)** Summarizing representation of all monosynaptic sensory-to-output connections (grouped targets: mNSCs, Se0ens, Se0ph and PMNs), and their alternative paths through interneurons to reach one cell of the target group, using a synaptic threshold of 2. Note that nearly all alternative paths (interneurons) of layer 2 and 3 (L2, L3) receive monosynaptic input from other sensory neurons (synaptic threshold = 2), thus integrating a completely different set of sensory neurons onto the basic reflex circuits. Percentages represent fraction of synapses from upstream neurons (arrows). Numbers within circles represent number of neurons. Percentage sensory composition (the three left donut circles) is shown by sensory compartment. **(E)** EM reconstruction of all interneurons that as paths to the different output neuron classes. Neurons are colored based on path layers to respective output neurons.

common output, and the interneurons ‘H1’ (a huginPC neuron) and ‘S’ (not previously described) as two of the polysynaptic paths (layer 2) onto the common output. One consequence of such superimposition is that the amount of sensory information that can reach a common output neuron can be significantly increased. In this case, the Dilp 1L neuron, in addition to receiving inputs from four sensory neurons (from monosynaptic paths, layer 1), now receives inputs from seven new sensory neurons through the interneuron ‘S’, and eight new sensory neurons from interneuron ‘H1’. Furthermore, these additional sensory neurons derive from new peripheral regions (e.g., pharyngeal ‘ACp’ in addition to enteric ‘ACa’ and ’AVa’). Note also that the two interneurons themselves interact, thus increasing the number paths available between any sensory-output pair (also see **Fig 4.33**). The interneurons could also sharpen sensory information by inhibiting parallel pathways, for example through feed-forward inhibition. Another circuit layer comes into play when tri-synaptic (3-hop) paths are analyzed (**Fig 4.32 A**, layer 3). For example, the interneuron ‘Ag’ (not previously described) brings in a different set of new sensory inputs that converge onto a comon target (Dilp 1L). In addition, it receives sensory inputs from layer 2 sensory neurons.

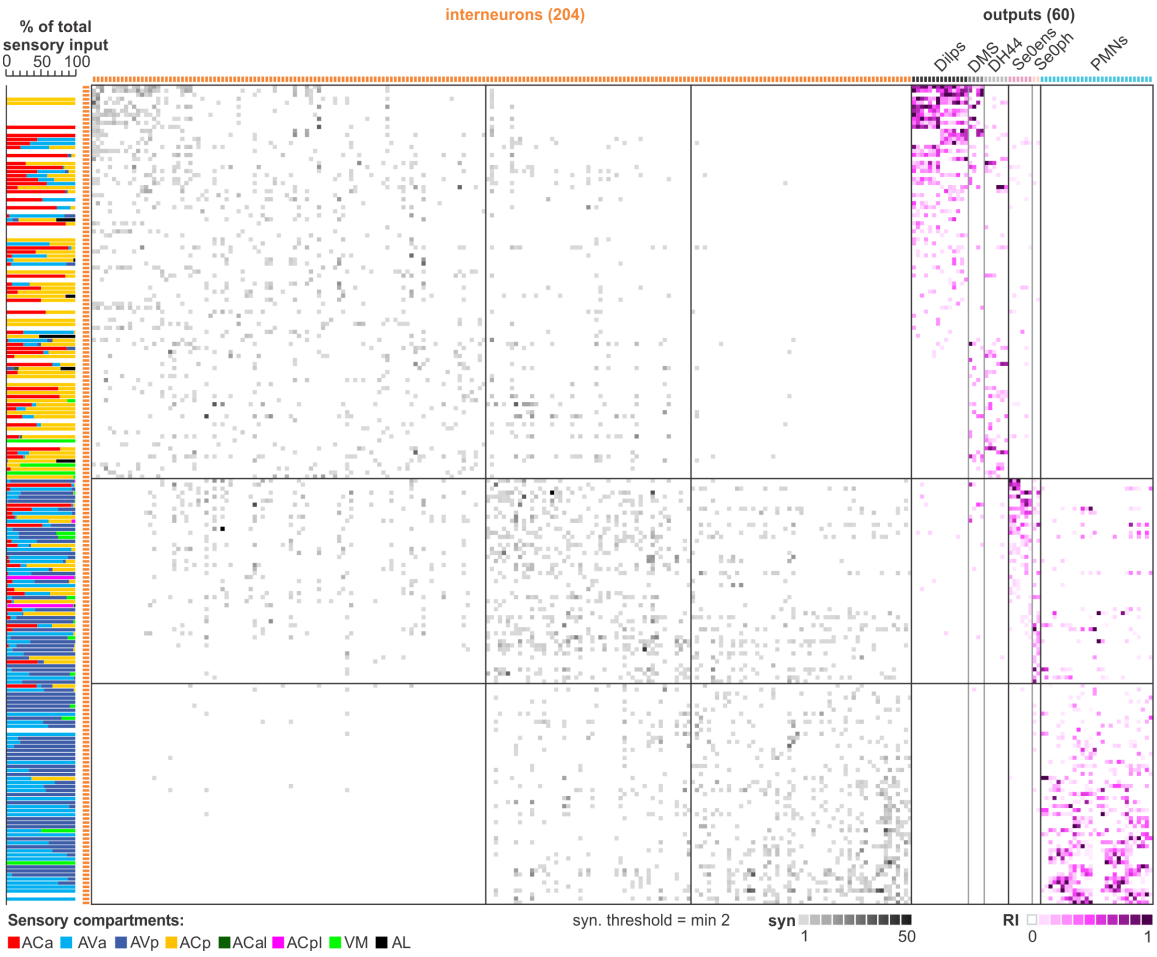

FIGURE 4.33. Connectivity of interneurons within the feeding circuits. Adjacency matrix showing all 204 'layer2 – and 'layer 3' interneurons, their sensory inputs and their connections to the mNSCs, Se0ens, Se0ph and PMNs. Left panel represents the percentage sensory composition (as shown by sensory compartments) of the total sensory input of each interneuron. Interneuron-to-interneuron connections (orange): each entry represents the number of synapses from a row to a column neuron. Interneurons are arranged by their connectivity to the output target groups. Ranking index (RI) for interneuron-to-ouput connections shows the relative synaptic strength of every connection compared to the total synaptic input of a single output neuron (1.0 represents the highest from all possible inputs to the output neuron).

Thus, a circuit architecture is observed where new interneurons that target the same output neurons are successively layered, and which receive sensory input from the previous layer as well as from completely new set of inputs. Extending this to the full set of feeding output neurons (mNSCs, Se0ens, Se0ph and PMNs) illustrates the increase in the interneuron number used as alternative paths, in the sensory neuron number and in the peripheral origin that can be gained by integrating polysynaptic connections onto monosynaptic reflex circuits (**Fig 4.32 B,C,D; Fig 4.33**). For example, monosynaptic paths to the mNSCs would

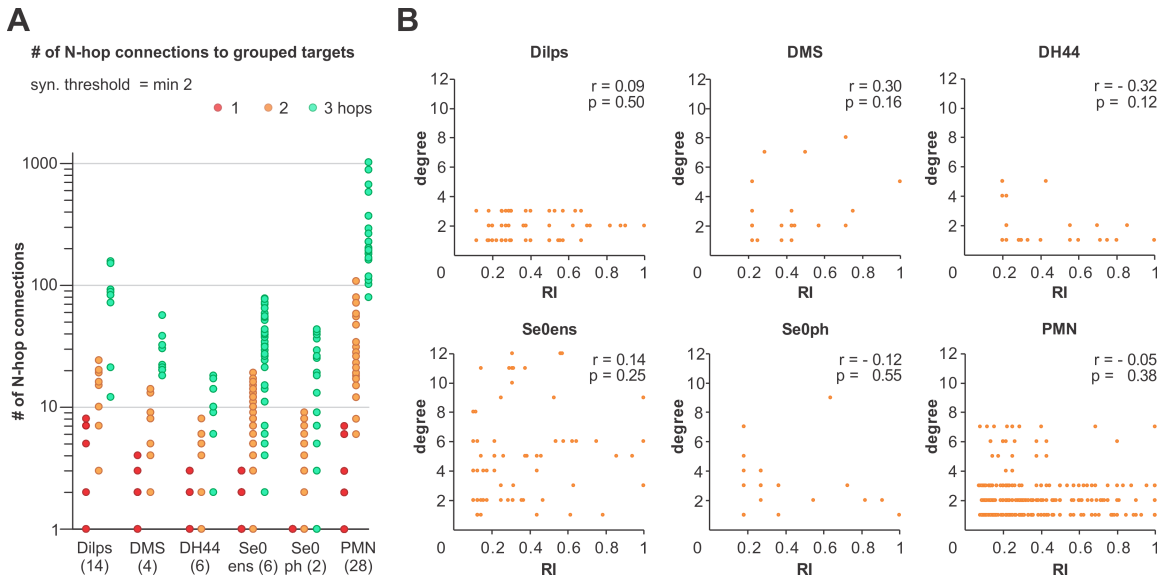

FIGURE 4.34. Quantification of alternative paths onto output neurons. (A) Number of alternative N-hop connections for each monosynaptic sensory-to-target connection. Paths are calculated for grouped targets. Paths to PMNs are calculated on a to 70% reconstructed CNS. (B) Relationship between degree (frequency of use as alternative path) and ranking index of the different presynaptic interneurons of the different target groups. R = Pearson's r, p = p value.

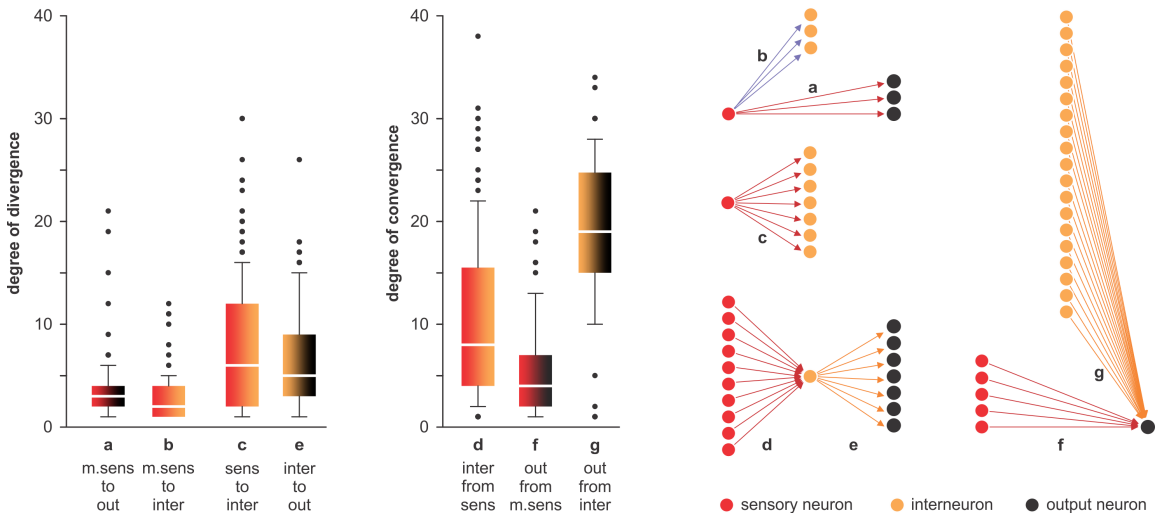

FIGURE 4.35. Degree of divergence and convergence within the feeding circuits. (Left) Quantification of divergent and convergent connectivity levels for monosynaptic sensory neurons (m.sens), sensory neurons (sens), interneurons (inter) and output neurons (out) based on the connectivity maps in **Fig. 4.33** and **Apendix, Fig A.1 – A.3** (no synaptic threshold). Degree represents the in-degree and out-degree of single node which are defined as the number of afferent and efferent edges respectively. Neurons without synaptic contacts to respective neurons within the feeding network were excluded from analysis. (Right) Schematics of mean divergence and convergence degrees for every individual neuron type.

only allow sensory inputs from enteric origin, whereas polysynaptic paths would allow sensory inputs from enteric, pharyngeal and external origins. Note that nearly every synaptic upstream partner of the Se0 and PMN cluster (synaptic threshold = 2) receives monosynaptic input from sensory neurons, each with an individual sensory profile (composition of sensory input). This does not apply to 27 percent of the synaptic upstream partners of the mNSCs. Here, layer 3 is divided into interneurons which receive monosynaptic sensory inputs (L3a) and those which do not receive monosynaptic input from any sensory neuron (L3b) (**Fig 4.32 B,D,E; Fig 4.33**), suggesting that these interneurons integrate sensory independent information onto the mNSCs.

So far, the analysis of the network was based on the shortest paths between inputs and outputs. Proceeding from this, all reconstructed upstream partners (premotor neurons) of the output neurons and their synaptic input from sensory neurons could be layered in relation to the monosynaptic input-to-output connections resulting in a compact circuit motif **(Fig 4.32 D)**. To further describe the structure and connectedness of the feeding network **(Fig 4.33)**, the degree of divergence and convergence was quantified for every individual neuron type (sensory neuron, interneuron, output neuron) **(Fig 4.35)**. In detail, a sensory neuron makes synaptic contact to three output neurons on average (mean=3.5, SD=3.1). The same sensory is connected to three interneurons on average (mean=3.0, SD=2.3). In general, sensory neurons diverge onto seven interneurons on average (mean=7.5, SD=6.4). An interneuron in turn receives synaptic input from ten sensory neurons (mean=10.4, SD=7.8) and is connected to seven output neurons on average (mean=6.6, SD=4.8). Finally, a single output neuron receives synaptic contacts from five sensory neurons (mean=5.5, SD=4.8) and 19 interneurons on average (mean=18.8; SD=7.7).

4.8 Integration of mushroom body associative memory circuits onto the feeding circuits

Finally, this study tackles the question whether and how any output neurons of the mushroom body (MBONs, Eichler et al. 2017) connect to the feeding circuits. In other words, do the MBONs target any of the interneurons that comprise the different layers of the feeding circuits, that in turn target the outputs (see **Fig 4.32 D**). Therefore, all MBONs described in Eichler et al. 2017 were analyzed for outputs to the alternative path layers identified in

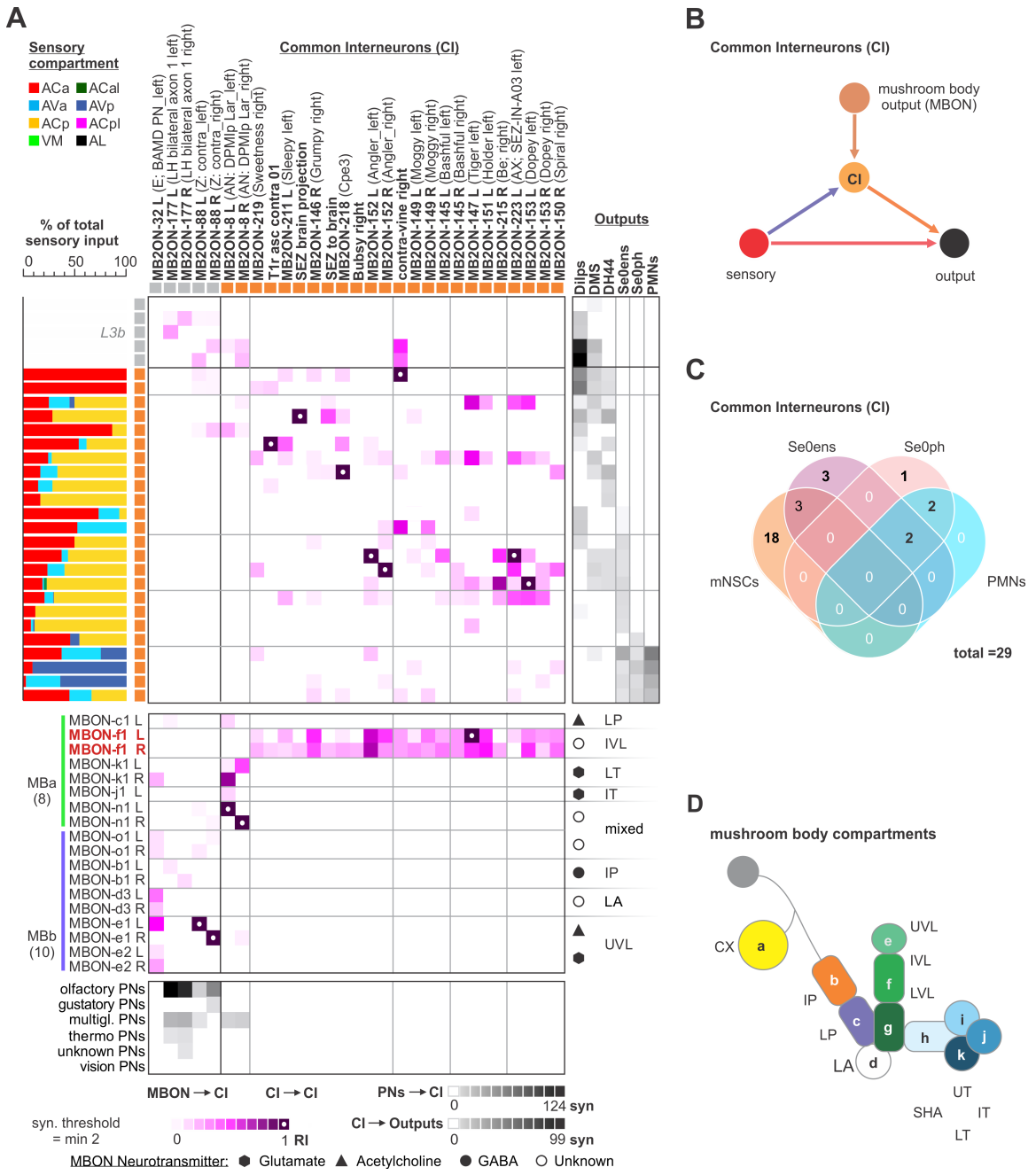

FIGURE 4.36. Connectivity of mushroom body output neurons onto the feeding circuits I. (A) Connectivity matrix showing connections between projection neurons to the MB calyx (PNs), mushroom body output neurons (MBONs), common interneurons (CI) and output neurons (mNSCs, Se0ens, Se0ph and PMNs). Left panel represents the percentage sensory composition (shown by sensory compartment) of the total sensory input to each CI. 5 of the CIs (L3b) do not receive monosynaptic contacts from sensory neurons. Each entry for MBON-to-CI and CI-to-CI connections represents the ranking index (RI). Ranking index (RI) shows the relative synaptic strength of every connection compared to the total synaptic input of a single interneuron. Each entry for PN-to-CI and CI-to-output connections represents the number of synapses from a row to a column neuron. CIs are arranged by their connectivity to the output target groups. MBONs are divided into two groups: MBa, 8 MBONs which primarily

synapse onto interneurons that receive monosynaptic contacts from sensory neurons and MBb, 10 MBONs which synapse onto interneurons that do not receive monosynaptic sensory input. **(B)** Illustration of direct (1-hop) sensory to output neuron connections and indirect (2-hop) paths which connect mushroom body output neurons (MBONs) to reach the same output neuron, thus representing final common interneurons (CI). **(C)** Venn diagram shows overlap and difference between presynaptic common interneurons of the different target groups. **(D)** Schematic of the different larval mushroom body compartments. Calyx (CX), intermediate and lower penduncle (IP, LP), lateral appendix (LA), upper, intermediate and lower peduncle (UVL, IVL, LVL), shaft, upper, intermediate and lower toe of the medial lobe (SHA, UT, IT, LT) (Eichler et al., 2017; Saumweber et al., 2018). These abbreviations are used in (A).

Fig 4.36). Only 18 of 48 MBONs make monosynaptic contacts to 29 interneurons that target the different output neuron groups (**Fig 4.36 A,B**). The MBONs have been divided into two groups. One group of 8 MBONS (MBa) making synaptic contacts to sensory information integrating interneurons and the other (MBb), making synaptic contacts to those interneurons (L3b) that do not receive monosynaptic contacts from sensory neurons (see **Fig 4.32 B,D,E; Fig 4.33**). Strikingly, the MBON-f1 of the MBa (the only MBON with projections to the SEZ) makes monosynaptic connections to a large number of interneurons that target all classes of feeding output neurons (**Fig 4.36 A**). Furthermore, this MB module (consisting of ORNs, projection neurons to the Kenyon cells and MBONs) can be placed on top of the existing feeding circuits, since the interneurons targeted by MBON-f1 are shared by those that comprise the previous layers of the feeding circuit (**Fig 4.37**). This MBON may thus be representative of a 'psychomotor' neuron described by Cajal **(see Fig 1.1)** (Ramón y Cajal 1894; see also Swanson 2011), which acts higher and in parallel to a reflex circuit.

In addition, a similar divergent and reconvergent architecture can be observed for all PNs (except vision PNs) targeting L3b interneurons which in turn target the mNSCs. In this case, the mushroom body (Calyx and MBONs) can be placed, in turn, on top of the existing monosynaptic pathways from PNs to L3b interneurons and may act here as well as a parallel and alternative processing route.

In summary, this work proposes that the different path possibilities allow different strength and combination of sensory inputs to be integrated and evaluated, which would then determine which synaptic path will dominate to a given output. Such multisensory integration via multiple parallel pathways would be necessary to make sense of a complex, multimodal world, and to better choose a behavioral response.

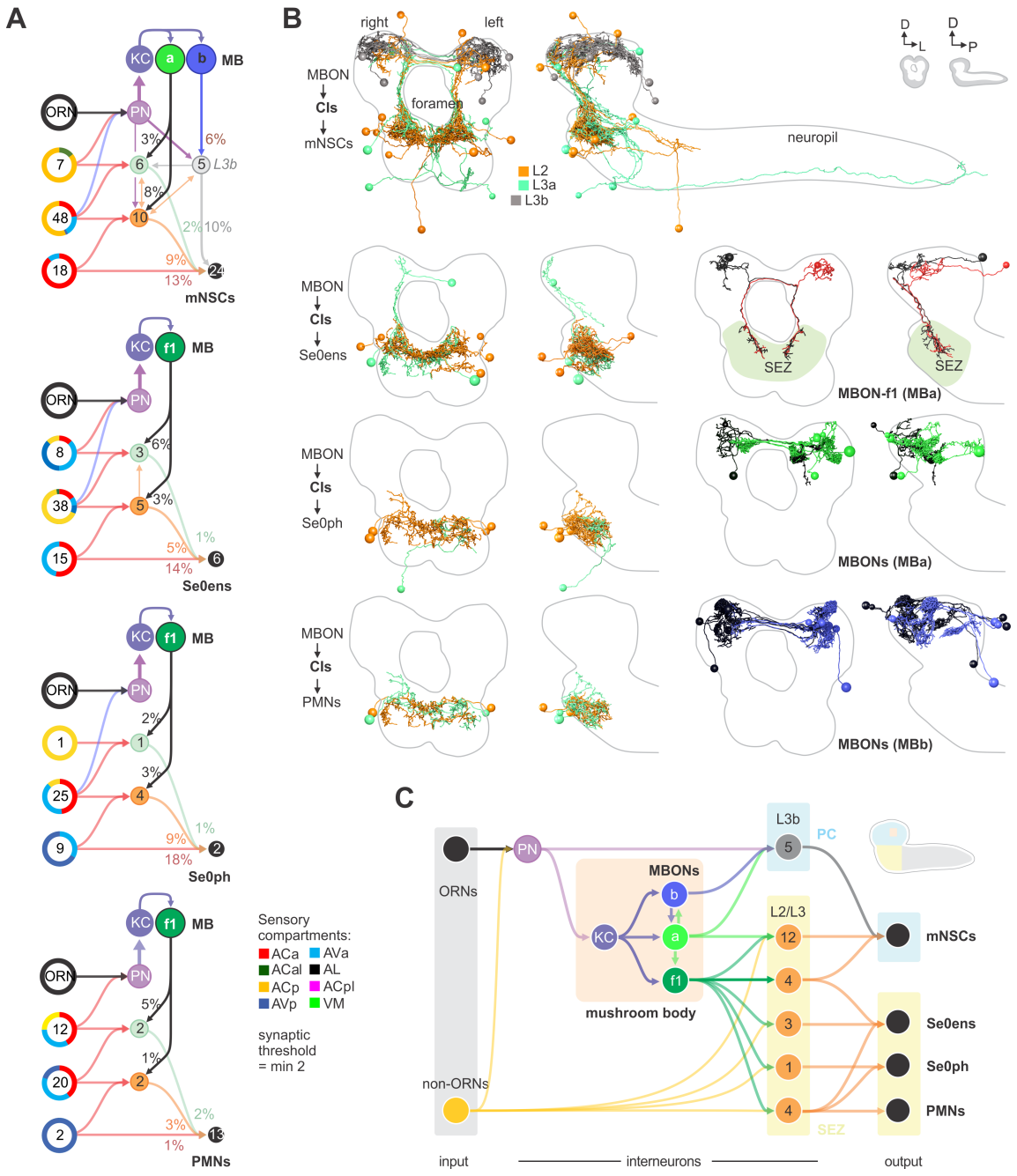

FIGURE 4.37. Connectivity of mushroom body output neurons onto the feeding circuits II. (A) Representation of all common interneurons to mNSCs, Se0ens, Se0ph and PMNs that receive monosynaptic input from MBONs. Exclusive sensory-to-output connections are not shown. Note that the PNs to the calyx (PN) also act as part of 3-hop paths from olfactory, layer 2 and layer 3 sensory neurons to the mNSCs. The MBON-f1 (IVL) connects to a wide range of interneurons that essentially target all feeding output neurons. Percentages represent fraction of synapses from MBONs to Cis and Cis to outputs. Numbers within circles represent number of neurons. Percentage sensory composition (the four left donut circles) is shown by sensory compartment. **(B)** EM reconstruction of all common interneurons (Cis) to mNSCs, Se0ens, Se0ph and PMNs that receive monosynaptic input from MBONs. Neurons are color coded based on path layers to respective output neurons. EM reconstruction of all

MBONs which target interneurons that connect to the feeding output neurons. Note that MBON-f1 is the only MBON with projections to the SEZ. MBONs are divided into two groups. MBa, which primarily synapses onto interneurons that receive monosynaptic contacts from sensory neurons and MBb, which synapses onto interneurons that do not receive monosynaptic sensory input. **(C)** Summarizing connectivity graph of all paths from olfactory and non-olfactory sensory neurons to mNSCs, Se0ens, Se0ph and PMNs. Common interneurons are grouped dependent on their downstream targets (outputs). Numbers within circles represent number of neurons.

CHAPTER 5

DISCUSSION

5.1 A feeding connectome

Almost every organism is faced with the problem of making the right decisions. This ranges from evaluation and integration of information to selection of the right action leading to an appropriate behavior. Often, these processes are also guided by past experience. In other words, decision-making involves interaction between many brain systems: sensory, sensory processing, learning and memory, and premotor and motor systems (Barron et al., 2015). Feeding as one of the most fundamental behaviors of animals involves all these neuronal systems. Nearly all of them are located within the subesophageal zone (SEZ) of *Drosophila*, a brain region analogous to the vertebrate brainstem (Ghysen, 2003). Although the SEZ has been studied on various levels of analysis (Colomb et al., 2007; Hartenstein et al., 2017; Kendroud et al., 2017; Kwon et al., 2011; Schlegel et al., 2016; Schoofs et al., 2014a; Scott, 2018), a circuit map for feeding connecting all sensory inputs to motor outputs could not be constructed so far.

On that account, the objective of this study was to provide a comprehensive synaptic map of sensory and output neurons that underlie food intake and metabolic homeostasis in *Drosophila* larva **(Fig 5.1)**. This included a complete EM reconstruction of all neurons connecting the brain with anterior sensory organs, feeding related muscles and the enteric

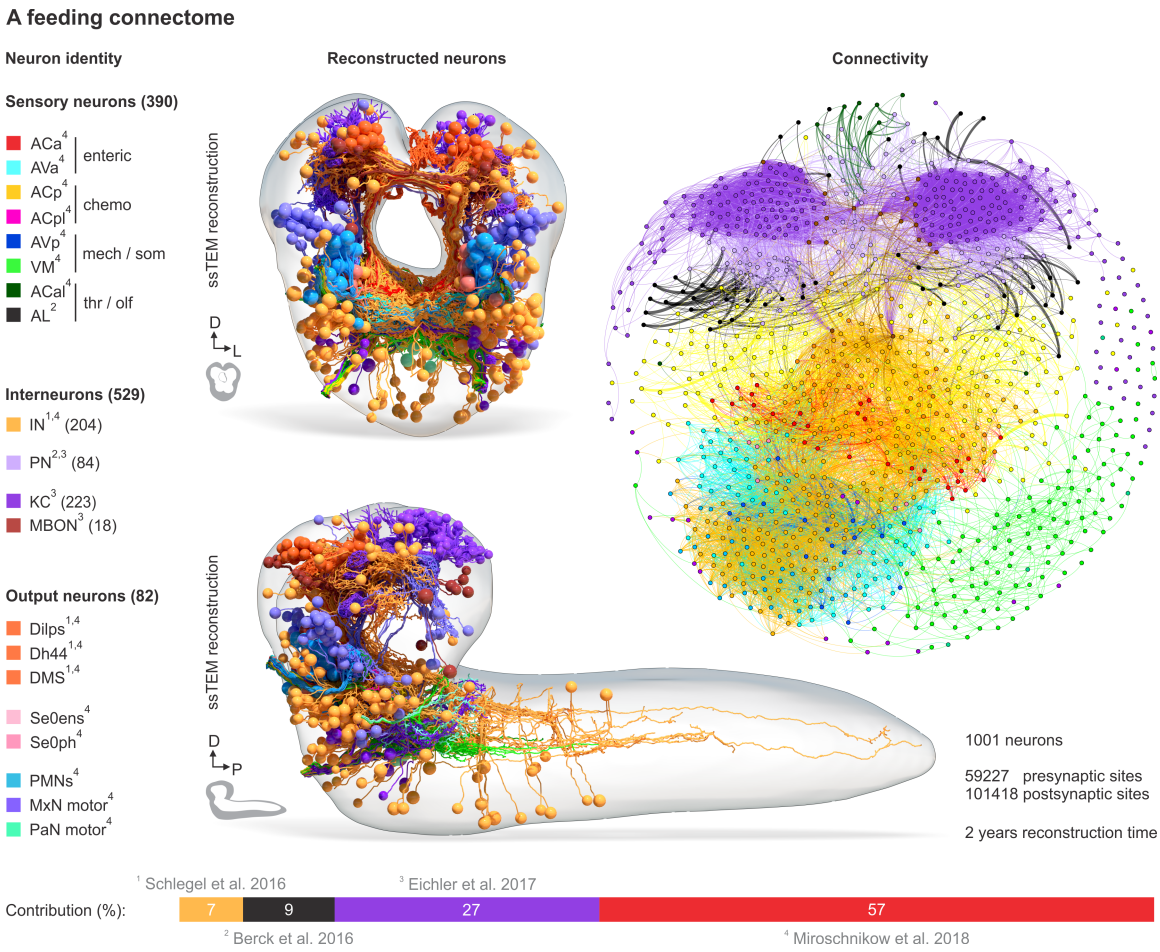

FIGURE 5.1. A feeding connectome. (Middle panel) EM reconstruction of all neurons used in the present study. Neurons are color coded based on their identity (left panel). Sensory neurons are grouped by synaptic compartments and origin or likely type (enteric = enteric nervous system, chemo = pharyngeal and external chemosensory neurons, mech /som = pharyngeal and external mechano- and somatosensory neurons, thr / olf = thermosensory- and olfactory receptor neurons). Interneurons that act as parallel paths to the different output neuron classes (IN). Projection neurons to the calyx (PN). Kenyon cells (KC) and mushroom body output neurons (MBON). Feeding related output neurons: median neurosecretory cells (mNSCs), modulatory serotonergic output neurons (Se0ens and Se0ph) and feeding motor neurons (PMNs, MxN motor and PaN motor). The numbers in parenthesis represent number of respective neurons. Index numbers refer to studies that published respective neurons (Berck et al., 2016; Eichler et al., 2017; Miroschnikow et al., 2018; Schlegel et al., 2016). (Right panel) A connectivity diagram of 1001 sensory, output and interneurons. Neurons are color coded based in their identity. (Lower panel) Percentage contribution of respective studies.

nervous system through the three pharyngeal nerves of the *Drosophila* larva. Applying a morphological clustering algorithm to the reconstructed neurons demonstrated that the SEZ can be divided into smaller, putative functional units: seven topographical distinct

sensory compartments subdividing the SEZ based on modality and peripheral origin **(Fig 5.2)**. Comparing sensory neurons connectivity with their peripheral origin showed that sensory neurons forming monosynaptic connections to feeding related output neurons are mostly of enteric origin, and are distinct from those that form multisynaptic connections to the mushroom body memory circuit.

Finally, the presence of different polysynaptic connections which are superimposed on the monosynaptic input-output pairs that comprise the reflex arc gives rise to a compact circuit architecture that may be used for controlling feeding and other instinctive behaviors **(Fig 5.3 – 5.4)**.

5.2 Architecture of the larval brainstem

5.2.1 Sensory input compartments

A common feature of the central nervous system is the structural division in different domains which can be observed even at the level of external appearance. Each domain can be further subdivided in a multitude of segments, compartments or nuclei based on different structures and functions. Well described examples in which structure follows function are the olfactory bulbs in vertebrates and the antennal lobes in insects. In both cases, the basic organization of the olfactory projection relies on the convergence of sensory axons that share the same olfactory receptor onto a single projection center - a glomerulus (Ghysen, 2003; Hildebrand and Shepherd, 1997). Other sensory projections like the somatosensory systems were also shown to converge in a topological and modality-specific manner in different subregions of the brain of flies and mammals (Abraira and Ginty, 2013; Sakurai et al., 2013; Tsubouchi et al., 2017). Numerous studies in *Drosophila* proposed similar structural and functional compartmentalizations of the SEZ based on fiber tracts, secondary lineages, gustatory and mechanosensory receptor expression (Chen and Dahanukar, 2020; Colomb et al., 2007; Gendre et al., 2004; Hartenstein et al., 2017; Kwon et al., 2011). This is further supported by the fact, that the SEZ sensory projections do not follow a metameric scheme which is in contrast to the overall organization of the insect sensory system (Kendroud et al., 2017). In agreement with this, the sensory compartments described in the present study propose a glomeruli-like organization of the SEZ based on the similarity in distribution of sensory neuron synaptic sites and their broader peripheral origin and sensory modality.

The primary gustatory center (ACp), which resembles the “primary taste center” of Colomb et al., 2007 and the “anterior central sensory column” of Kendroud et al., 2017 is a prime example for such a modality-specific convergence zone defined by afferents of at least six different external and pharyngeal chemosensory organs projecting through four nerves to the SEZ. Within this compartment, we observe a layered organization in which pharyngeal sensory inputs are found anteriorly and external sensory inputs found posteriorly. This suggests a somatotopic organization of sensory projections within the compartment which in turn would allow the larva to distinguish between different locations of food and taste during food intake. Furthermore, it would be reasonable to investigate if this segregated projection fits to a more functional ‘chemotopic’ organization in the SEZ.

The primary gustatory center is laterally flanked by the ACpl sensory projections. They form a to-date undescribed sensory compartment in the larva which is likely comparable to the antenno-subesophageal tract (AST) in adults (Ito et al., 2014). In the context of the present study, the ACpl neurons make synaptic contacts exclusively to the multiglomerular projection neurons to the Calyx and the lateral horn (Berck et al., 2016).

The sensory projections from the foregut and enteric nervous system form two adjacent but distinct compartments (ACa and AVa) in the tritocerebral neuropil, anterior to the primary gustatory center (ACp), and resemble the “anterior ventral sensory column” described by Kendroud et al., 2017. These two sensory compartments consists of internal sensory projections that mediate metabolic and non-nutritive signals from all enteric ganglia and foregut structures to regulate feeding in *Drosophila* (Copenhaver, 2007; Mishra et al., 2013; Miyamoto and Amrein, 2014; Olds and Xu, 2014). The prominent monosynaptic input from ACa and AVa sensory neurons onto median neurosecretory cells and pharyngeal motor neurons, respectively, suggests a segregation of enteric chemo- and mechanosensory projection. Conceivably, the ACa could comprise all internal chemosensory and the AVa all internal mechanosensory neurons. A similar adjacent but distinct organization has been shown for central representation of nutrient-responsive GPR65 and vagal mechanoreceptive GLP1R afferents in the NTS of mice, suggesting engagement of different neural circuits (Williams et al., 2016).

Mechanoreception is the least well understood among feeding-related sensory modalities. In addition to gustation, physical properties like the texture of food are critical factors

affecting food preference in vertebrates and invertebrates (Jeltema et al., 2015; Kudow et al., 2019; Sako et al., 2002; Sánchez-Alcañiz et al., 2017). Several studies reported the existence of mechanosensory neurons in taste organs in the head of *Drosophila* larva (Apostolopoulou et al., 2015; Rist and Thum, 2017; Singh and Singh, 1984). However, the central representation and circuits mediating mechanical properties of food are unknown. In adult flies, nompC, a TRP-family mechanosensory channel localizes to the sensory dendrites of neurons housed within gustatory sensilla in the labellum and was suggested to be required for food texture preference. The projections of these neurons innervate a ventral region in the SEZ which is adjacent but discrete from those of any class of gustatory neurons (Sánchez-Alcañiz et al., 2017). In the larva, the AVp sensory compartment, which is ventral and adjacent to the primary gustatory center (ACp), could represent a convergence zone of such taste organ specific mechanosensory neurons, which in turn suggests a segregation of pharyngeal and external chemo-and mechanosensory projection. This assumption is further underpinned by the striking direct synaptic input of serotonergic modulatory and pharyngeal motor neurons from AVp sensory neurons.

Compared to the other sensory compartments discussed here, the ventromedial sensory compartment (VM) is the largest and stretches from the labial and maxillary neuromere of the larval SEZ deep into the neuropil of the VNC. The VM sensory projections enter the brain through all three pharyngeal nerves except the enteric bundle of the antennal nerve. This sensory compartment corresponds to the "ventromedial sensory column" described by Kendroud et al., 2017 and houses terminal arborizations of mechanosensory trichoid, campaniform sensilla, subepidermally located multidendritic neurons and so far unidentified mechanosensory neurons from the larval head.

The ACal sensory compartment at the posterior surface of the antennal lobe is the smallest among the seven synaptic compartments. It contains terminal arborizations of three thermosensory neurons from the dorsal organ ganglion. These neurons are required to navigate along temperature gradients towards preferred temperatures (Apostolopoulou et al., 2015; Klein et al., 2015).

5.2.2 Feeding related output compartments

The feeding related output neurons of larval *Drosophila* have been characterized partially in several studies (Hückesfeld et al., 2015; Schlegel et al., 2016) using dye backfills (PMNs),

electrophysiological recordings (PMNs, MxN and PaN motor) and EM reconstruction (mNSCs). The present work provides a complete EM based neuron and synapse reconstruction of the median neurosecretory cells (mNSCs), modulatory serotonergic output neurons (Se0ens and Se0ph) and feeding motor neurons (PMNs, MxN motor and PaN motor). The dendritic arborizations and nearly non-overlapping synapse compartments of the different output neuron classes show a varying and non-metameric organization in comparison to the motor neuropils of the ventral nerve chord of the larva (Fushiki et al., 2016). For example, the synapses of the mNSCs form two elongated bilateral compartments extending from the dorsal surface of the protocerebral neuropil down to the SEZ. In accordance with other neuroanatomical studies in *Drosophila* (Kendroud et al., 2017), the dendrites of the Se0 and PMNs locate around the nerve entry points of the antennal nerve. Their synaptic compartments are organized in compact layers and form, together with the MxN and PaN motor compartments, a continuous shell along the ventrolateral surface of the neuropil.

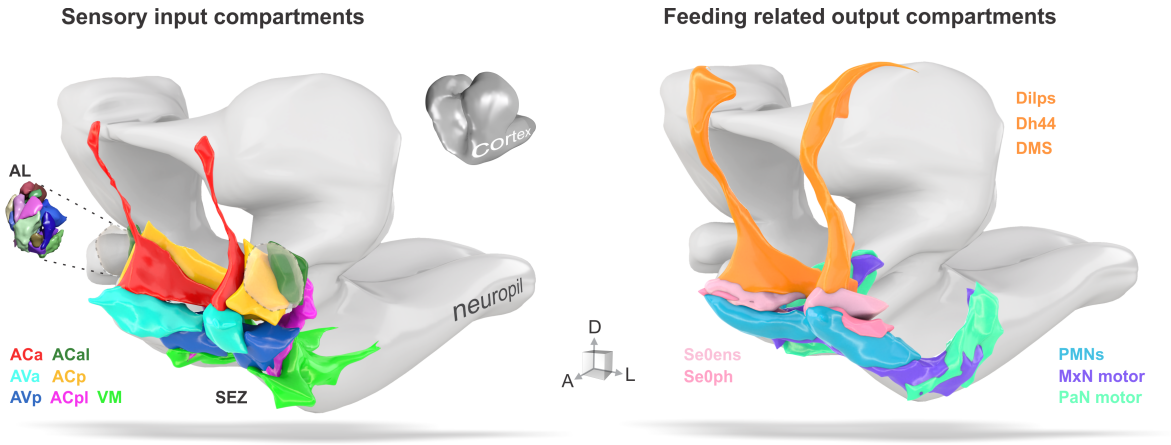

FIGURE 5.2. Input-output synaptic organization of the larval feeding system. Sensory input compartments: Glomerular compartmentalization of the larval antennal lobe (AL) compared to the glomerular-like compartmentalization of the subesophageal zone (SEZ). Non-overlapping digital 3D model delineates likely modality specific compartments based on synapse similarity score. Feeding related output compartments: 3D model summarizes the synaptic compartments of median neurosecretory cells (mNSCs), modulatory serotonergic output neurons (Se0ens and Se0ph) and feeding motor neurons (PMNs, MxN motor and PaN motor). Figure modified from Miroschnikow et al., 2018

In summary, the compartmentalization of the sensory and motor neuropil based on synapse similarity may illustrate and confirm a fundamental structural organization principle of the larval subesophageal zone (Kendroud et al., 2017), which may help to unravel

the complete encoding of complex behaviors like feeding from perception to action (see **Fig 5.2** for a summarized representation of all sensory input – and feeding related output compartments). Regardless, to underpin these findings, future work should continue to examine the central and peripheral projection patterns of feeding related sensory and output neurons, respectively. In this context, the existing lack of specific genetic driver lines to identify reconstructed neurons could be an obstacle, which, however, with the current state of art, could be overcome easily by an EM volume of an entire animal.

5.3 Intersensory communication

EM reconstruction of all sensory neurons of the three pharyngeal nerves showed a high number of monosynaptic connections between sensory neurons within the central sensory compartments. These synaptic connections are to a lesser extend reciprocal and in that appear to establish a hierarchy. Their influence is likely to be considerable, as they provide a major input to the axons of sensory neurons in the enteric, primary gustatory and somatosensory compartments. Interestingly, within a given compartment, synaptic connections are made even between sensory neurons from different nerves, further supporting the concept of convergence zones discussed before and suggesting that similar sensory modalities from different peripheral origins influence each other. Assuming that the synaptic connections are excitatory and hence facilitate each other, they could be a way of amplifying a specific sensory signal (via entrainment) or in case of connections between different sensory neurons (different sub-modalities) even a form of early sensory processing.

By contrast, very few monosynaptic connections exist between the larval olfactory, chordotonal or nociceptive class IV sensory neurons (Gerhard et al., 2017; Jovanic et al., 2016; Ohyama et al., 2015). There is, however, a much higher percentage of intersensory connections between olfactory receptor neurons in adults as compared to the larva. These could function in gain modulation of low signal intensities (Tobin et al., 2017). This might be a consequence of adult flies navigating larger areas hence requiring higher sensory sensitivity and faster processing of olfactory information during flight (or mating), and/or to reduce the metabolic costs of information processing (Niven and Laughlin, 2008).

A connectomic study of the posterior nervous system of the *C.elegans* adult male reported monosynaptic connectivity among sensory neurons as well. Around 60 % of all

sensory neurons are reciprocally and recurrently connected by both chemical and gap junctions suggesting an amplification of input signals through loop gain (Jarrell et al., 2012).

Intersensory communication has also been studied in the moth *Manduca sexta* in the context of gustation. Here, electrophysiological experiments showed that individual tastant chemicals are represented as unique temporally structured patterns of spiking activity distributed across populations of receptor neurons (Reiter et al., 2015) which is inconsistent with a basic taste model of gustation (labeled line connectivity) or basic taste categories such as sweet, salty bitter and sour (Erickson, 2008, 1984). In this context, synaptic intersensory connections may help to enhance spatiotemporal integration and regulate the impact of specific sensory signals. Whether this also applies to the intersensory connections between the different types of sensory neurons in *Drosophila* remains to be determined.

5.4 Elemental feeding circuits

A complex, adaptive and goal-directed behavior like feeding is a coordinated composition of elemental behavioral acts based on the dualism of stimulus and response. The simplest and fastest form of stimulus response mechanisms are reflex actions. Further, the neuronal circuits of reflexes represent the most basic circuit architecture of the nervous system, whose anatomical and physiological foundations were laid down by Cajal and Sherrington (Ramón y Cajal, 1894; Sherrington, 1906; Swanson, 2011).

One of the key findings of the present study was the existence of monosynaptic connections between feeding relevant sensory and output neurons. The output neurons consist of motor neurons innervating muscles that drive pharyngeal pumping and two clusters of serotonergic neurons innervating the pharyngeal muscles and the entire enteric nervous system. The outputs also include the neuroendocrine cells that target the endocrine organs. The vast majority of output neurons are targeted monosynaptically from a set of the described sensory compartments in an overlapping manner: the ACa targets all neuroendocrine cells as well as the serotonergic neurons; the AVa targets a subset of neuroendocrine cells, the serotonergic neurons and most of the pharyngeal motor neurons; the AVp targets the serotonergic neurons and a different set of pharyngeal motor neurons.

5.4.1 Motor neurons

The pharyngeal motor neurons and their repetitive, stereotyped motor program are a core feeding component controlling food transport into the esophagus - in other words 'swallowing'. In general, such rhythmic motor output is generated by neural networks called central pattern generators (CPGs) even in the absence of any sensory input or voluntary control (Grillner, 2006; Marder and Bucher, 2001). Nevertheless, reflex control mechanisms - which include sensory feedback - are essential to either induce, modulate and stop the swallowing motor sequence depending on bolus type, size and consistency in the pharynx (Barlow, 2009; Jean, 2001, 1984) or to coordinate the different phases of swallowing (Lang, 2009). In the blow fly *Calliphora erythrocephala*, cibarial pump proprioceptor neurons have been shown to monitor sequential tension of the pharynx and perhaps modulate the rate and type of cibarial pumping through positive and negative feedback to the motor neurons dependend on volume and viscosity of the food (McKellar, 2016; Rice, 1970). However, knowledge about the underlying neuronal circuits is very limited and the cellular components that comprise a feeding CPG have been characterized only in a few instances including the stomatogastric nervous system in crabs (Marder and Bucher, 2007) and the feeding system of the snail *Lymnia stagnalis* (Benjamin and Rose, 1979).

In addition, there are several points of views concerning the involvement of motor neurons in regulating CPG function. It is anticipated that in most of the vertebrate CPGs, motor neurons are just passive output cells (Guertin and Steuer, 2009; Kiehn, 2011, 2006), with the exception of a few spinal circuits in the chick embryo (Wenner and O'Donovan, 2001) and neonatal rodents (Mentis et al., 2005), swimming CPGs in the *Xenopus* tadpole (Roberts et al., 2012) and zebrafish (Song et al., 2016), and *Xenopus laevis* vocal CPG (Lawton et al., 2017) in which premotor rhythms are tuned by motor neuron activity. In several invertebrate CPGs like the stomatogastric ganglion (STG) of lobster and crab or the feeding system of *Aplysia* and *Tritonia*, just to name a few, motor neurons exhibit functional connections with other motor and premotor neurons, thus being an integral part of the circuit (Barkan and Zornik, 2019; García-Crescioni and Miller, 2011; Marder and Bucher, 2007).

Surprisingly, the *Drosophila* larva exhibits a high number of monosynaptic sensorimotor reflex connections that originate from the enteric and pharyngeal mechanosensory compartments AVa and AVp. Further, nearly all sensory neurons of these two compartments are integrated by pharyngeal premotor neurons. Based on this, hypotheses can be

suggested: First, these findings support the view that CPGs for swallowing and the spatio-temporal control of the pharyngeal muscles involved in food intake are modifiable based on mechanosensory stimulus. Second, the decision to swallow or expunge a harmful substance, once in the mouth, may require a very fast and local response. To accomplish this, the CNS has to process information as rapidly as possible and does so by minimizing the number of synaptic relays in any given circuit and parallelizing central computations to avoid neural processing delays (Tuthill and Wilson, 2016a).

The MxN and PaN motor neurons that control mouth hook movements and head tilting, movements which are involved in both feeding and locomotion, also receive a small number of monosynaptic reflex connections that originate from the somatosensory compartment (VM). With this in mind, it is important to note that monosynaptic sensorimotor connections are also found in the larval ventral cord, which generates locomotion - albeit to a lesser degree (unpublished data from Ohyama et al., 2015). An analogous situation exists in *C.elegans*, where the majority of monosynaptic reflex circuits are found in the head motor neurons and not in the body (Yan et al., 2017). One reason could be due to the relative complexity in the response necessary for food intake as compared to locomotion and the potential behavioral contexts of the specific muscle groups. For example, the motor units of the pharynx are primarily used for feeding and swallowing behaviors in invertebrates and additionally for breathing and vocalization in vertebrates. In contrast, the activity of specific body motor units can be common to different foraging, locomotion and escape behaviors and has to be coordinated with respect to the body movements involved. Therefore, it is reasonable to assume that in this context a high number of monosynaptic arcs might be too restrictive for the coordination and the behavioral repertoire. Accordingly, in *Drosophila* larva it was shown that even the selection of the fastest mode of escape locomotion employs multimodal sensory integration via a multi layered circuit (Ohyama et al., 2015).

5.4.2 Serotonergic modulatory neurons

The serotonergic modulatory neurons (Se0) stand out because of the amount of monosynaptic inputs they receive from the sensory compartments. Serotonin is one of the oldest and most widely distributed neurotransmitters and has been implicated in regulating both invertebrate and vertebrate feeding behavior at various levels (Azmitia, 2001; Donovan and Tecott, 2013; Gillette, 2006; Lee et al., 2017; Schoofs et al., 2014b). Recently, Schoofs et al., 2018 showed that serotonergic neurons are part of the feeding motor control in

Drosophila and their neuronal activity and release of serotonin modulates the larval feeding motor pattern. This could be mediated by the monosynaptic sensory contacts to the Se0 cluster. For example, AN motor neurons drive the pharyngeal pump, sensory neurons feedback movement to Se0 leading to an increased response and serotonin release which in turn could facilitate the formation of stereotypic motor patterns of the pharyngeal pump (Bailey et al., 2000; Brunelli et al., 1976; Jacobs and Fornal, 1999; Wallis, 1994). In zebrafish larvae, the serotonergic system was also shown to perform such sensorimotor computations with persistent responses to repeated exposure to sensory feedback indicative of excessive movements, a form of short-term motor learning behavior to increase the effectiveness of swimming (Kawashima et al., 2016).

5.4.3 Median neurosecretory cells

The neurosecretory cells of the pars intercerebralis are a major direct target of sensory neurons. The existence of monosynaptic connections between sensory neurons and median neurosecretory cells has already been shown on the EM level in *Drosophila* larva (Schlegel et al., 2016). However, origin and identity of the sensory neurons had not been determined. The present study now shows that median neurosecretory cells receive monosynaptic input exclusively from enteric sensory neurons. Further, these sensory neuron projections originate, inter alia, from the three enteric ganglia (EG, HCG, PVG) which are in direct contact with the gastrointestinal tissue and concurrently with the hemolymph. Some of these ganglionic sensory neurons express gustatory receptors (Gr28a, Gr43a) and thus may play a role in transmitting post-ingestive information on nutritional quality, metabolic state, and regulating larval food intake.

From an evolutionary perspective, such direct sensory-to-neurosecretory connections may be explained by the 'protoneuron concept', which suggested a phylogenetically old neurosecretory cell type with a binary sensory-neurosecretory function, which may have existed already in the common bilaterian ancestor or even in the common metazoan ancestor (Smith et al., 2014; Tessmar-Raible et al., 2007; Vígh et al., 2004). In *Drosophila*, such primordial binary function might be preserved since in adults, Dilps and DMS releasing cells of the pars intercerebralis directly innervate the enteric nervous system and the gut where they express several receptors to receive various signals from the circulation, fat body or intestine (Dickerson et al., 2012; Hentze et al., 2015; Nässel et al., 2013). However,

larval mNSCs do not innervate the enteric nervous system and may therefore receive monosynaptic input from enteric sensory neurons.

In summary, with the outputs discussed here, one can in principle fulfill the most basic physiological and behavioral needs for feeding: pharyngeal motor neurons for feeding, serotonergic neurons for modulation and stabilization of feeding related motor patterns and neurosecretory cells for metabolic regulation. The set of monosynaptic connections between the input and output neurons can thus be seen to represent an elemental circuit for feeding, since these connections cannot be broken down any further.

5.5 Direct and indirect pathways

Adaptive behavior requires variability and flexibility, meaning that the nervous system has to adequately adjust its output to a large number of different external and internal input combinations. This applies particularly if monosynaptic reflexes are core components of a certain behavior. Neuronal networks in vertebrates and invertebrates achieve such functional flexibility and accuracy through parallel divergent and convergent interactions which involve the operation of interneurons that intervene between afferents and output neurons (Brezina, 1997; Burke, 1999; Jeanne and Wilson, 2015; Man et al., 2013; Rumelhart and McClelland, 1986).

In support of this, EM data of the *Drosophila* larva revealed four major network features connecting the sensory and feeding related output neurons. First, the existence of directly connected sensory-output pairs as a core network element. Second, effectively every monosynaptic sensory→output pair is additionally connected via indirect pathways: sensory neurons that connect directly to an output neuron also connect to interneurons which then target the same output neuron. Third, nearly all interneurons used in these 'triplet' motifs receive sensory inputs from more sensory neurons than those that connect directly to the output neurons. Fourth, each individual interneuron receives inputs from a set of other interneurons **(Fig 5.3)**.

Analysis of the feeding connectome suggests that the circuit architecture of the monosynaptic sensory to output pairs and their associated alternative paths is a consistently appearing three-neuron pattern in the SEZ **(Fig 5.3)**. This so-called feedforward loop (FFL)

(Fig 5.3 B2) is one of the most significant network motifs, previously noticed in the neural network of *C.elegans* (Hall and Russell, 1991; White, 1985) and in transcription networks of *Escherichia coli* and *Sacharomyces cerevisiae* (Milo, 2002; Shen-Orr et al., 2002). Depending on whether the signs of the two paths to the common target are the same (coherent) or opposite (incoherent), the FFL was proposed to serve as a mechanism for persistence detection (coherent) or pulse generation and response time acceleration (incoherent) **(Fig 5.3 C)**. Further, the combination of two feedforward loops can be useful for decision making or provide memory of an input signal, even after the input signal is gone (Alon, 2007; Mangan and Alon, 2003). In general, network motifs are significantly expressed sub-circuits that have been proposed as building blocks for natural and engineered networks (Gorochowski et al., 2018). However, inferring functional significance of these circuits in *Drosophila* appears difficult without additional information (e.g. signs of connections, neurotransmitters, behavioral/physiological data). Nevertheless, the described network organization represents a framework which does allow to speculate about the benefits of the observed layout.

Sensory information can (and will) take multiple paths as it propagates through the network to converge on a common output (Sherrington, 1906), finding always the paths of least resistance. A very strong sensory signal may be capable of immediately activating a monosynaptic reflex path and propagate via the shortest path to an output neuron. However, a weaker sensory signal may result in using at first a divergent path through an interneuron, such as one with less threshold for activation to influence the same target neuron. Even weaker subthreshold signals might require multi-sensory, multi-modal spatio-temporal integration via interneurons. For instance, a low sensory signal may not be adequate to activate neither an output neuron nor an indirect path. However, if the same signal persists, it may be merged and summed with other subthreshold sensory signals for a sufficient activation of the indirect path and consequently of the output neuron, for example, to initiate an EPSP on a post-synaptic target (Kien, 1979). Conversely, this would also allow a rapid deactivation of the output neuron when one of the sensory inputs silences. This way of processing information can be useful for a multi-modal sensorimotor network to reject transient input fluctuations that are inherent in a variable or noisy environment (Milo, 2002).

Producing and maintaining (inter-)neurons is energetically expensive. Consequently, the various indirect paths between inputs and outputs have to serve a purpose other than

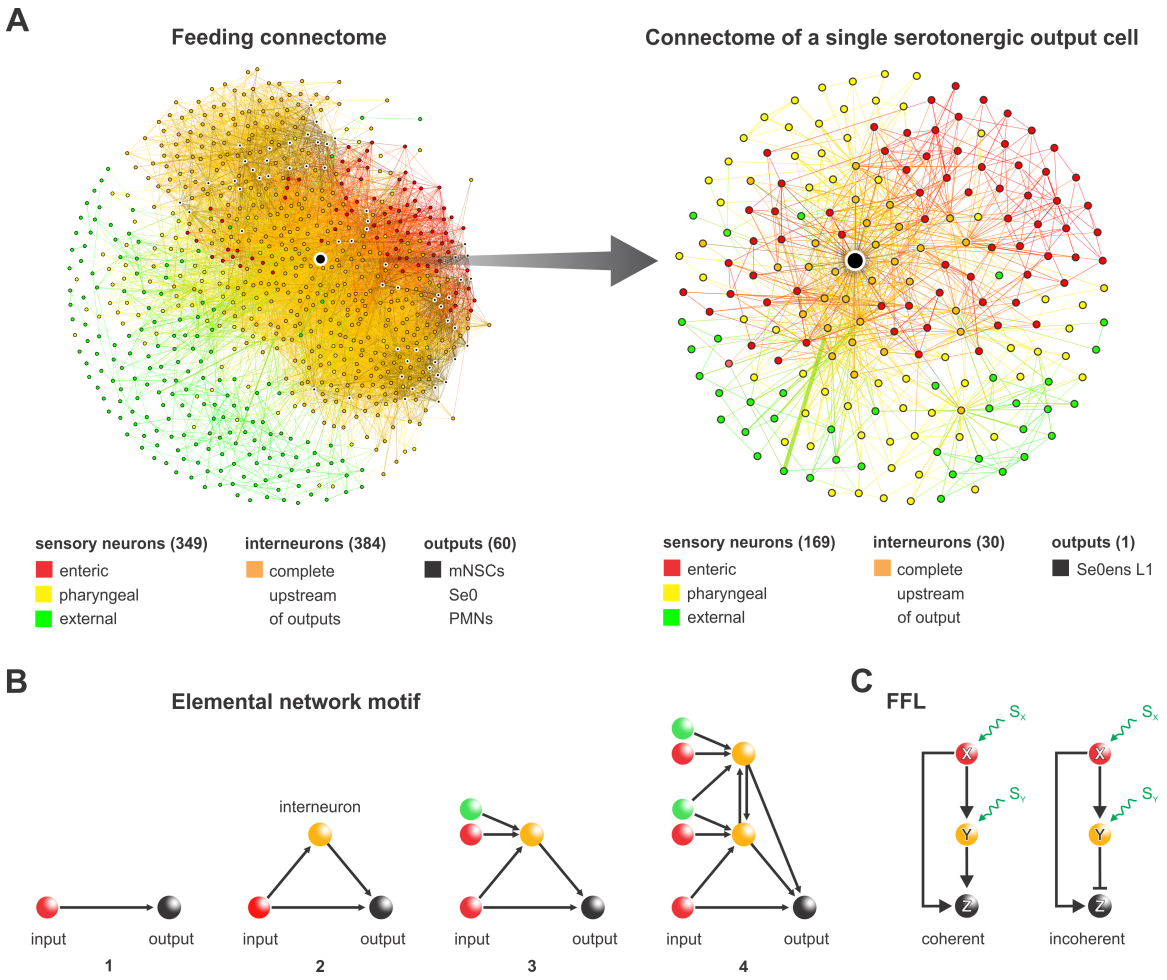

FIGURE 5.3. Elemental network motif. **(A)** Left: A connectivity diagram of all sensory neurons, median neurosecretory cells (mNSCs), modulatory serotonergic output neurons (Se0), pharyngeal motor neurons (PMNs) and the complete upstream of the respective output neurons without synaptic threshold. The numbers in parenthesis represent number of respective neurons. Right: Complete connectome of a single output neuron (Se0ens L1) is shown as a blow-up of the left panel. **(B)** Circuit architecture of the feeding network. The simplest is the monosynaptic connection between sensory and motor output (1). Interneurons are added that provide alternative paths. This architecture corresponds to a feedforward loop (2). Interneurons receive a new set of sensory inputs (3). Additional layer of interneurons is added, these are connected to the previous interneurons and receive inputs from a different set of sensory neurons. All layers target a common output. **(C)** For comparison, feedforward loop motif found in the transcription networks: a regulator X, which regulates Y, and a gene Z, which is regulated by both x and Y. S_X and S_Y are input signals (inducer) for X and Y. The function of the FFL is dependent on whether the signs of the two paths to Z are the same (coherent) or opposite (incoherent). Figure modified from Miroschnikow et al., 2020.

being simple alternative routes. Indeed, the indirect paths allow the transformation of sensory signals and convergent integration of additional information onto the same path.

However, there is still the question why the brain needs this plethora of parallel paths to any given output neuron. Processing of sensory information through parallel paths is a commonly used strategy that provides a compact, efficient input to the brain for a unified and coherent percept. This has been extensively studied in other sensory systems like the visual (Nassi and Callaway, 2009; Stone and Dreher, 1982) and olfactory system. For example in early olfactory processing, activity of some second order interneurons (called "projection neurons", PNs) is much less noisy and more specific than that of their sensory inputs - a consequence of integrating across many sensory neurons and lateral inhibition via GABAergic local neurons (Wilson, 2013). Third order olfactory neurons are then thought to extract more abstract features, e.g. by categorizing odors (Frechter et al., 2019). The work on somatosensory processing and central integration in adult *Drosophila* is yet another example of parallel integration. Here, leg touch receptors diverge onto three different interneuron classes, which in turn encode additional and different somatosensory stimuli (touch and proprioception) from same or opposite legs. The CNS integrates across submodalities on the level of second order neurons that perform distinct computations in parallel which allows transformation of finer spatio-temporal features sensory signals, reduces noise and redundancy, increases metabolic efficiency and the speed of information extraction (Tuthill and Wilson, 2016a, 2016b).

Once behaviorally relevant information has been extracted it must reach and modulate the output nodes in order to affect behavior. The present study shows that both ascending and descending paths diverge and reconverge at essentially every layer of the network. This makes sense if we assume that features about the outside world are extracted at different points in the network: some - like 'food tastes bitter, stop eating' - may emerge early, others - like 'lack of protein, find new food source' - may emerge later. However, these features must not only be extracted but also processed with each other. In support of this, the connectivity between the interneurons adds another layer of complexity and gives rise to a myriad of possible routes to converge multimodal sensory information onto the same behavioral output, e.g. the quality of a food stimulus (taste, texture, odor).

Post-ingestive effects and the nutritional state of an animal may also play an important role in shaping the networks response and could be integrated in the same fashion during early sensory processing. Using the huginPC neurons as an example illustrates a potential functional consequence for the larva in more concrete terms. The Dilps receive

monosynaptic input exclusively from enteric sensory neurons, which are potentially in contact with the hemolymph and the gut. These sensory neurons use huginPC neurons as an alternative di-synaptic path to the Dilps. Hugin neurons in turn integrate additional sensory neurons from the same sensory compartment and from a completely new peripheral origin (primary gustatory center). Thus, the hugin interneurons enable sensory inputs from different peripheral origins, for example to integrate enteric inputs with pharyngeal gustatory inputs, to influence under the right conditions an output response, which in this case, is to stop feeding (Schoofs et al., 2014a).

Network control theory provides a complementary explanation. It assumes that two nodes (i.e. neurons) that receive the exact same input will have highly correlated activity and can hence not be independently controlled. A more illustrative and less abstract example would be two motor neurons that each control a different muscle. If both motor neurons received monosynaptic input from the same (type of) sensory neuron, the muscles could not move independently. By adding layers of interneurons that provide indirect paths from the sensory to either motor neuron, we can decorrelate their activity and thereby increasing their controllability. Layering direct and indirect pathways in such a way might be a cost-effective way for biological networks to achieve controllability (Liu and Barabási, 2016; Yan et al., 2017).

An open issue is how the different sensory neurons connect to the feeding central pattern generators (CPGs). Their existence in the SEZ have been demonstrated (Hückesfeld et al., 2015; Schoofs et al., 2010), however, the neurons being integral parts of such CPGs haven't yet been characterized on the EM level. A complete reconstruction of the larval SEZ may shed more light on feeding circuits and the structure of involved CPGs. When that point has been reached, it would be fascinating to see whether the elemental network motif presented in this study occurs on other monosynaptic steps, for example between all interneurons in the SEZ, or how many other motifs can be detected. Undoubtedly, uncovering the basic building blocks will gain insight into nervous system function and its dynamical behavior which in turn underpins the importance of connectomic analysis on the level of synapses.

5.6 Early sensory convergence across modalities onto memory circuits

A more complex circuit architecture is represented by the mushroom body (MB), the site of associative learning and memory in insects. Connectomes of the larval antennal lobe and the MB, which have recently been reconstructed (Berck et al., 2016; Eichler et al., 2017), allowed the mapping of the respective neurons onto the non-olfactory sensory neurons and core feeding circuits described in the present study.

In comparison to the monosynaptic feeding circuits, a completely different set of sensory synaptic compartments (ACp, ACpl, ACal) connects via various projection neurons to the MB calyx. Thus, the MB module is not superimposed onto the monosynaptic reflex circuits but rather forms a separate unit. Further, certain multiglomerular projection neurons receive input from both olfactory as well as non-olfactory (e.g. gustatory and thermosensory) sensory neurons, thereby representing an early cross-modal convergence and likely context-dependent integration at the level of second order neurons (Balkenius and Balkenius, 2016; Ikeda et al., 2020; Maimon, 2011; Vogt, 2020). Their multi-modal input to the MB calyx might convey information about food taste or quality, and enable the animal to form positive (e.g. pleasant odor and caloric content) or negative (e.g. unpleasant taste and temperature, and toxic substances) associative memories that help to evaluate food sources in the future.

A complete ‘mushroom body module’ can be seen to consist of inputs from olfactory and other sensory neurons, projection neurons that carry information in parallel to the MB kenyon cells, intrinsic MB neurons and the MB output neurons (MBONs) (Eichler et al., 2017; Thum and Gerber, 2019). However, significantly less is known about the details how information is conveyed from the mushroom bodies to the motor regions of the brain responsible for feeding behavior. The present study shows that the MBON-f1, the only descending MBON, connects directly to the premotor neurons of the core feeding network. In this context, the subesophageal zone and the core feeding network might serve as a control center primarily concerned with rapid coordination and proper timing of feeding motor programs dependent on immediate gustatory and mechanosensory inputs that are functionally important for intaking of food. The indirect paths with several subsequent synaptic steps through higher brain centers such as the mushroom body would enable

independent processing of the same gustatory information, additional concurrent processing of olfactory and gustatory signals (e.g. perception of flavor) (Small, 2012) and incorporation of previous experience. Finally, the MBON encodes a valence (e.g. aversive or appetitve value) and its altered activity directly biases the premotor network for feeding. In this scenario, the MB module can be seen to represent a more complex form of 'stored' sensory information that converges onto the motor outputs to select an action. Functional studies on MB output neurons such as the MBON-f1, which may be part of a 'psychomotor' pathway (Ramón y Cajal, 1894) (also see **Fig 1.1**) and which targets a number of interneurons that connect to the neurosecretory, seretonergic and pharyngeal motor neurons, may help to adress how associative memory circuits interact with feeding circuits.

5.7 Control of feeding reflexes and decisions

Feeding is one of our most basic behaviors and permeates human life like hardly any other. As such it manifests in many psychological and social aspects. While looking simply on the surface, the act of feeding is in fact an incredibly complex process that involves higher brain functions as well a plethora of sensory and motor systems: a simple odor can make our mouths water in anticipation (or churn our stomachs), we consciously and subconsciously assess food quality with all our senses (visual → odor → taste → mechano) and the actual ingestion involves tightly controlled movement of many muscles and sudden reflex reactions, for example upon unexpectedly biting down on hard seed or shell. While humans might be the only animals capable of (or at least interested in) contemplating the merits of French cuisine for hours on end, more fundamental aspects of feeding are found in many if not all animals. *Drosophila* larvae, for example, are mainly focused on feeding (Green et al., 1983). The behavioral sequence includes foraging, evaluation of a potential food source by integrating and processing multi-modal sensory information from different external and internal sensory organs, and even previous experience to finally make a nearly universal decision: to eat or not to eat.

The architecture of the feeding circuit described in the present study allows speculating about how this decision-making might be implemented at the circuit level. First, for a given sensory input there are multiple paths (i.e. chains of neurons) connecting it to any given output. Second, these paths can be short (e.g. direct connections between sensory and motor neurons) or rather long (e.g. sensory neuron → PN → MB → descending neuron →

premotor → motor neuron). Third, the main path between any two points in the network is often not immediately apparent. With this in mind, experimentally assigning a singular function or role to any given neuron or even a short chain of connected neurons is likely to be an oversimplification. We can however speculate about general circuit motifs and use them to implicate brain regions in feeding decisions and thereby gaining insights into the cellular and molecular mechanisms by which different systems of the brain converge to a final and fundamental action.

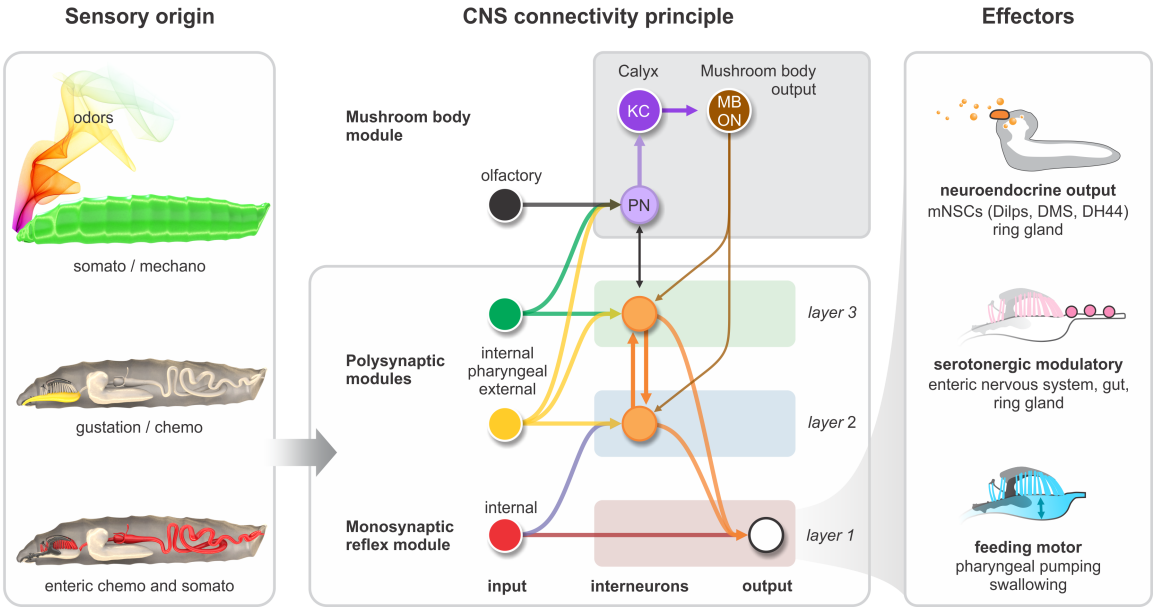

FIGURE 5.4. The larval feeding system and its connectivity architecture in the brain. Sensory origin: Representation of the different sensory types and origins. CNS connectivity principle: Different polysynaptic modules are integrated onto existing monosynaptic circuits, or added separately as new multisynaptic circuits, for example the mushroom body. Effectors: The CNS connectivity principle applies to all feeding related output neurons and their effectors. Figure modified from Miroschnikow et al., 2018.

The feeding circuitry is divided into three main axes that connect the input to the output systems: the sensory-neurosecretory cell axis (neuroendocrine), the sensory-modulatory neuron axis (autonomic) and the sensory-motor neuron axis (somatic) (Swanson, 2011). The sensory system targets the output neurons directly in overlapping domains. Here, the direct monosynaptic pathways, which derive mostly from the internal organs, could be employed when fast feedback and reflex-like response is required. The presence of polysynaptic paths might enable slower and finer control of these reflex events by allowing different sensory inputs, strengths or modalities to act on the monosynaptic circuits. Additional

multisynaptic circuits, such as CPGs, those involving sensory signals from somatosensory systems (external inputs), or those comprising memory circuits, are integrated or added in parallel to expand the behavioral repertoire of the animal **(Fig 5.4)**. Although the circuits appear to be layered from internal to external, this sequence is reversed during feeding behavior: the first sensory cues are external (olfactory), resulting in locomotion (somatic muscles) that can be influenced by memory of previous experience; this is followed by external taste cues, resulting in food intake into the mouth; the ultimate decision and action is the swallowing of food, involving pharyngeal and enteric signals and reflex circuits. Finally, post-ingestive sensory feedback from the enteric nervous system or the metabolic state of the animal may then modulate activity of the feeding circuits, e.g. in order to terminate food intake or steer the animal towards a better food source.

Regardless of the types of sensory inputs, their timing or whether they are transmitted through a reflex arc, memory circuits or some other multisynaptic circuits in the brain, they will likely converge in parallel onto a certain set of output neurons - Sherrington refers to this concept as the 'final common path' (Sherrington, 1906). Thus, instead of considering the sensorimotor pathways as merely a set of task-specific neurons (e.g. integrating unisensory modalities or controlling a motor neuron), they can be seen as a palette of complex sensory information representations that are flexibly combined and modulated without a strict hierarchy to make meaningful feeding decisions and drive instinctive behaviors such as food intake.

Further investigating this issue not only requires comprehensive mapping of the brain to build circuits from sensory in- all the way to motor outputs but also cellular and molecular tools to probe them functionally. To date, there is no vertebrate model that meets all these requirements. Fortunately, as demonstrated many times in the past, work on invertebrate models such as *Drosophila* has the potential to extract fundamental principles that apply across the animal kingdom.

Acronyms

ACa	anterior part of the Anterior Central sensory compartment
ACal	anterior-lateral part of the Anterior Central sensory compartment
ACp	posterior part of the Anterior Central sensory compartment
ACpl	posterior-lateral part of the Anterior Central sensory compartment
AL	antennal lobe
AN	antennal nerve
AST	antenno-subesophageal tract
AVa	anterior part of the Anterior Ventral sensory compartment
AVp	posterior part of the Anterior Ventral sensory compartment
B1	bundle one
B2	bundle two
B3	bundle three
CDM	cibarial dilator muscles
CNS	central nervous system
CPG	central pattern generator
CPS	cephalopharyngeal sceleton
CX	calyx
DCV	dense core vesicle
DH44	diuretic hormone 44
Dilps	*Drosophila* insulin-like peptides
DMS	dromyosuppressin
DO	dorsal organ
DOG	dorsal organ ganglion

DPO	dorsal pharyngeal organ
DPS	dorsal pharyngeal sensilla
EG	esophageal ganglion
EM	electron miscroscopy
ENS	enteric nervous system
Eso	esophagus
FFL	feedforward loop
FN	frontal nerve
FNJ	frontal nerve junction
GR	gustatory receptor
HCG	hypocerebral ganglion
huginPC	hugin protocerebrum
huginPH	hugin pharynx
IN	interneurons
KC	kenyon cells
L2	layer two
L3	layer three
LBO	labial organ
LR	labial retractor
MB	mushroom body
MBON	mushroom body output neuron
mech	mechano
MHD	mouth hook depressors
MHE	mouth hook elevators
mNSCs	median neurosecretory cells
MxN	maxilllary nerve
ORN	olfactory receptor neuron
PaN	prothoracic accessory nerve
PC	protocerebrum
ph	pharynx
PI	pars intercerebralis
PMN	pharyngeal motor neuron
PN	projection neuron
PPS	posterior pharyngeal sensilla

$Pro_{do}A$	dorsal protractor A
$Pro_{do}B$	dorsal protractor B
PVG	proventricular ganglion
RG	ring gland
RI	ranking index
RN	recurrent nerve
Se0	serotonergic modulatory neuron
SEZ	subesophageal zone
SGDO	salivary gland ductus opener
som	somato
ssTEM	serial section transmission electron miscroscopy
STG	stomatogastric ganglion
syn	synapse
T1	thoracic segment 1
TEM	transmission electron microscopy
TO	terminal orga
TOG	terminal organ ganglion
UAS	upstream activation sequence
VM	Ventromedial sensory compartment
VO	ventral organ
VPS	ventral pharyngeal sensilla

APPENDIX

The following figures and tables were modified from Miroschnikow et al., 2018.

SUPPLEMENTARY DATA

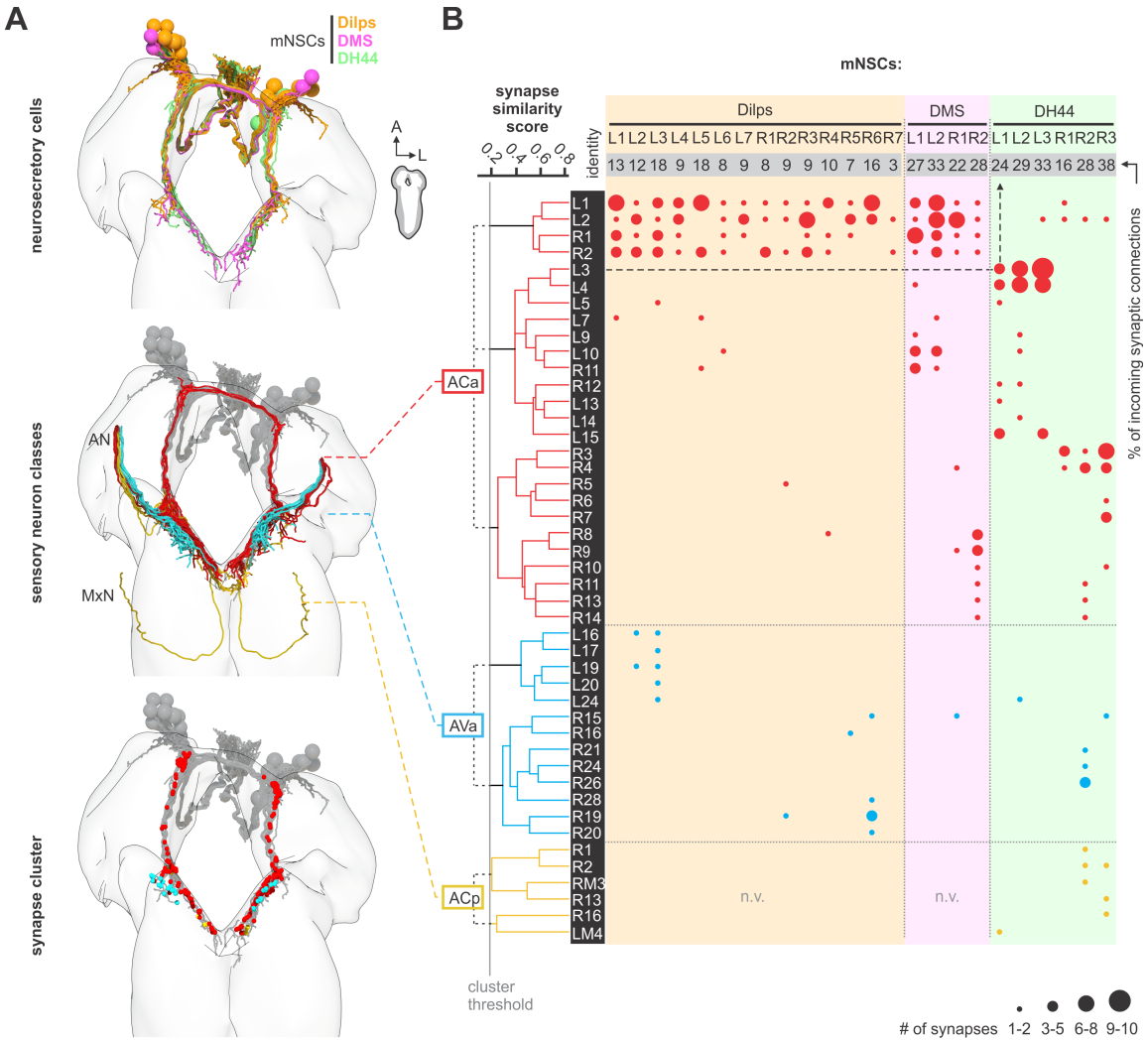

Figure A.1: Sensory neuron to mNSC connectivity. (A) EM reconstruction of mNSCs (Dilps, DMS, DH44). The mNSCs were clustered based on connectivity similarity since they are not anatomically distinguishable (Schlegel et al., 2016) (upper panel). EM reconstruction of sensory neurons (middle panel) and their synaptic contacts (lower panel) with mNSCs. Each dot represents a synaptic site. Neurons and synaptic sites are colored based on their sensory compartment (ACa, AVa and ACp). **(B)** All presynaptic sensory neurons of mNSCs clustered based on synapse similarity. Connectivity matrix shows that Dilps- and DMS-producing cells receive monosynaptic contacts from 2 of the 7 SEZ sensory compartments. DH44-producing neurons are the only cells that receive a very limited number of monosynaptic inputs from the primary gustatory center (ACp).

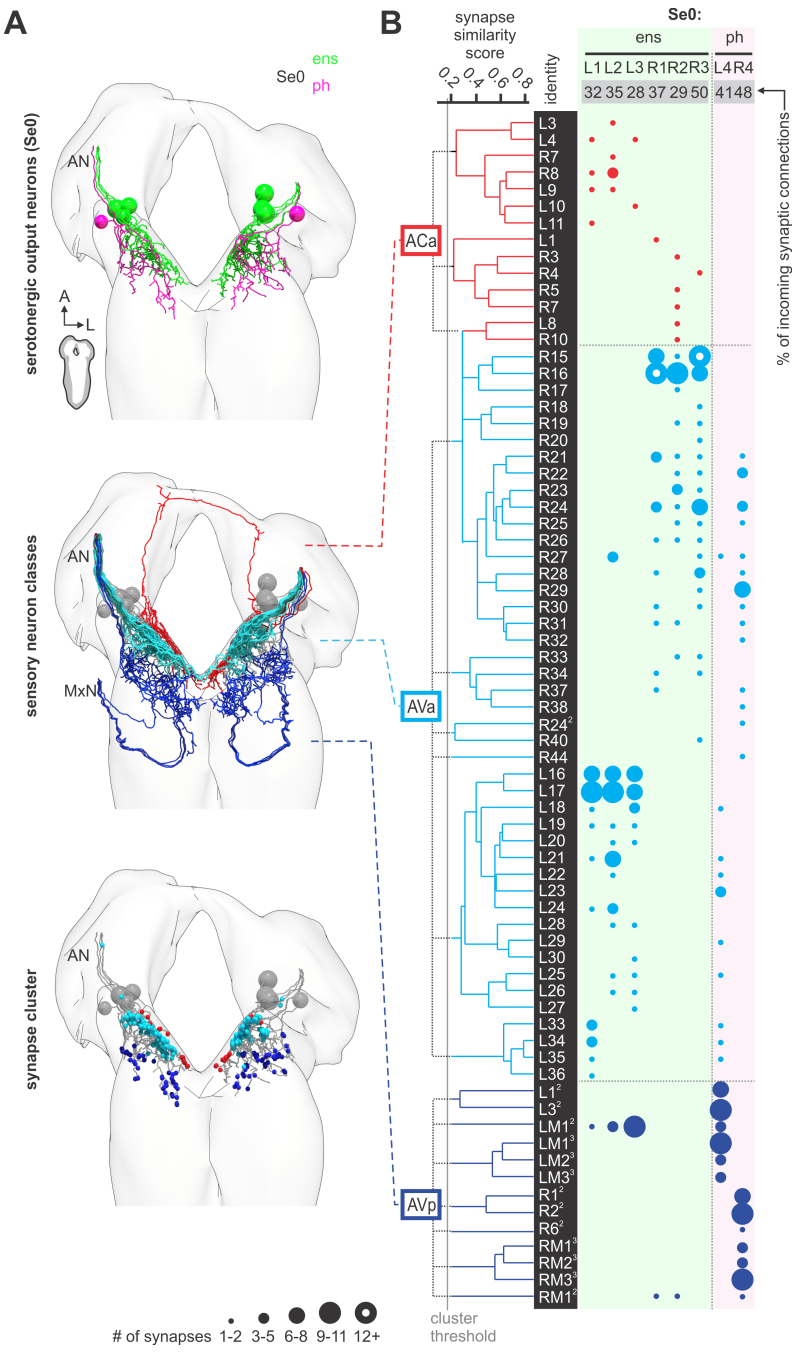

Figure A.2: Sensory neuron to Se0 connectivity. (A) EM reconstruction of the Se0 cluster (Se0ens, Se0ph) (upper panel). EM reconstruction of sensory neurons (middle panel) and their synaptic contacts (lower panel) with Se0. Each dot represents a synaptic site. Neurons and synaptic sites are colored based on their sensory compartment (ACa, AVa and AVp). **(B)** All presynaptic sensory neurons of Se0 clustered based on synapse similarity. Connectivity matrix shows that up to 50% of all incoming synaptic connections to the Se0 cells are made by sensory neurons from 3 of the 7 SEZ sensory compartments. Se0ens and Se0ph are mainly targeted by AVa and AVp sensory neurons, respectively.

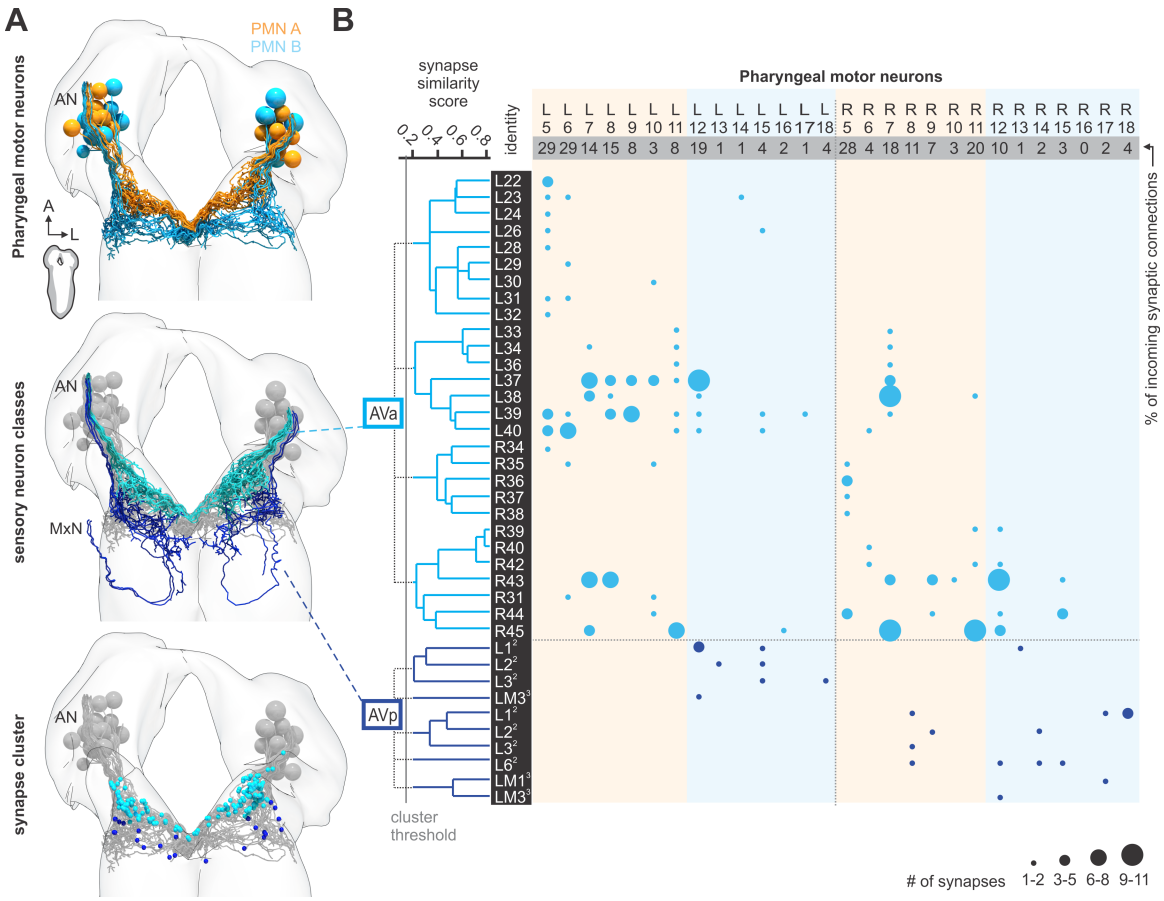

Figure A.3: Sensory neuron to PMN connectivity. (A) EM reconstruction of the pharyngeal motor neurons (upper panel). EM reconstruction of sensory neurons (middle panel) and their synaptic contacts (lower panel) with pharyngeal motor neurons. Each dot represents a synaptic site. Neurons and synaptic sites are colored based on their sensory compartment (AVa and AVp). **(B)** All presynaptic sensory neurons of pharyngeal motor neurons clustered based on synapse similarity. Connectivity matrix shows that pharyngeal motor neurons receive monosynaptic contacts from 2 of the 7 SEZ sensory compartments. Most of the AVa contacts are made to motor neurons 5–12 consistently across both hemi sides.

Nerve name (in larva)	Axon bundles	Terminology (in embryo and larva)	Source
Antennal nerve (AN)	**1,2,3**	Antennennerv (an)	Hertweck, 1931
		Antenna nerve (en)	Bodenstein, 1950
		Antennal nerve (an)	Schoofs, 2010
		Compound pharyngeal nerve (phn)	Hartenstein, 2017
		Pharyngeal nerve (phn)	Kendroud, 2017
	1	Medial root of pharyngeal nerve (pn_m)	Hartenstein, 2017
	2	Labral nerve (ln)	Campos-Ortega, 1985
		Hypopharyngeal nerve (hpn)	Campos-Ortega, 1985
		Anterior root of pharyngeal nerve (pn_a)	Kendroud, 2017
		Posterior root of pharyngeal nerve (pn_p)	Kendroud, 2017
	3	Antennal nerve (an)	Kendroud, 2017
		Posterior antennal nerve (an_p)	Kendroud, 2017
Maxillary nerve (MxN)	**1,2,3**	MN Nerv (mn)	Hertweck, 1931
		Maxillary nerve (mn)	Bodenstein, 1950
		Maxillary nerve (mn)	Schoofs, 2010
		Combined maxillary-labial nerve (lbn)	Hartenstein, 2017
		Labial nerve (lbn)	Kendroud, 2017
		Combined labial nerve (lbn)	Kendroud, 2017
		Compound labial nerve (lbn)	Kendroud, 2017
	1	Labial nerve (lbn)	Campos-Ortega, 1985
		Labial segmental nerve (ln)	Hartenstein, 2017
		Anterior root of labial nerve (ln_a)	Kendroud, 2017
	2	Maxillary nerve (mn)	Campos-Ortega, 1985
		Maxillary segmental nerve (mn)	Hartenstein, 2017
		Maxillary root of labial nerve (mn)	Kendroud, 2017
		Anterior bundle of the mn (mn_a)	Kendroud, 2017
		Posterior bundle of the mn (mn_p)	Kendroud, 2017
	3	Labial nerve (lbn)	Campos-Ortega, 1985
		Labial segmental nerve (ln)	Hartenstein, 2017
		Posterior root of labial nerve (ln_p)	Kendroud, 2017
Prothoracic accessory nerve (PaN)	**1**	Prothoracic accessory nerve (PaN)	Ludwig, 1949
		Prothoracic accessory nerve (PaN)	Schoofs, 2010

Table A.1: Nerve nomenclature of *Drosophila melanogaster* larva. Different names exist from analysis of structures analyzed at different stages of development (embryo, larva) and imaging methodology by different authors (Bodenstein, 1950; Campos-Ortega and Hartenstein, 1985; Hartenstein et al., 2017; Hertweck, 1931; Kendroud et al., 2017; Schoofs et al., 2010). The table provides a cross-reference for the readers but should not be taken as a definitive canonical version. At the larval stage, the different nerves enter the CNS from the periphery as single entities. These then split apart into different branches, each with a new set of nerve names, within the CNS. The usage of the term PaN derives from an analogous nerve described in *Calliphora* (Ludwig, 1949) and *Drosophila* (Schoofs et al., 2010).

BIBLIOGRAPHY

Abraira VE, Ginty DD. 2013. The sensory neurons of touch. *Neuron* **79**:618–639. doi:10.1016/j.neuron.2013.07.051

Adams MD, Celniker SE, Holt RA, Evans CA, Gocayne JD, Amanatides PG, Scherer SE, Li PW, Hoskins RA, Galle RF, George RA, Lewis SE, Richards S, Ashburner M, Henderson SN, Sutton GG, Wortman JR, Yandell MD, Zhang Q, Chen LX, Brandon RC, Rogers YHC, Blazej RG, Champe M, Pfeiffer BD, Wan KH, Doyle C, Baxter EG, Helt G, Nelson CR, Gabor Miklos GL, Abril JF, Agbayani A, An HJ, Andrews-Pfannkoch C, Baldwin D, Ballew RM, Basu A, Baxendale J, Bayraktaroglu L, Beasley EM, Beeson KY, Benos P V., Berman BP, Bhandari D, Bolshakov S, Borkova D, Botchan MR, Bouck J, Brokstein P, Brottier P, Burtis KC, Busam DA, Butler H, Cadieu E, Center A, Chandra I, Michael Cherry J, Cawley S, Dahlke C, Davenport LB, Davies P, de Pablos B, Delcher A, Deng Z, Deslattes Mays A, Dew I, Dietz SM, Dodson K, Doup LE, Downes M, Dugan-Rocha S, Dunkov BC, Dunn P, Durbin KJ, Evangelista CC, Ferraz C, Ferriera S, Fleischmann W, Fosler C, Gabrielian AE, Garg NS, Gelbart WM, Glasser K, Glodek A, Gong F, Harley Gorrell J, Gu Z, Guan P, Harris M, Harris NL, Harvey D, Heiman TJ, Hernandez JR, Houck J, Hostin D, Houston KA, Howland TJ, Wei MH, Ibegwam C, Jalali M, Kalush F, Karpen GH, Ke Z, Kennison JA, Ketchum KA, Kimmel BE, Kodira CD, Kraft C, Kravitz S, Kulp D, Lai Z, Lasko P, Lei Y, Levitsky AA, Li J, Li Z, Liang Y, Lin X, Liu X, Mattei B, McIntosh TC, McLeod MP, McPherson D, Merkulov G, Milshina N V., Mobarry C, Morris J, Moshrefi A, Mount SM, Moy M, Murphy B, Murphy L, Muzny DM, Nelson DL, Nelson DR, Nelson KA, Nixon K, Nusskern DR, Pacleb JM, Palazzolo M, Pittman GS, Pan S, Pollard J, Puri V, Reese

MG, Reinert K, Remington K, Saunders RDC, Scheeler F, Shen H, Christopher Shue B, Siden-Kiamos I, Simpson M, Skupski MP, Smith T, Spier E, Spradling AC, Stapleton M, Strong R, Sun E, Svirskas R, Tector C, Turner R, Venter E, Wang AH, Wang X, Wang ZY, Wassarman DA, Weinstock GM, Weissenbach J, Williams SM, Woodage T, Worley KC, Wu D, Yang S, Alison Yao Q, Ye J, Yeh RF, Zaveri JS, Zhan M, Zhang G, Zhao Q, Zheng L, Zheng XH, Zhong FN, Zhong W, Zhou X, Zhu S, Zhu X, Smith HO, Gibbs RA, Myers EW, Rubin GM, Craig Venter J. 2000. The genome sequence of *Drosophila melanogaster*. *Science (80-)* **287**:2185–2195. doi:10.1126/science.287.5461.2185

Albertson DG, Thompson JN. 1976. The pharynx of *Caenorhabditis elegans*. *Philos Trans R Soc London B, Biol Sci* **275**:299–325. doi:10.1098/rstb.1976.0085

Almeida-Carvalho MJ, Berh D, Braun A, Chen Y-C, Eichler K, Eschbach C, Fritsch PMJ, Gerber B, Hoyer N, Jiang X, Kleber J, Klämbt C, König C, Louis M, Michels B, Miroschnikow A, Mirth C, Miura D, Niewalda T, Otto N, Paisios E, Pankratz MJ, Petersen M, Ramsperger N, Randel N, Risse B, Saumweber T, Schlegel P, Schleyer M, Soba P, Sprecher SG, Tanimura T, Thum AS, Toshima N, Truman JW, Yarali A, Zlatic M. 2017. The Ol1mpiad: Concordance of behavioural faculties of stage 1 and stage 3 *Drosophila* larvae. *J Exp Biol* **220**. doi:10.1242/jeb.156646

Alon U. 2007. Network motifs: theory and experimental approaches. *Nat Rev Genet* **8**:450–461. doi:10.1038/nrg2102

Andrade I V., Riebli N, Nguyen BCM, Omoto JJ, Cardona A, Hartenstein V. 2019. Developmentally Arrested Precursors of Pontine Neurons Establish an Embryonic Blueprint of the *Drosophila* Central Complex. *Curr Biol* **29**:412-425.e3. doi:10.1016/j.cub.2018.12.012

Apostolopoulou AA, Rist A, Thum AS. 2015. Taste processing in *Drosophila* larvae. *Front Integr Neurosci* **9**:1–9. doi:10.3389/fnint.2015.00050

Azevedo FAC, Carvalho LRB, Grinberg LT, Farfel JM, Ferretti REL, Leite REP, Filho WJ, Lent R, Herculano-Houzel S. 2009. Equal numbers of neuronal and nonneuronal cells make the human brain an isometrically scaled-up primate brain. *J Comp Neurol* **513**:532–541. doi:10.1002/cne.21974

Azmitia EC. 2001. Modern views on an ancient chemical: serotonin effects on cell proliferation, maturation, and apoptosis. *Brain Res Bull* **56**:413–424. doi:10.1016/S0361-9230(01)00614-1

Bailey CH, Giustetto M, Zhu H, Chen M, Kandel ER. 2000. A novel function for serotonin-

mediated short-term facilitation in Aplysia: Conversion of a transient, cell-wide homosynaptic Hebbian plasticity into a persistent, protein synthesis-independent synapse-specific enhancement. *Proc Natl Acad Sci U S A* **97**:11581–11586. doi:10.1073/pnas.97.21.11581

Balkenius A, Balkenius C. 2016. Multimodal interaction in the insect brain. *BMC Neurosci* **17**:29. doi:10.1186/s12868-016-0258-7

Bargmann CI, Marder E. 2013. From the connectome to brain function. *Nat Methods* **10**:483–490. doi:10.1038/nmeth.2451

Barkan CL, Zornik E. 2019. Feedback to the future: Motor neuron contributions to central pattern generator function. *J Exp Biol* **222**. doi:10.1242/jeb.193318

Barlow SM. 2009. Central pattern generation involved in oral and respiratory control for feeding in the term infant. *Curr Opin Otolaryngol Head Neck Surg* **17**:187–193. doi:10.1097/MOO.0b013e32832b312a

Barron AB, Gurney KN, Meah LFS, Vasilaki E, Marshall JAR. 2015. Decision-making and action selection in insects: inspiration from vertebrate-based theories. *Front Behav Neurosci* **9**:1–14. doi:10.3389/fnbeh.2015.00216

Bellen HJ, Tong C, Tsuda H. 2010. History of *Drosophila* Neuroscience **11**.

Bels V, Whishaw IQ. 2019. Feeding in Vertebrates, Fascinating Life Sciences. Cham: Springer International Publishing. doi:10.1007/978-3-030-13739-7

Benjamin PR, Rose RM. 1979. Central generation of bursting in the feeding system of the snail, *Lymnaea stagnalis*. *J Exp Biol* **80**:93–118.

Berck ME, Khandelwal A, Claus L, Hernandez-Nunez L, Si G, Tabone CJ, Li F, Truman JW, Fetter RD, Louis M, Samuel AD, Cardona A. 2016. The wiring diagram of a glomerular olfactory system. *Elife* **5**:1–21. doi:10.7554/eLife.14859

Bodenstein D. 1950. The postembryonic development of *Drosophila* In: Demerec M, editor. Biology of *Drosophila*. John Wiley & Sons, N.Y. pp. 275–367.

Borst A, Helmstaedter M. 2015. Common circuit design in fly and mammalian motion vision. *Nat Neurosci* **18**:1067–1076. doi:10.1038/nn.4050

Braganza O, Beck H. 2018. The Circuit Motif as a Conceptual Tool for Multilevel Neuroscience. *Trends Neurosci* **41**:128–136. doi:10.1016/j.tins.2018.01.002

Braitenberg V, Schüz A. 1998. Cortex: Statistics and Geometry of Neuronal Connectivity. Berlin, Heidelberg: Springer Berlin Heidelberg. doi:10.1007/978-3-662-03733-1

Brand AH, Perrimon N. 1993. Targeted gene expression as a means of altering cell fates and generating dominant phenotypes. *Development* **118**:401–415.

Brezina V. 1997. Functional consequences of divergence and convergence in physiological signaling pathways. *Mol Psychiatry* **2**:9–11. doi:10.1038/sj.mp.4000191

Briggman KL, Helmstaedter M, Denk W. 2011. Wiring specificity in the direction-selectivity circuit of the retina. *Nature* **471**:183–188. doi:10.1038/nature09818

Brunelli M, Castellucci V, Kandel ER. 1976. Synaptic facilitation and behavioral sensitization in *Aplysia*: Possible role of serotonin and cyclic AMP. *Science (80-)* **194**:1178–1181. doi:10.1126/science.186870

Brunet Avalos C, Maier GL, Bruggmann R, Sprecher SG. 2019. Single cell transcriptome atlas of the *Drosophila* larval brain. *Elife* **8**:1–25. doi:10.7554/eLife.50354

Bucher D, Haspel G, Golowasch J, Nadim F. 2015. Central Pattern GeneratorsELS. Chichester, UK: John Wiley & Sons, Ltd. pp. 1–12. doi:10.1002/9780470015902.a0000032.pub2

Bullock TH. 1959. Neuron Doctrine and Electrophysiology: A quiet revolution has been taking place in our concepts of how the nerve cells act alone and in concert. *Science (80-)* **129**:997–1002. doi:10.1126/science.129.3355.997

Bullock TH, Horridge GA. 1965. Structure and Function in the Nervous System of Invertebrates. Freeman: San Francisco.

Burke RE. 1999. The use of state-dependent modulation of spinal reflexes as a tool to investigate the organization of spinal interneurons. *Exp Brain Res* **128**:263–277. doi:10.1007/s002210050847

Burrows M. 1975. Monosynaptic connexions between wing stretch receptors and flight motoneurones of the locust. *J Exp Biol* **62**:189–219.

Campos-Ortega JA, Hartenstein V. 1985. The Embryonic Development of *Drosophila melanogaster*. Berlin, Heidelberg: Springer Berlin Heidelberg. doi:10.1007/978-3-662-02454-6

Chen Y-CD, Dahanukar A. 2020. Recent advances in the genetic basis of taste detection in *Drosophila*. *Cell Mol Life Sci* **77**:1087–1101. doi:10.1007/s00018-019-03320-0

Clyne PJ. 2000. Candidate Taste Receptors in *Drosophila*. *Science (80-)* **287**:1830–1834. doi:10.1126/science.287.5459.1830

Cocanougher BT, Wittenbach JD, Long X, Kohn AB, Norekian TP, Yan J, Colonell J, Masson J-B, Truman JW, Cardona A, Turaga S, Singer RH, Moroz LL, Zlatic M. 2019. Comparative single-cell transcriptomics of complete insect nervous systems. *bioRxiv*. doi:https://doi.org/10.1101/785931

Colomb J, Grillenzoni N, Ramaekers A, Stocker RF. 2007. Architecture of the primary

taste center of *Drosophila melanogaster* larvae. *J Comp Neurol* **502**:834–847. doi:10.1002/cne.21312

Cook SJ, Jarrell TA, Brittin CA, Wang Y, Bloniarz AE, Yakovlev MA, Nguyen KCQ, Tang LTH, Bayer EA, Duerr JS, Bülow HE, Hobert O, Hall DH, Emmons SW. 2019. Whole-animal connectomes of both *Caenorhabditis elegans* sexes. *Nature* **571**:63–71. doi:10.1038/s41586-019-1352-7

Copenhaver PF. 2007. How to Innervate a Simple Gut : Familiar Themes and Unique Aspects in the Formation of the Insect Enteric Nervous System 1841–1864. doi:10.1002/dvdy.21138

Cordes SP. 2001. Molecular genetics of cranial nerve development in mouse. *Nat Rev Neurosci* **2**:611–623. doi:10.1038/35090039

Corl AB, Berger KH, Ophir-Shohat G, Gesch J, Simms JA, Bartlett SE, Heberlein U. 2009. Happyhour, a Ste20 Family Kinase, Implicates EGFR Signaling in Ethanol-Induced Behaviors. *Cell* **137**:949–960. doi:10.1016/j.cell.2009.03.020

D'Agostino G, Lyons DJ, Cristiano C, Burke LK, Madara JC, Campbell JN, Garcia AP, Land BB, Lowell BB, Dileone RJ, Heisler LK. 2016. Appetite controlled by a cholecystokinin nucleus of the solitary tract to hypothalamus neurocircuit. *Elife* **5**:1–15. doi:10.7554/eLife.12225

De Velasco B, Shen J, Go S, Hartenstein V. 2004. Embryonic development of the *Drosophila* corpus cardiacum, a neuroendocrine gland with similarity to the vertebrate pituitary, is controlled by sine oculis and glass. *Dev Biol* **274**:280–294. doi:10.1016/j.ydbio.2004.07.015

DeFelipe J. 2010. From the connectome to the synaptome: An epic love story. *Science (80-)* **330**:1198–1201. doi:10.1126/science.1193378

Delsuc F, Brinkmann H, Chourrout D, Philippe H. 2006. Tunicates and not cephalochordates are the closest living relatives of vertebrates. *Nature* **439**:965–968. doi:10.1038/nature04336

Denk W, Horstmann H. 2004. Serial Block-Face Scanning Electron Microscopy to Reconstruct Three-Dimensional Tissue Nanostructure. *PLoS Biol* **2**:e329. doi:10.1371/journal.pbio.0020329

Diao Feici, Elliott AD, Diao Fengqiu, Shah S, White BH. 2017. Neuromodulatory connectivity defines the structure of a behavioral neural network. *Elife* **6**:1–30. doi:10.7554/eLife.29797

Dickerson M, McCormick J, Mispelon M, Paisley K, Nichols R. 2012. Structure–activity

and immunochemical data provide evidence of developmental- and tissue-specific myosuppressin signaling. *Peptides* **36**:272–279. doi:10.1016/j.peptides.2012.05.002

Dickinson PS. 2006. Neuromodulation of central pattern generators in invertebrates and vertebrates. *Curr Opin Neurobiol* **16**:604–614. doi:10.1016/j.conb.2006.10.007

Donovan MH, Tecott LH. 2013. Serotonin and the regulation of mammalian energy balance. *Front Neurosci* **7**:1–15. doi:10.3389/fnins.2013.00036

Duffy JB. 2002. GAL4 system in *Drosophila*: a fly geneticist's Swiss army knife. *Genesis* **34**:1–15. doi:10.1002/gene.10150

Dumstrei K, Wang F, Nassif C, Hartenstein V. 2003. Early development of the *Drosophila* brain: V. Pattern of postembryonic neuronal lineages expressing DE-cadherin. *J Comp Neurol* **455**:451–462. doi:10.1002/cne.10484

Dus M, Lai JS-Y, Gunapala KM, Min S, Tayler TD, Hergarden AC, Geraud E, Joseph CM, Suh GSB. 2015. Nutrient Sensor in the Brain Directs the Action of the Brain-Gut Axis in *Drosophila*. *Neuron* **87**:139–151. doi:10.1016/j.neuron.2015.05.032

Eccles JC, Gibson WC. 1979. Sherrington: His Life and Thought, This includes an account of Sherrington's Linacre Lecture, delivered at St John's College, Cambridge, on 6 May 1924. Springer Verlag Berlin.

Eichler K, Li F, Litwin-Kumar A, Park Y, Andrade I, Schneider-Mizell CM, Saumweber T, Huser A, Eschbach C, Gerber B, Fetter RD, Truman JW, Priebe CE, Abbott LF, Thum AS, Zlatic M, Cardona A. 2017. The complete connectome of a learning and memory centre in an insect brain. *Nature* **548**:175–182. doi:10.1038/nature23455

Emmons SW. 2015. The beginning of connectomics: a commentary on White et al. (1986) 'The structure of the nervous system of the nematode *Caenorhabditis elegans* .' *Philos Trans R Soc B Biol Sci* **370**:20140309. doi:10.1098/rstb.2014.0309

Erickson RP. 2008. A study of the science of taste: On the origins and influence of the core ideas. *Behav Brain Sci* **31**:59–75. doi:10.1017/S0140525X08003348

Erickson RP. 1984. Öhrwall, Henning and von Skramlik; The foundations of the four primary position in taste. *Neurosci Biobehav Rev* **8**:105–106. doi:10.1016/0149-7634(84)90024-1

Eschbach C, Fushiki A, Winding M, Schneider-Mizell CM, Shao M, Arruda R, Eichler K, Valdes-Aleman J, Ohyama T, Thum AS, Gerber B, Fetter RD, Truman JW, Litwin-Kumar A, Cardona A, Zlatic M. 2020. Recurrent architecture for adaptive regulation of learning in the insect brain. *Nat Neurosci* **23**:544–555. doi:10.1038/s41593-020-0607-9

Flanders M. 2011. What is the biological basis of sensorimotor integration? *Biol Cybern* **104**:1–8. doi:10.1007/s00422-011-0419-9

Fornito A, Bullmore ET, Zalesky A, editors. 2016. Fundamentals of Brain Network Analysis. Elsevier. doi:10.1016/C2012-0-06036-X

Foster M, Sherrington CS. 1897. A Textbook of Physiology. With C.S. Sherrington. Part 3. The Central Nervous System. London : Macmillan.

Frechter S, Bates AS, Tootoonian S, Dolan M-J, Manton J, Jamasb AR, Kohl J, Bock D, Jefferis G. 2019. Functional and anatomical specificity in a higher olfactory centre. *Elife* **8**:1–39. doi:10.7554/eLife.44590

Friedman JM. 2019. Leptin and the endocrine control of energy balance. *Nat Metab* **1**:754–764. doi:10.1038/s42255-019-0095-y

Friesen WO. 2009. Central Pattern Generators: Sensory FeedbackEncyclopedia of Neuroscience. Elsevier. pp. 701–709. doi:10.1016/B978-008045046-9.01949-5

Fushiki A, Zwart MF, Kohsaka H, Fetter RD, Cardona A, Nose A. 2016. A circuit mechanism for the propagation of waves of muscle contraction in *Drosophila*. *Elife* **5**:e13253. doi:10.7554/eLife.13253

García-Crescioni K, Miller MW. 2011. Revisiting the reticulum: feedforward and feedback contributions to motor program parameters in the crab cardiac ganglion microcircuit. *J Neurophysiol* **106**:2065–2077. doi:10.1152/jn.01128.2010

Gelperin A. 2019. Recent Trends in Invertebrate Neuroscience In: Byrne JH, editor. The Oxford Handbook of Invertebrate Neurobiology. Oxford University Press. pp. 2–30. doi:10.1093/oxfordhb/9780190456757.013.1

Gendre N, Lüer K, Friche S, Grillenzoni N, Ramaekers A, Technau GM, Stocker RF. 2004. Integration of complex larval chemosensory organs into the adult nervous system of *Drosophila*. *Development* **131**:83–92. doi:10.1242/dev.00879

Gerber B, Stocker RF, Tanimura T, Thum AS. 2009. Smelling, Tasting, Learning: *Drosophila* as a Study CaseResults and Problems in Cell Differentiation. pp. 187–202. doi:10.1007/400_2008_9

Gerhard S, Andrade I, Fetter RD, Cardona A, Schneider-Mizell CM. 2017. Conserved neural circuit structure across *Drosophila* larval development revealed by comparative connectomics. *Elife* **6**:1–17. doi:10.7554/eLife.29089

Getting PA, Lennard PR, Hume RI. 1980. Central pattern generator mediating swimming in *Tritonia*. I. Identification and synaptic interactions. *J Neurophysiol* **44**:151–164. doi:10.1152/jn.1980.44.1.151

Ghysen A. 2003. The origin and evolution of the nervous system. *Int J Dev Biol* **47**:555–562.

Gillette R. 2006. Evolution and Function in Serotonergic Systems. *Integr Comp Biol* **46**:838–846. doi:10.1093/icb/icl024

Giniger E, Varnum SM, Ptashne M. 1985. Specific DNA binding of GAL4, a positive regulatory protein of yeast. *Cell* **40**:767–774. doi:10.1016/0092-8674(85)90336-8

Gorochowski TE, Grierson CS, di Bernardo M. 2018. Organization of feed-forward loop motifs reveals architectural principles in natural and engineered networks. *Sci Adv* **4**:eaap9751. doi:10.1126/sciadv.aap9751

Grant G. 2007. How the 1906 Nobel Prize in Physiology or Medicine was shared between Golgi and Cajal. *Brain Res Rev* **55**:490–498. doi:10.1016/j.brainresrev.2006.11.004

Green CH, Burnet B, Connolly KJ. 1983. Organization and patterns of inter- and intraspecific variation in the behaviour of *Drosophila* larvae. *Anim Behav* **31**:282–291. doi:10.1016/S0003-3472(83)80198-5

Grillner S. 2009. Pattern GenerationEncyclopedia of Neuroscience. Elsevier. pp. 487–494. doi:10.1016/B978-008045046-9.01341-3

Grillner S. 2006. Biological Pattern Generation: The Cellular and Computational Logic of Networks in Motion. *Neuron* **52**:751–766. doi:10.1016/j.neuron.2006.11.008

Grillner S, Hellgren J, Ménard A, Saitoh K, Wikström MA. 2005. Mechanisms for selection of basic motor programs - Roles for the striatum and pallidum. *Trends Neurosci*. doi:10.1016/j.tins.2005.05.004

Guertin PA, Steuer I. 2009. Key central pattern generators of the spinal cord. *J Neurosci Res* **87**:2399–2405. doi:10.1002/jnr.22067

Hall D, Russell R. 1991. The posterior nervous system of the nematode *Caenorhabditis elegans*: serial reconstruction of identified neurons and complete pattern of synaptic interactions. *J Neurosci* **11**:1–22. doi:10.1523/JNEUROSCI.11-01-00001.1991

Harris-Warrick RM, Flamm RE, Johnson BR, Katz PS, Kiehn O, Zhang B. 1992. Neuromodulation of Small Neural Networks in Crustacea.Neurotox ’91. Springer Netherlands. pp. 305–321. doi:10.1007/978-94-011-2898-8_22

Hartenstein V, Omoto JJ, Ngo KT, Wong D, Kuert PA, Reichert H, Lovick JK, Younossi-Hartenstein A. 2017. Structure and development of the subesophageal zone of the *Drosophila* brain. I. Segmental architecture, compartmentalization, and lineage anatomy. *J Comp Neurol* **526**:6–32. doi:10.1002/cne.24287

Hartenstein V, Younossi-Hartenstein A, Lovick JK, Kong A, Omoto JJ, Ngo KT, Viktorin G.

2015. Lineage-associated tracts defining the anatomy of the *Drosophila* first instar larval brain. *Dev Biol* **406**:14–39. doi:10.1016/j.ydbio.2015.06.021

Hassenstein B, Reichardt W. 1956. Systemtheoretische Analyse der Zeit-, Reihenfolgen- und Vorzeichenauswertung bei der Bewegungsperzeption des Rüsselkäfers *Chlorophanus*. *Zeitschrift für Naturforsch B* **11**:513–524. doi:10.1515/znb-1956-9-1004

Häusser M. 2000. The Hodgkin-Huxley theory of the action potential. *Nat Neurosci* **3**:1165–1165. doi:10.1038/81426

Hayworth KJ, Xu CS, Lu Z, Knott GW, Fetter RD, Tapia JC, Lichtman JW, Hess HF. 2015. Ultrastructurally smooth thick partitioning and volume stitching for large-scale connectomics. *Nat Methods* **12**:319–322. doi:10.1038/nmeth.3292

Heisenberg M, Borst A, Wagner S, Byers D. 1985. *Drosophila* Mushroom Body Mutants are Deficient in Olfactory Learning. *J Neurogenet* **2**:1–30. doi:10.3109/01677068509100140

Helmstaedter M. 2013. Cellular-resolution connectomics : challenges of dense neural circuit reconstruction **10**:501–507. doi:10.1038/nmeth.2476

Helmstaedter M, Briggman KL, Turaga SC, Jain V, Seung HS, Denk W. 2013. Connectomic reconstruction of the inner plexiform layer in the mouse retina. *Nature* **500**:168–174. doi:10.1038/nature12346

Hentze JL, Carlsson MA, Kondo S, Nässel DR, Rewitz KF. 2015. The Neuropeptide Allatostatin A Regulates Metabolism and Feeding Decisions in *Drosophila*. *Sci Rep* **5**:11680. doi:10.1038/srep11680

Hertweck H. 1931. Anatomie und Variabilität des Nervensystems und der Sinnesorgane von *Drosophila melanogaster* (Meigen). *Zeitschrift f wissensch Zool* **139**:559–663.

Hildebrand JG, Shepherd GM. 1997. MECHANISMS OF OLFACTORY DISCRIMINATION: Converging Evidence for Common Principles Across Phyla. *Annu Rev Neurosci* **20**:595–631. doi:10.1146/annurev.neuro.20.1.595

Hodgkin AL, Huxley AF. 1952. A quantitative description of membrane current and its application to conduction and excitation in nerve. *J Physiol* **117**:500–544. doi:10.1113/jphysiol.1952.sp004764

Hodgkin AL, Huxley AF. 1939. Action Potentials Recorded from Inside a Nerve Fibre. *Nature* **144**:710–711. doi:10.1038/144710a0

Hoke KL, Hebets EA, Shizuka D. 2017. Neural Circuitry for Target Selection and Action Selection in Animal Behavior. *Integr Comp Biol* **57**:808–819. doi:10.1093/icb/icx109

Hooper SL, Büschges A. 2017. Neurobiology of Motor Control. Hoboken, NJ, USA: John Wiley & Sons, Inc. doi:10.1002/9781118873397

Hückesfeld S, Peters M, Pankratz MJ. 2016. Central relay of bitter taste to the protocerebrum by peptidergic interneurons in the *Drosophila* brain. *Nat Commun* **7**:12796. doi:10.1038/ncomms12796

Hückesfeld S, Schoofs A, Schlegel P, Miroschnikow A, Pankratz MJ. 2015. Localization of Motor Neurons and Central Pattern Generators for Motor Patterns Underlying Feeding Behavior in *Drosophila* Larvae. *PLoS One* **10**:e0135011. doi:10.1371/journal.pone.0135011

Hummel T, Krukkert K, Roos J, Davis G, Klämbt C. 2000. *Drosophila* Futsch/22C10 Is a MAP1B-like Protein Required for Dendritic and Axonal Development. *Neuron* **26**:357–370. doi:10.1016/S0896-6273(00)81169-1

Huser A, Rohwedder A, Apostolopoulou AA, Widmann A, Pfitzenmaier JE, Maiolo EM, Selcho M, Pauls D, von Essen A, Gupta T, Sprecher SG, Birman S, Riemensperger T, Stocker RF, Thum AS. 2012. The Serotonergic Central Nervous System of the *Drosophila* Larva: Anatomy and Behavioral Function. *PLoS One* **7**:e47518. doi:10.1371/journal.pone.0047518

Huston SJ, Jayaraman V. 2011. Studying sensorimotor integration in insects. *Curr Opin Neurobiol* **21**:527–534. doi:10.1016/j.conb.2011.05.030

Ikeda M, Nakano S, Giles AC, Xu L, Costa WS, Gottschalk A, Mori I. 2020. Context-dependent operation of neural circuits underlies a navigation behavior in *Caenorhabditis elegans*. *Proc Natl Acad Sci U S A* **117**:6178–6188. doi:10.1073/pnas.1918528117

International Human Genome Sequencing Consortium. 2001. Correction: Initial sequencing and analysis of the human genome. *Nature* **412**:565–566. doi:10.1038/35087627

Ito K, Shinomiya K, Ito M, Armstrong JD, Boyan G, Hartenstein V, Harzsch S, Heisenberg M, Homberg U, Jenett A, Keshishian H, Restifo LL, Rössler W, Simpson JH, Strausfeld NJ, Strauss R, Vosshall LB. 2014. A Systematic Nomenclature for the Insect Brain. *Neuron* **81**:755–765. doi:10.1016/j.neuron.2013.12.017

Jacobs BL, Fornal CA. 1999. Activity of serotonergic neurons in behaving animals. *Neuropsychopharmacology* **21**:9S-15S. doi:10.1016/S0893-133X(99)00012-3

Januszewski M, Kornfeld J, Li PH, Pope A, Blakely T, Lindsey L, Maitin-Shepard J, Tyka M, Denk W, Jain V. 2018. High-precision automated reconstruction of neurons with

flood-filling networks. *Nat Methods* **15**:605–610. doi:10.1038/s41592-018-0049-4

Jarrell TA, Wang Y, Bloniarz AE, Brittin CA, Xu M, Thomson JN, Albertson DG, Hall DH, Emmons SW. 2012. The Connectome of a Decision-Making Neural Network. *Science (80-)* **337**:437–444. doi:10.1126/science.1221762

Jean A. 2001. Brain stem control of swallowing: Neuronal network and cellular mechanisms. *Physiol Rev* **81**:929–969. doi:10.1152/physrev.2001.81.2.929

Jean A. 1984. Control of the central swallowing program by inputs from the peripheral receptors. A review. *J Auton Nerv Syst* **10**:225–233. doi:10.1016/0165-1838(84)90017-1

Jeanne JM, Wilson RI. 2015. Convergence, Divergence, and Reconvergence in a Feedforward Network Improves Neural Speed and Accuracy. *Neuron* **88**:1014–1026. doi:10.1016/j.neuron.2015.10.018

Jeltema M, Beckley J, Vahalik J. 2015. Model for understanding consumer textural food choice. *Food Sci Nutr* **3**:202–212. doi:10.1002/fsn3.205

Jones WD, Cayirlioglu P, Grunwald Kadow I, Vosshall LB. 2007. Two chemosensory receptors together mediate carbon dioxide detection in *Drosophila*. *Nature* **445**:86–90. doi:10.1038/nature05466

Jovanic T, Schneider-Mizell CM, Shao M, Masson JB, Denisov G, Fetter RD, Mensh BD, Truman JW, Cardona A, Zlatic M. 2016. Competitive Disinhibition Mediates Behavioral Choice and Sequences in *Drosophila*. *Cell* **167**:858-870.e19. doi:10.1016/j.cell.2016.09.009

Kandel ER. 2001. The Molecular Biology of Memory Storage: A Dialogue Between Genes and Synapses. *Science (80-)* **294**:1030–1038. doi:10.1126/science.1067020

Kasthuri N, Hayworth KJ, Berger DR, Schalek RL, Conchello JA, Knowles-Barley S, Lee D, Vázquez-Reina A, Kaynig V, Jones TR, Roberts M, Morgan JL, Tapia JC, Seung HS, Roncal WG, Vogelstein JT, Burns R, Sussman DL, Priebe CE, Pfister H, Lichtman JW. 2015. Saturated Reconstruction of a Volume of Neocortex. *Cell* **162**:648–661. doi:10.1016/j.cell.2015.06.054

Katz P, Grillner S, Wilson R, Borst A, Greenspan R, Buzsáki G, Martin K, Marder E, Kristan W, Friedrich R, Chklovskii DM. 2013. Vertebrate versus invertebrate neural circuits. *Curr Biol* **23**:504–506. doi:10.1016/j.cub.2013.05.039

Kawashima T, Zwart MF, Yang C-T, Mensh BD, Ahrens MB. 2016. The Serotonergic System Tracks the Outcomes of Actions to Mediate Short-Term Motor Learning. *Cell* **167**:933-946.e20. doi:10.1016/j.cell.2016.09.055

Kendroud S, Bohra AA, Kuert PA, Nguyen B, Guillermin O, Sprecher SG, Reichert H, VijayRaghavan K, Hartenstein V. 2017. Structure and development of the subesophageal zone of the *Drosophila* brain. II. Sensory compartments. *J Comp Neurol* **526**:33–58. doi:10.1002/cne.24316

Kiehn O. 2011. Development and functional organization of spinal locomotor circuits. *Curr Opin Neurobiol* **21**:100–109. doi:10.1016/j.conb.2010.09.004

Kiehn O. 2006. Locomotor Circuits in the Mammalian Spinal Cord. *Annu Rev Neurosci* **29**:279–306. doi:10.1146/annurev.neuro.29.051605.112910

Kien J. 1979. Variability of locust motoneuron responses to sensory stimulation: A possible substrate for motor flexibility. *J Comp Physiol □ A* **134**:55–68. doi:10.1007/BF00610277

Klein M, Afonso B, Vonner AJ, Hernandez-Nunez L, Berck M, Tabone CJ, Kane EA, Pieribone VA, Nitabach MN, Cardona A, Zlatic M, Sprecher SG, Gershow M, Garrity PA, Samuel ADT, Sternberg PW. 2015. Sensory determinants of behavioral dynamics in *Drosophila* thermotaxis. *Proc Natl Acad Sci U S A* **112**:E220–E229. doi:10.1073/pnas.1416212112

Knott G, Marchman H, Wall D, Lich B. 2008. Serial Section Scanning Electron Microscopy of Adult Brain Tissue Using Focused Ion Beam Milling. *J Neurosci* **28**:2959–2964. doi:10.1523/JNEUROSCI.3189-07.2008

Kohl J, Ostrovsky AD, Frechter S, Jefferis GSXE. 2013. A Bidirectional Circuit Switch Reroutes Pheromone Signals in Male and Female Brains. *Cell* **155**:1610–1623. doi:10.1016/j.cell.2013.11.025

Kornfeld J, Denk W. 2018. Progress and remaining challenges in high-throughput volume electron microscopy. *Curr Opin Neurobiol* **50**:261–267. doi:10.1016/j.conb.2018.04.030

Kudow N, Kamikouchi A, Tanimura T. 2019. Softness sensing and learning in *Drosophila* larvae. *J Exp Biol* **222**:jeb196329. doi:10.1242/jeb.196329

Kwon JY, Dahanukar A, Weiss L a., Carlson JR. 2011. Molecular and Cellular Organization of the Taste System in the *Drosophila* Larva. *J Neurosci* **31**:15300–15309. doi:10.1523/JNEUROSCI.3363-11.2011

Lang IM. 2009. Brain stem control of the phases of swallowing. *Dysphagia* **24**:333–348. doi:10.1007/s00455-009-9211-6

Larderet I, Fritsch PMJ, Gendre N, Neagu-Maier GL, Fetter RD, Schneider-Mizell CM, Truman JW, Zlatic M, Cardona A, Sprecher SG. 2017. Organization of the *Drosophila*

larval visual circuit. *Elife* **6**. doi:10.7554/eLife.28387

Lawton KJ, Perry WM, Yamaguchi A, Zornik E. 2017. Motor Neurons Tune Premotor Activity in a Vertebrate Central Pattern Generator. *J Neurosci* **37**:3264–3275. doi:10.1523/JNEUROSCI.2755-16.2017

Lee KS, Iwanir S, Kopito RB, Scholz M, Calarco JA, Biron D, Levine E. 2017. Serotonin-dependent kinetics of feeding bursts underlie a graded response to food availability in *C. elegans*. *Nat Commun* **8**:14221. doi:10.1038/ncomms14221

Leonardo A. 2005. Degenerate coding in neural systems. *J Comp Physiol A* **191**:995–1010. doi:10.1007/s00359-005-0026-0

Lichtman JW, Denk W. 2011. The Big and the Small: Challenges of Imaging the Brain's Circuits. *Science (80-)* **334**:618–623. doi:10.1126/science.1209168

Lichtman JW, Pfister H, Shavit N. 2014. The big data challenges of connectomics. *Nat Neurosci* **17**:1448–1454. doi:10.1038/nn.3837

Liu Y-Y, Barabási A-L. 2016. Control principles of complex systems. *Rev Mod Phys* **88**:035006. doi:10.1103/RevModPhys.88.035006

Llinás RR. 2003. The contribution of Santiago Ramon y Cajal to functional neuroscience. *Nat Rev Neurosci* **4**:77–80. doi:10.1038/nrn1011

Ludwig CE. 1949. Embryology and morphology of the larval head of *Calliphora erythrocephala* (Meigen). *Microentomology* **14**:75–111.

Luo L, Callaway EM, Svoboda K. 2018. Genetic Dissection of Neural Circuits: A Decade of Progress. *Neuron* **98**:256–281. doi:10.1016/j.neuron.2018.03.040

Maimon G. 2011. Modulation of visual physiology by behavioral state in monkeys, mice, and flies. *Curr Opin Neurobiol* **21**:559–564. doi:10.1016/j.conb.2011.05.001

Man K, Kaplan J, Damasio H, Damasio A. 2013. Neural convergence and divergence in the mammalian cerebral cortex: From experimental neuroanatomy to functional neuroimaging. *J Comp Neurol* **521**:4097–4111. doi:10.1002/cne.23408

Mangan S, Alon U. 2003. Structure and function of the feed-forward loop network motif. *Proc Natl Acad Sci* **100**:11980–11985. doi:10.1073/pnas.2133841100

Marder E, Bucher D. 2007. Understanding Circuit Dynamics Using the Stomatogastric Nervous System of Lobsters and Crabs. *Annu Rev Physiol* **69**:291–316. doi:10.1146/annurev.physiol.69.031905.161516

Marder E, Bucher D. 2001. Central pattern generators and the control of rhythmic movements. *Curr Biol* **11**:R986–R996. doi:10.1016/S0960-9822(01)00581-4

Marder E, Jorge-Rivera JC, Kilman V, Weimann JM. 1997. Peptidergic Modulation of

Synaptic Transmission in a Rhythmic Motor SystemAdvances in Organ Biology. pp. 213–233. doi:10.1016/S1569-2590(08)60187-1

Marder E, Weimann JM. 1992. Modulatory control of multiple task processing in the stomatogastric nervous system.Neurobiology of Motor Programme Selection. Elsevier. pp. 3–19. doi:10.1016/B978-0-08-041986-2.50006-0

Matsuo K, Palmer JB. 2009. Coordination of mastication, swallowing and breathing. *Jpn Dent Sci Rev* **45**:31–40. doi:10.1016/j.jdsr.2009.03.004

McCormick DA, Nusbaum MP. 2014. Editorial overview: Neuromodulation: Tuning the properties of neurons, networks and behavior. *Curr Opin Neurobiol* **29**:4–7. doi:10.1016/j.conb.2014.10.010

McKellar CE. 2016. Motor control of fly feeding. *J Neurogenet* **30**:101–111. doi:10.1080/01677063.2016.1177047

Mei N. 1978. Vagal glucoreceptors in the small intestine of the cat. *J Physiol* **282**:485–506. doi:10.1113/jphysiol.1978.sp012477

Melcher C, Bader R, Walther S, Simakov O, Pankratz MJ. 2006. Neuromedin U and Its Putative *Drosophila* Homolog hugin. *PLoS Biol* **4**:e68. doi:10.1371/journal.pbio.0040068

Mentis GZ, Alvarez FJ, Bonnot A, Richards DS, Gonzalez-Forero D, Zerda R, O'Donovan MJ. 2005. Noncholinergic excitatory actions of motoneurons in the neonatal mammalian spinal cord. *Proc Natl Acad Sci* **102**:7344–7349. doi:10.1073/pnas.0502788102

Mikhailov AT, Gilbert SF. 2002. From development to evolution: The re-establishment of the "Alexander Kowalevsky Medal." *Int J Dev Biol* **46**:693–698. doi:10.1387/ijdb.12216980

Milo R. 2002. Network Motifs: Simple Building Blocks of Complex Networks. *Science (80-)* **298**:824–827. doi:10.1126/science.298.5594.824

Miroschnikow A, Schlegel P, Pankratz MJ. 2020. Making Feeding Decisions in the *Drosophila* Nervous System. *Curr Biol* **30**:R831–R840. doi:10.1016/j.cub.2020.06.036

Miroschnikow A, Schlegel P, Schoofs A, Hückesfeld S, Li F, Schneider-Mizell CM, Fetter RD, Truman JW, Cardona A, Pankratz MJ. 2018. Convergence of monosynaptic and polysynaptic sensory paths onto common motor outputs in a Drosohila feeding connectome. *Elife* **7**. doi:10.7554/eLife.40247

Mishra D, Miyamoto T, Rezenom YH, Broussard A, Yavuz A, Slone J, Russell DH, Amrein

H. 2013. The molecular basis of sugar sensing in *Drosophila* larvae. *Curr Biol* **23**:1466–1471. doi:10.1016/j.cub.2013.06.028

Mishra D, Thorne N, Miyamoto C, Jagge C, Amrein H. 2018. The taste of ribonucleosides: Novel macronutrients essential for larval growth are sensed by *Drosophila* gustatory receptor proteins. *PLOS Biol* **16**:e2005570. doi:10.1371/journal.pbio.2005570

Miyamoto T, Amrein H. 2014. Diverse roles for the *Drosophila* fructose sensor Gr43a. *Fly (Austin)* **8**:19–25. doi:10.4161/fly.27241

Morgan JL, Lichtman JW. 2017. Digital tissue and what it may reveal about the brain. *BMC Biol* **15**:101. doi:10.1186/s12915-017-0436-9

Morgan JL, Lichtman JW. 2013. Why not connectomics? *Nat Methods* **10**:494–500. doi:10.1038/nmeth.2480

Mulcahy B, Witvliet D, Holmyard D, Mitchell J, Chisholm AD, Samuel ADT, Zhen M. 2018. A pipeline for volume electron microscopy of the *Caenorhabditis elegans* nervous system. *Front Neural Circuits* **12**. doi:10.3389/fncir.2018.00094

Nässel DR, Kubrak OI, Liu Y, Luo J, Lushchak O V. 2013. Factors that regulate insulin producing cells and their output in *Drosophila*. *Front Physiol* **4**:1–12. doi:10.3389/fphys.2013.00252

Nassi JJ, Callaway EM. 2009. Parallel processing strategies of the primate visual system. *Nat Rev Neurosci* **10**:360–372. doi:10.1038/nrn2619

Nichols TR. 2009. Reflex CircuitsEncyclopedia of Neuroscience. Elsevier. pp. 73–79. doi:10.1016/B978-008045046-9.01344-9

Niven JE, Laughlin SB. 2008. Energy limitation as a selective pressure on the evolution of sensory systems. *J Exp Biol* **211**:1792–1804. doi:10.1242/jeb.017574

Ohyama T, Schneider-Mizell CM, Fetter RD, Aleman JV, Franconville R, Rivera-Alba M, Mensh BD, Branson KM, Simpson JH, Truman JW, Cardona A, Zlatic M. 2015. A multilevel multimodal circuit enhances action selection in *Drosophila*. *Nature* **520**:633–639. doi:10.1038/nature14297

Olds WH, Xu T. 2014. Regulation of food intake by mechanosensory ion channels in enteric neurons. *Elife* **3**:e04402. doi:10.7554/eLife.04402

Oppliger FY, M. Guerin P, Vlimant M. 2000. Neurophysiological and behavioural evidence for an olfactory function for the dorsal organ and a gustatory one for the terminal organ in *Drosophila melanogaster* larvae. *J Insect Physiol* **46**:135–144. doi:10.1016/S0022-1910(99)00109-2

Park JH, Kwon JY. 2011. Heterogeneous expression of *Drosophila* gustatory receptors in

enteroendocrine cells. *PLoS One* **6**. doi:10.1371/journal.pone.0029022

Plaza SM, Scheffer LK, Chklovskii DB. 2014. Toward large-scale connectome reconstructions. *Curr Opin Neurobiol* **25**:201–210. doi:10.1016/j.conb.2014.01.019

Pool AH, Scott K. 2014. Feeding regulation in *Drosophila*. *Curr Opin Neurobiol* **29**:57–63. doi:10.1016/j.conb.2014.05.008

Prokop A, Meinertzhagen IA. 2006. Development and structure of synaptic contacts in *Drosophila*. *Semin Cell Dev Biol* **17**:20–30. doi:10.1016/j.semcdb.2005.11.010

Raka F, Farr S, Kelly J, Stoianov A, Adeli K. 2019. Metabolic control via nutrient-sensing mechanisms: role of taste receptors and the gut-brain neuroendocrine axis. *Am J Physiol Metab* **317**:E559–E572. doi:10.1152/ajpendo.00036.2019

Ramón y Cajal S. 1894. Les nouvelles idées sur la structure du système nerveux chez l'homme et chez les vertébrés, Édition Fr. ed. Paris : Reinwald.

Reiter S, Campillo Rodriguez C, Sun K, Stopfer M. 2015. Spatiotemporal Coding of Individual Chemicals by the Gustatory System. *J Neurosci* **35**:12309–12321. doi:10.1523/JNEUROSCI.3802-14.2015

Rice MJ. 1970. Cibarial stretch receptors in the tsetse fly (*Glossina austeni*) and the blowfly (*Calliphora erythrocephala*). *J Insect Physiol* **16**:277–289. doi:10.1016/0022-1910(70)90170-8

Rist A, Thum AS. 2017. A map of sensilla and neurons in the taste system of *Drosophila* larvae. *J Comp Neurol* **525**:3865–3889. doi:10.1002/cne.24308

Roberts A, Li WC, Soffe SR. 2012. A functional scaffold of CNS neurons for the vertebrates: The developing *Xenopus laevis* spinal cord. *Dev Neurobiol* **72**:575–584. doi:10.1002/dneu.20889

Rolls E. 2005. Taste, olfactory, and food texture processing in the brain, and the control of food intake. *Physiol Behav* **85**:45–56. doi:10.1016/j.physbeh.2005.04.012

Rumelhart DE, McClelland JL. 1986. Parallel Distributed Processing: Explorations in the Microstructure of Cognition. Volume 1: Foundations. The MIT Press. doi:10.7551/mitpress/5236.001.0001

Ryan K, Lu Z, Meinertzhagen IA. 2018. The peripheral nervous system of the ascidian tadpole larva: Types of neurons and their synaptic networks. *J Comp Neurol* **526**:583–608. doi:10.1002/cne.24353

Ryan K, Lu Z, Meinertzhagen IA. 2017. Circuit Homology between Decussating Pathways in the *Ciona* Larval CNS and the Vertebrate Startle-Response Pathway. *Curr Biol* **27**:721–728. doi:10.1016/j.cub.2017.01.026

Ryan K, Lu Z, Meinertzhagen IA. 2016. The CNS connectome of a tadpole larva of *Ciona intestinalis* (L.) highlights sidedness in the brain of a chordate sibling. *Elife* **5**:1–34. doi:10.7554/eLife.16962

Saalfeld S, Cardona A, Hartenstein V, Tomancak P. 2009. CATMAID: collaborative annotation toolkit for massive amounts of image data. *Bioinformatics* **25**:1984–6. doi:10.1093/bioinformatics/btp266

Sako N, Okamoto K, Mori T, Yamamoto T. 2002. The hardness of food plays an important role in food selection behavior in rats. *Behav Brain Res* **133**:377–382. doi:10.1016/S0166-4328(02)00031-1

Sakurai K, Akiyama M, Cai B, Scott A, Han BX, Takatoh J, Sigrist M, Arber S, Wang F. 2013. The Organization of Submodality-Specific Touch Afferent Inputs in the Vibrissa Column. *Cell Rep* **5**:87–98. doi:10.1016/j.celrep.2013.08.051

Sánchez-Alcañiz JA, Zappia G, Marion-Poll F, Benton R. 2017. A mechanosensory receptor required for food texture detection in *Drosophila*. *Nat Commun* **8**:14192. doi:10.1038/ncomms14192

Saumweber T, Rohwedder A, Schleyer M, Eichler K, Chen Y, Aso Y, Cardona A, Eschbach C, Kobler O, Voigt A, Durairaja A, Mancini N, Zlatic M, Truman JW, Thum AS, Gerber B. 2018. Functional architecture of reward learning in mushroom body extrinsic neurons of larval *Drosophila*. *Nat Commun* **9**:1104. doi:10.1038/s41467-018-03130-1

Sawin ER, Ranganathan R, Horvitz HR. 2000. *C. elegans* locomotory rate is modulated by the environment through a dopaminergic pathway and by experience through a serotonergic pathway. *Neuron* **26**:619–631. doi:10.1016/S0896-6273(00)81199-X

Scheffer LK, Xu CS, Januszewski M, Lu Z, Takemura Shin-ya, Hayworth KJ, Huang G, Shinomiya K, Maitlin-Shepard J, Berg S, Clements J, Hubbard PM, Katz WT, Umayam L, Zhao T, Ackerman D, Blakely T, Bogovic J, Dolafi T, Kainmueller D, Kawase T, Khairy K, Leavitt L, Li PH, Lindsey L, Neubarth N, Olbris DJ, Otsuna H, Trautman ET, Ito M, Goldammer J, Wolff T, Svirskas R, Schlegel P, Neace E, Knecht C, Alvarado CX, Bailey DA, Ballinger S, Borycz JA, Canino BS, Cheatham N, Cook M, Dreher M, Duclos O, Eubanks B, Fairbanks K, Finley S, Forknall N, Francis A, Hopkins GP, Joyce EM, Kim S, Kirk NA, Kovalyak J, Lauchie S, Lohff A, Maldonado C, Manley EA, McLin S, Mooney C, Ndama M, Ogundeyi O, Okeoma N, Ordish C, Padilla N, Patrick CM, Paterson T, Phillips EE, Phillips EM, Rampally N, Ribeiro C, Robertson MK, Rymer JT, Ryan SM, Sammons M, Scott AK, Scott AL, Shinomiya A,

Smith C, Smith K, Smith NL, Sobeski MA, Suleiman A, Swift J, Takemura Satoko, Talebi I, Tarnogorska D, Tenshaw E, Tokhi T, Walsh JJ, Yang T, Horne JA, Li F, Parekh R, Rivlin PK, Jayaraman V, Ito K, Saalfeld S, George R, Meinertzhagen I, Rubin GM, Hess HF, Jain V, Plaza SM. 2020. A Connectome and Analysis of the Adult *Drosophila* Central Brain. *bioRxiv* 2020.04.07.030213.

Schlegel P, Costa M, Jefferis GS. 2017. Learning from connectomics on the fly. *Curr Opin Insect Sci* **24**:96–105. doi:10.1016/j.cois.2017.09.011

Schlegel P, Texada MJ, Miroschnikow A, Schoofs A, Hückesfeld S, Peters M, Schneider-Mizell CM, Lacin H, Li F, Fetter RD, Truman JW, Cardona A, Pankratz MJ. 2016. Synaptic transmission parallels neuromodulation in a central food-intake circuit. *Elife* **5**:1–28. doi:10.7554/eLife.16799

Schneider-Mizell CM, Gerhard S, Longair M, Kazimiers T, Li F, Zwart MF, Champion A, Midgley FM, Fetter RD, Saalfeld S, Cardona A. 2016. Quantitative neuroanatomy for connectomics in *Drosophila*. *Elife* **5**:1–36. doi:10.7554/eLife.12059

Schoofs A, Hückesfeld S, Pankratz MJ. 2018. Serotonergic network in the subesophageal zone modulates the motor pattern for food intake in *Drosophila*. *J Insect Physiol* **106**:36–46. doi:10.1016/j.jinsphys.2017.07.007

Schoofs A, Hückesfeld S, Schlegel P, Miroschnikow A, Peters M, Zeymer M, Spieß R, Chiang AS, Pankratz MJ. 2014a. Selection of Motor Programs for Suppressing Food Intake and Inducing Locomotion in the *Drosophila* Brain. *PLoS Biol* **12**:e1001893. doi:10.1371/journal.pbio.1001893

Schoofs A, Hückesfeld S, Surendran S, Pankratz MJ. 2014b. Serotonergic pathways in the *Drosophila* larval enteric nervous system. *J Insect Physiol* **69**:118–125. doi:10.1016/j.jinsphys.2014.05.022

Schoofs A, Niederegger S, van Ooyen A, Heinzel H-G, Spieß R. 2010. The brain can eat: Establishing the existence of a central pattern generator for feeding in third instar larvae of *Drosophila virilis* and *Drosophila melanogaster*. *J Insect Physiol* **56**:695–705. doi:10.1016/j.jinsphys.2009.12.008

Scott K. 2018. Gustatory Processing in *Drosophila melanogaster*. *Annu Rev Entomol* **63**:15–30. doi:10.1146/annurev-ento-020117-043331

Scott K, Brady R, Cravchik A, Morozov P, Rzhetsky A, Zuker C, Axel R. 2001. A Chemosensory Gene Family Encoding Candidate Gustatory and Olfactory Receptors in *Drosophila*. *Cell* **104**:661–673. doi:10.1016/S0092-8674(01)00263-X

Selverston AI, Russell DF, Miller JP, King DG. 1976. The stomatogastric nervous system:

Structure and function of a small neural network. *Prog Neurobiol* **7**:215–289. doi:10.1016/0301-0082(76)90008-3

Seymour B. 2012. Hodgkin and Huxley's legacy: the science of neural supercomputing. *Brain* **135**:2892–2895. doi:10.1093/brain/aws184

Shen-Orr SS, Milo R, Mangan S, Alon U. 2002. Network motifs in the transcriptional regulation network of *Escherichia coli*. *Nat Genet* **31**:64–68. doi:10.1038/ng881

Shepherd GM. 2011. Neurogastronomy: How the Brain Creates Flavor and Why It Matters. New York Chichester, West Sussex: Columbia University Press. doi:10.7312/shep15910

Shepherd GM. 1987. Neurobiology, 2nd ed. Oxford University Press.

Sherrington CS. 1906. The integrative action of the nervous system. New Haven: Yale University Press. doi:10.1037/13798-000

Shimada-Niwa Y, Niwa R. 2014. Serotonergic neurons respond to nutrients and regulate the timing of steroid hormone biosynthesis in *Drosophila*. *Nat Commun* **5**:5778. doi:10.1038/ncomms6778

Siegmund T, Korge G. 2001. Innervation of the ring gland of *Drosophila melanogaster*. *J Comp Neurol* **431**:481–491. doi:10.1002/1096-9861(20010319)431:4<481::AID-CNE1084>3.0.CO;2-7

Simon SA, de Araujo IE, Gutierrez R, Nicolelis MAL. 2006. The neural mechanisms of gustation: a distributed processing code. *Nat Rev Neurosci* **7**:890–901. doi:10.1038/nrn2006

Simpson JH. 2009. Mapping and Manipulating Neural Circuits in the Fly Brain.Chapter 3 in: Genetic Dissection of Neuroal Circuits and Behavior. pp. 79–143. doi:10.1016/S0065-2660(09)65003-3

Singh RN, Singh K. 1984. Fine structure of the sensory organs of *Drosophila melanogaster* Meigen larva (Diptera : Drosophilidae). *Int J Insect Morphol Embryol* **13**:255–273. doi:10.1016/0020-7322(84)90001-1

Small DM. 2012. Flavor is in the brain. *Physiol Behav* **107**:540–552. doi:https://doi.org/10.1016/j.physbeh.2012.04.011

Smith CL, Varoqueaux F, Kittelmann M, Azzam RN, Cooper B, Winters CA, Eitel M, Fasshauer D, Reese TS. 2014. Novel Cell Types, Neurosecretory Cells, and Body Plan of the Early-Diverging Metazoan *Trichoplax adhaerens*. *Curr Biol* **24**:1565–1572. doi:10.1016/j.cub.2014.05.046

Song J, Ampatzis K, Björnfors ER, El Manira A. 2016. Motor neurons control locomotor

circuit function retrogradely via gap junctions. *Nature* **529**:399–402. doi:10.1038/nature16497

Spearman DG, Poliacek I, Rose MJ, Bolser DC, Pitts T. 2014. Variability of the Pharyngeal Phase of Swallow in the Cat. *PLoS One* **9**:e106121. doi:10.1371/journal.pone.0106121

Spieß R, Schoofs A, Heinzel H-G. 2008. Anatomy of the stomatogastric nervous system associated with the foregut in *Drosophila melanogaster* and *Calliphora vicina* third instar larvae. *J Morphol* **269**:272–282. doi:10.1002/jmor.10581

Spindler SR, Hartenstein V. 2010. The *Drosophila* neural lineages: A model system to study brain development and circuitry. *Dev Genes Evol* **220**:1–10. doi:10.1007/s00427-010-0323-7

Sporns O. 2011. The Non-Random Brain: Efficiency, Economy, and Complex Dynamics. *Front Comput Neurosci* **5**:1–13. doi:10.3389/fncom.2011.00005

Sporns O, Kötter R. 2004. Motifs in Brain Networks. *PLoS Biol* **2**:e369. doi:10.1371/journal.pbio.0020369

Sporns O, Tononi G, Kötter R. 2005. The human connectome: A structural description of the human brain. *PLoS Comput Biol* **1**:e42. doi:10.1371/journal.pcbi.0010042

Stein W. 2014. Sensory Input to Central Pattern Generators In: Jaeger D, Jung R, editors. Encyclopedia of Computational Neuroscience. New York, NY: Springer New York. pp. 1–11. doi:10.1007/978-1-4614-7320-6_465-3

Steuer I, Guertin PA. 2019. Central pattern generators in the brainstem and spinal cord: an overview of basic principles, similarities and differences. *Rev Neurosci* **30**:107–164. doi:10.1515/revneuro-2017-0102

Stone J, Dreher B. 1982. Parallel processing of information in the visual pathways. *Trends Neurosci* **5**:441–446. doi:10.1016/0166-2236(82)90237-5

Stradmeyer L. 1989. A behavioural method to test feeding responses of fish to pelleted diets. *Aquaculture* **79**:303–310. doi:10.1016/0044-8486(89)90471-7

Swanson LW. 2011. Brain Architecture: Understanding the Basic Plan, 2nd ed. Oxford University Press. doi:10.1093/med/9780195378580.001.0001

Swanson LW, Lichtman JW. 2016. From Cajal to Connectome and Beyond. *Annu Rev Neurosci* **39**:197–216. doi:10.1146/annurev-neuro-071714-033954

Szigeti B, Gleeson P, Vella M, Khayrulin S, Palyanov A, Hokanson J, Currie M, Cantarelli M, Idili G, Larson S. 2014. OpenWorm: an open-science approach to modeling *Caenorhabditis elegans*. *Front Comput Neurosci* **8**:1–7.

doi:10.3389/fncom.2014.00137

Takemura SY, Bharioke A, Lu Z, Nern A, Vitaladevuni S, Rivlin PK, Katz WT, Olbris DJ, Plaza SM, Winston P, Zhao T, Horne JA, Fetter RD, Takemura S, Blazek K, Chang LA, Ogundeyi O, Saunders MA, Shapiro V, Sigmund C, Rubin GM, Scheffer LK, Meinertzhagen IA, Chklovskii DB. 2013. A visual motion detection circuit suggested by *Drosophila* connectomics. *Nature* **500**:175–181. doi:10.1038/nature12450

Tastekin I, Riedl J, Schilling-Kurz V, Gomez-Marin A, Truman JW, Louis M. 2015. Role of the subesophageal zone in sensorimotor control of orientation in *Drosophila* larva. *Curr Biol* **25**:1448–1460. doi:10.1016/j.cub.2015.04.016

Tecott LH. 2007. Serotonin and the Orchestration of Energy Balance. *Cell Metab* **6**:352–361. doi:10.1016/j.cmet.2007.09.012

Tessmar-Raible K, Raible F, Christodoulou F, Guy K, Rembold M, Hausen H, Arendt D. 2007. Conserved Sensory-Neurosecretory Cell Types in Annelid and Fish Forebrain: Insights into Hypothalamus Evolution. *Cell* **129**:1389–1400. doi:10.1016/j.cell.2007.04.041

Thum AS, Gerber B. 2019. Connectomics and function of a memory network: the mushroom body of larval *Drosophila*. *Curr Opin Neurobiol* **54**:146–154. doi:10.1016/j.conb.2018.10.007

Tobin WF, Wilson RI, Lee W-CA. 2017. Wiring variations that enable and constrain neural computation in a sensory microcircuit. *Elife* **6**:1–26. doi:10.7554/eLife.24838

Todorov E. 2004. Optimality principles in sensorimotor control. *Nat Neurosci* **7**:907–915. doi:10.1038/nn1309

Towlson EK, Vertes PE, Ahnert SE, Schafer WR, Bullmore ET. 2013. The Rich Club of the *C. elegans* Neuronal Connectome. *J Neurosci* **33**:6380–6387. doi:10.1523/JNEUROSCI.3784-12.2013

Tsubouchi A, Yano T, Yokoyama TK, Murtin C, Otsuna H, Ito K. 2017. Topological and modality-specific representation of somatosensory information in the fly brain. *Science (80-)* **358**:615–623. doi:10.1126/science.aan4428

Tuthill JC, Wilson RI. 2016a. Mechanosensation and Adaptive Motor Control in Insects. *Curr Biol* **26**:R1022–R1038. doi:10.1016/j.cub.2016.06.070

Tuthill JC, Wilson RI. 2016b. Parallel Transformation of Tactile Signals in Central Circuits of *Drosophila*. *Cell* **164**:1046–1059. doi:10.1016/j.cell.2016.01.014

Varshney LR, Chen BL, Paniagua E, Hall DH, Chklovskii DB. 2011. Structural properties of the *Caenorhabditis elegans* neuronal network. *PLoS Comput Biol* **7**.

doi:10.1371/journal.pcbi.1001066

Venken KJT, Simpson JH, Bellen HJ. 2011. Genetic Manipulation of Genes and Cells in the Nervous System of the Fruit Fly. *Neuron* **72**:202–230. doi:10.1016/j.neuron.2011.09.021

Vígh B, Manzano e Silva MJ, Frank CL, Vincze C, Czirok SJ, Szabó A, Lukáts A, Szél A. 2004. The system of cerebrospinal fluid-contacting neurons. Its supposed role in the nonsynaptic signal transmission of the brain. *Histol Histopathol* **19**:607–628. doi:10.14670/HH-19.607

Vogt K. 2020. Towards a functional connectome in *Drosophila*. *J Neurogenet* **34**:156–161. doi:10.1080/01677063.2020.1712598

Vosshall LB, Stocker RF. 2007. Molecular architecture of smell and taste in *Drosophila*. *Annu Rev Neurosci* **30**:505–533. doi:10.1146/annurev.neuro.30.051606.094306

Waldeyer-Hartz W von. 1891. Ueber einige neuere Forschungen im Gebiete der Anatomie des Centralnervensystems. Leipzig : Verlag von Georg Thieme.

Wallis DI. 1994. 5-HT receptors involved in initiation or modulation of motor patterns: Opportunities for drug development. *Trends Pharmacol Sci* **15**:288–292. doi:10.1016/0165-6147(94)90009-4

Watanabe K, Toba G, Koganezawa M, Yamamoto D. 2011. Gr39a, a Highly Diversified Gustatory Receptor in *Drosophila*, has a Role in Sexual Behavior. *Behav Genet* **41**:746–753. doi:10.1007/s10519-011-9461-6

Wenner P, O'Donovan MJ. 2001. Mechanisms That Initiate Spontaneous Network Activity in the Developing Chick Spinal Cord. *J Neurophysiol* **86**:1481–1498. doi:10.1152/jn.2001.86.3.1481

White JG. 1985. Neuronal connectivity in *Caenorhabditis elegans*. *Trends Neurosci* **8**:277–283. doi:10.1016/0166-2236(85)90102-X

White JG, Southgate E, Thomson JN, Brenner S. 1986. The Structure of the Nervous System of the Nematode *Caenorhabditis elegans*. *Philos Trans R Soc B Biol Sci* **314**:1–340. doi:10.1098/rstb.1986.0056

White JG, Southgate E, Thomson JN, Brenner S. 1976. The structure of the ventral nerve cord of *Caenorhabditis elegans*. *Philos Trans R Soc London B, Biol Sci* **275**:327–348. doi:10.1098/rstb.1976.0086

Williams EA, Verasztó C, Jasek S, Conzelmann M, Shahidi R, Bauknecht P, Mirabeau O, Jékely G. 2017. Synaptic and peptidergic connectome of a neurosecretory center in the annelid brain. *Elife* **6**:1–22. doi:10.7554/eLife.26349

Williams EK, Chang RB, Strochlic DE, Umans BD, Lowell BB, Liberles SD. 2016. Sensory Neurons that Detect Stretch and Nutrients in the Digestive System. *Cell* **166**:209–221. doi:10.1016/j.cell.2016.05.011

Wilson RI. 2013. Early Olfactory Processing in *Drosophila*: Mechanisms and Principles. *Annu Rev Neurosci* **36**:217–241. doi:10.1146/annurev-neuro-062111-150533

Wolpert DM, Ghahramani Z. 2000. Computational principles of movement neuroscience. *Nat Neurosci* **3**:1212–1217. doi:10.1038/81497

Wu Q, Zhang Y, Xu J, Shen P. 2005. Regulation of hunger-driven behaviors by neural ribosomal S6 kinase in *Drosophila*. *Proc Natl Acad Sci* **102**:13289–13294. doi:10.1073/pnas.0501914102

Xiang Y, Yuan Q, Vogt N, Looger LL, Jan LY, Jan YN. 2010. Light-avoidance-mediating photoreceptors tile the *Drosophila* larval body wall. *Nature* **468**:921–926. doi:10.1038/nature09576

Xu CS, Hayworth KJ, Lu Z, Grob P, Hassan AM, García-Cerdán JG, Niyogi KK, Nogales E, Weinberg RJ, Hess HF. 2017. Enhanced FIB-SEM systems for large-volume 3D imaging. *Elife* **6**:1–36. doi:10.7554/eLife.25916

Xu CS, Pang S, Hayworth KJ, Hess HF. 2019. Enabling FIB-SEM Systems for Large Volume Connectomics and Cell Biology. *bioRxiv* **C**:852863. doi:10.1101/852863

Yan G, Vértes PE, Towlson EK, Chew YL, Walker DS, Schafer WR, Barabási A-L. 2017. Network control principles predict neuron function in the *Caenorhabditis elegans* connectome. *Nature* **550**:519–523. doi:10.1038/nature24056

Yang Z, Huang R, Fu X, Wang G, Qi W, Mao D, Shi Z, Shen WL, Wang L. 2018. A post-ingestive amino acid sensor promotes food consumption in *Drosophila*. *Cell Res* **28**:1013–1025. doi:10.1038/s41422-018-0084-9

Yapici N, Cohn R, Schusterreiter C, Ruta V, Vosshall LB. 2016. A Taste Circuit that Regulates Ingestion by Integrating Food and Hunger Signals. *Cell* **165**:715–729. doi:10.1016/j.cell.2016.02.061

Zhang H, Liu J, Li CR, Momen B, Kohanski RA, Pick L. 2009. Deletion of *Drosophila* insulin-like peptides causes growth defects and metabolic abnormalities. *Proc Natl Acad Sci* **106**:19617–19622. doi:10.1073/pnas.0905083106

Zhen M, Samuel AD. 2015. *C. elegans* locomotion: small circuits, complex functions. *Curr Opin Neurobiol* **33**:117–126. doi:10.1016/j.conb.2015.03.009

Zheng Z, Lauritzen JS, Perlman E, Robinson CG, Nichols M, Milkie D, Torrens O, Price J, Fisher CB, Sharifi N, Calle-Schuler SA, Kmecova L, Ali IJ, Karsh B, Trautman ET,

Bogovic JA, Hanslovsky P, Jefferis GSXE, Kazhdan M, Khairy K, Saalfeld S, Fetter RD, Bock DD. 2018. A Complete Electron Microscopy Volume of the Brain of Adult *Drosophila melanogaster*. *Cell* **174**:730-743.e22. doi:10.1016/j.cell.2018.06.019

Zinke I, Kirchner C, Chao LC, Tetzlaff MT, Pankratz MJ. 1999. Suppression of food intake and growth by amino acids in *Drosophila*: the role of pumpless, a fat body expressed gene with homology to vertebrate glycine cleavage system. *Development* **126**:5275–84.

Zwart MF, Pulver SR, Truman JW, Fushiki A, Fetter RD, Cardona A, Landgraf M. 2016. Selective Inhibition Mediates the Sequential Recruitment of Motor Pools. *Neuron* **91**:615–628. doi:10.1016/j.neuron.2016.06.031

PUBLICATIONS

1. **Miroschnikow A**, Schlegel P, Pankratz MJ. 2020. Making Feeding Decisions in the *Drosophila* Nervous System. Curr Biol 30:R831–R840 *

2. **Miroschnikow A**, Schlegel P, Schoofs A, Hückesfeld S, Li F, Schneider-Mizell CM, Fetter RD, Truman JW, Cardona A, Pankratz MJ. 2018. Convergence of monosynaptic and polysynaptic sensory paths onto common motor outputs in a *Drosophila* feeding connectome. eLife. doi:10.7554/elife.40247 *

   preprint of the article:

   Miroschnikow A, Schlegel P, Schoofs A, Hückesfeld S, Li F, Schneider-Mizell CM, Fetter RD, Truman J, Cardona A, Pankratz MJ. 2018. The Feeding Connectome: Convergence of Monosynaptic and Polysynaptic Sensory Paths onto Common Motor Outputs. bioRxiv 368878. doi:10.1101/368878 *

3. Almeida-Carvalho MJ, Berh D, Braun A, Chen Y-C, Eichler K, Eschbach C, Fritsch PMJ, Gerber B, Hoyer N, Jiang X, Kleber J, Klämbt C, König C, Louis M, Michels B, **Miroschnikow A**, Mirth C, Miura D, Niewalda T, Otto N, Paisios E, Pankratz MJ, Petersen M, Ramsperger N, Randel N, Risse B, Saumweber T, Schlegel P, Schleyer M, Soba P, Sprecher SG, Tanimura T, Thum AS, Toshima N, Truman JW, Yarali A, Zlatic M. (2017). The Ol1mpiad: concordance of behavioural faculties of stage 1 and stage 3 *Drosophila* larvae. The Journal of Experimental Biology. doi:10.1242/jeb.156646

4. Schlegel P, Texada MJ, **Miroschnikow A**, Schoofs A, Hückesfeld S, Peters M, Schneider-Mizell CM, Lacin H, Li F, Fetter RD, Truman JW, Cardona A, Pankratz MJ. 2016. Synaptic transmission parallels neuromodulation in a central food-intake circuit. eLife. doi:10.7554/elife.16799

5. Hückesfeld S, Schoofs A, Schlegel P, **Miroschnikow A**, Pankratz MJ. 2015. Localization of Motor Neurons and Central Pattern Generators for Motor Patterns Underlying Feeding Behavior in *Drosophila* Larvae. PLOS ONE. doi:10.1371/journal.pone.0135011

6. Schoofs A, Hückesfeld S, Schlegel P, **Miroschnikow A**, Peters M, Zeymer M, Spieß R, Chiang A-S, Pankratz MJ. 2014. Selection of Motor Programs for Suppressing Food Intake and Inducing Locomotion in the *Drosophila* Brain. PLoS Biology. doi:10.1371/journal.pbio.1001893

PhD independent publications:

1. Kaiser W, Weber T, Otto D, **Miroschnikow A**. 2014. Oxygen supply of the heart and electrocardiogram potentials with reversed polarity in sleeping and resting honey bees. Apidologie. doi:10.1007/s13592-013-0229-2

2. Niederegger S, **Miroschnikow A**, Spieß R. 2013. Marked for life: muscle attachment site patterns in blowfly larvae are constant throughout development. Parasitology Research. doi:10.1007/s00436-012-3142-0

* Please note that these publications have been incorporated into this dissertation.